

**Development of Lipid Nanodisc Technology for the Formulation of
Poorly Water Soluble Drugs**

Andreea Ivona Petrache

**Submitted in accordance with requirements for the degree of
Doctor of Philosophy**

**The University of Leeds
School of Chemistry**

April 2016

The candidate confirms that the work submitted is her own, except where work which has formed part of jointly-authored publication has been included. The contribution of the candidate and the other authors to this work has been explicitly indicated below. The candidate confirms that appropriate credit has been given within the thesis where reference has been made to the work of others.

Chapter 5 – *Modified nanodiscs for traceable cellular delivery* includes content from the publication: "Sortase-mediated labelling of lipid nanodiscs for cellular tracing", Mol. BioSyst., 2016, Accepted Manuscript, A. I. Petrache, D. C. Machin, D. J. Williamson, M. E. Webb and P. A. Beales. The candidate reconstituted the nanodiscs and conducted the cleavage of His₆ tag attached to the N-terminus of MSP1D1, incorporated in nanodiscs. The candidate also conducted the Sortase A mediated reaction. TEV protease, Sortase A and fluorescein depsipeptide were prepared in HEPES buffer by Dr Daniel Williamson. General passage procedure, preparation of HeLa cells before transfection, the protein transfection procedure and cell fixation were conducted by Mr Darren Machin. The candidate immobilised the cells and performed the measurements on the confocal fluorescence microscopy. M. E. Webb, P. A. Beales and the candidate composed the manuscript.

This copy has been supplied on the understanding that it is a copyright material and that no quotation from the thesis may be published without proper acknowledgment.

Acknowledgements

Firstly I would like to thank all past and present members of lab 3.14 and lab 1.49. James W., Tom W., Wynn, Noha, Kat, Tom B, Heather, Darren, Dan, Chadamas, Matt, Tom Mc, James R. and Phil have made my working days in Leeds a joyful experience.

I would like to express my gratitude to my supervisors Paul Beales and Mike Webb for their support and encouraging feedback given throughout the project.

It is a pleasure to also thank Heather Cox, Darren Machin and Dan Williamson who had the patience to teach me all there is to know about the bio lab, protein labelling and cell culture. I cannot thank them enough for their helpful and smiley attitude.

I would like to warmly acknowledge the technical staff in School of Chemistry and Astbury Centre, with special thanks to Martin Huscroft and Dave Fogarty for their assistance with HPLC and UV spectrometry assays.

Special thanks go to James Warren and Tom Wild for their never-ending calm in stopping my panic moments, their enjoyable chemistry chats and general support during the dark days, with coffee breaks or after work pints – Tom is not fond of coffee.

Mami, îți mulțumesc din suflet că îmi ești alături și că întotdeauna ai încercat să mă ajuți la nevoie și să îmi susții alegerile. Mă bucur tare mult că amândouă ne-am schimbat în bine și că suntem mult mai aproape una de alta deși distanța nu ne permite. Te iubesc.

Finally, I would like to thank Joe Bradley. My PhD would not have been finished with my sanity intact without his patience, constant encouragement, silly faces and random dance moments in the house. His positive perspective was there when I most needed it. For all this I am truly thankful to him.

Abstract

The research surrounding delivery carriers of hydrophobic drugs has evolved with the help of efficient tools brought together by nature's most important process, self-assembly. This enabled scientists to create and tailor materials with multiple functionalities in order to suite specific needs. One such nanomaterial is the disc-shaped cargo carrier, named nanodiscs. Nanodiscs are noncovalent assemblies consisting of a phospholipid bilayer, whose hydrophobic edge is stabilized by two or more copies of membrane scaffold protein.

Despite an abundance of research directed towards the development of an effective nanosystem for delivery into mammalian cells, superficial focus is given to characterizing the incorporation of hydrophobic drugs. This thesis describes the development of a simple approach to systematically study the relation between physical parameters related to loading and release of poorly water soluble drugs from nanodisc systems.

For the nanodiscs reconstitution, two strategies have been studied, the first comprised of adding the protein to a mixture of lipid and detergent micelles, and second strategy involved adding protein stabilised in detergent micelles to the lipid. Two more strategies were employed for studying the loading of drugs into nanodiscs - the drugs were added either to a solution of nanodiscs, or loaded during the reconstitution of nanodiscs. The latter strategy showed an increase in drug incorporated per nanodiscs and a slower release rate. In the case of amiodarone and chlorambucil incorporation, a decrease in membrane thickness was seen to be correlated with the efficiency of drug loading within the POPC bilayer. In addition, the lipid composition within nanodiscs was varied in order to investigate its effect on nanodisc formation, drug loading and release kinetics. Finally, the protein component of empty and drug loaded nanodiscs was site-specifically modified *via* Sortase A mediated ligation, for traceable delivery in *in vitro* cell studies. Good internalisation of MSP by HeLa cells was observed when cells were treated with empty and chlorambucil loaded nanodiscs.

Abbreviations

AD	Alcohol dehydrogenase
AIM	Auto Induction media
AMB	Amphotericin B
AMD	Amiodarone
ApoA-I	Apolipoprotein A1
ApoE	Apolipoprotein E
APS	Ammonium persulphate
ATP	Adenosine triphosphate
ATRA	All <i>trans</i> retinoic acid
Au	Absorbance unit
BSA	Bovine serum albumin
CCM	Curcumin
CD	Circular dichroism
CLB	Chlorambucil
CLF	Clofazimine
CLQ	Chloroquine
CMC	Critical micelle concentration
CPR	Cytochrome P450 reductase
CPT	Camptothecin

CV	Column volume
DAPI	4',6-diamidino-2-phenylindole
DHPC	1, 2-diheptanoyl- <i>sn</i> -glycero-3-phosphocholine
DLPC	1, 2-dilauroyl- <i>sn</i> -glycero-3-phosphocholine
DLS	Dynamic light scattering
DMPC	1,2-dimyristoyl- <i>sn</i> -glycero-3-phosphocholine
DNA	Deoxyribonucleic acid
DOPE PEG550	1,2 – dioleoyl- <i>sn</i> -glycero-3-phosphoethanolamine – N - [methoxy (polyethylene glycol) - 550]
DOTAP	1,2-dioleoyl-3-trimethylammonium-propane
DPPC	1,2-dipalmitoyl- <i>sn</i> -glycero-3-phosphocholine
<i>E. coli</i>	Escherichia coli
FCS	Fluorescence correlation spectroscopy
FLC	Fluorescein
FRET	Förster resonance energy transfer
GPC	G-protein coupled receptor
HDL	High density lipoproteins
HEPES	4-(2-hydroxyethyl)-1-piperazineethanesulfonic acid
HepG2	Liver hepatocellular cells
His	Histidine
HPLC	High performance liquid chromatography

IND	Indomethacin
IPTG	Isopropyl β -D-1-thiogalactopyranoside
JC virus	John Cunningham virus
LB	Lysogeny broth
Log P	Logarithm of partition coefficient
MeCN	Acetonitrile
MLV	Multilamellar vesicles
MS	Mass spectroscopy
MSP	Membrane scaffold protein
MTT	(3-(4,5-dimethylthiazol-2-yl)-2,5-diphenyltetrazolium bromide) tetrazolium reduction
MW	Molecular weight
NADPH	Nicotinamide adenine dinucleotide phosphate
ND	Nanodiscs
ND AMD	Amiodarone loaded nanodiscs
ND CCM	Curcumin loaded nanodiscs
ND CLB	Chlorambucil loaded nanodiscs
ND CLF	Clofazimine loaded nanodiscs
ND CLQ	Chloroquine loaded nanodiscs
ND CPT	Camptothecin loaded nanodiscs
ND FLC	Fluorescein loaded nanodiscs

ND IND	Indomethacin loaded nanodiscs
ND NVB	Novobiocin loaded nanodiscs
ND OXM	Oxymethazoline loaded nanodiscs
ND RMD	Rimantadine loaded nanodiscs
ND TMX	Tamoxifen loaded nanodiscs
ND TRD	Thioridazine loaded nanodiscs
Ni	Nickel
nm	Nanometers
NMR	Nuclear magnetic resonance spectroscopy
NVB	Novobiocin
o/n	Overnight
OD	Optical density
OXM	Oxymethazoline
PAGE	Polyacrylamide gel electrophoresis
PB ₁₂₀₀ - <i>b</i> -PEO ₆₀₀	Poly(butadiene)- <i>b</i> -poly(ethylene oxide)
PB- <i>b</i> -PEO ND	Nanodiscs reconstituted with PB- <i>b</i> -PEO
PBS	Phosphate buffer saline
PE	Phosphoethanolamine
PEG	Poly(ethylene glycol)
PFA	Paraformaldehyde
POPC	1-palmitoyl-2-oleoyl- <i>sn</i> -glycero-3-phosphocholine

POPS	1-palmitoyl-2-oleoyl- <i>sn</i> -glycero-3-phospho-L-serine
QD	Quantum dots
RMD	Rimantadine
SAXS	Small-angle X-ray scattering
SDS	Sodium dodecyl sulfate
SEC	Size exclusion chromatography
SrtA	Sortase A
TB	Terrific Broth
TEMED	Tetramethylethylenediamine
TEV	Tobacco Etch Virus
TFA	Trifluoroacetic acid
TFE	2,2,2-Trifluoroethanol
TIRFM	Total internal reflection fluorescence microscopy
TMX	Tamoxifen
TRD	Thioridazine
Tris	Tris(hydroxymethyl)aminomethane
ULV	Unilamellar vesicles
UV	Ultraviolet

Contents

Acknowledgements.....	ii
Abstract.....	iii
Abbreviations.....	iv
Contents.....	ix
1 Chapter 1 - Introduction	1
1.1 The importance of nanotechnology.....	1
1.2 The field of nanomedicine.....	2
1.3 The principles behind self-assembled structures	3
1.4 Poorly water soluble (hydrophobic) drugs and their challenges	5
1.5 Self-assembled materials as nanocarriers for poorly water soluble drugs	6
1.5.1 Theranostic nanocarriers.....	8
1.5.2 Drug delivery systems	9
1.6 Nanodisc systems.....	15
1.6.1 Lipid discs – bicelles.....	16
1.6.2 HDL inspired discs	17
1.7 Outline of the project.....	24
2 Chapter 2 - Assembly and characterization of POPC nanodiscs	26
2.1 Introduction	26
2.2 MSP expression and purification	26
2.3 The reconstitution of POPC nanodisc assemblies	30
2.3.1 Original method of reconstitution.....	30
2.3.2 Improved method of reconstitution	31
2.3.3 Circular dichroism (CD)	33

2.4	Summary	34
3	Chapter 3 - Incorporation of poorly water soluble drugs into ND	36
3.1	The poorly water soluble small molecules	36
3.2	Finding the optimum approach for drug loading within ND	37
3.2.1	Nanodiscs loaded with amiodarone.....	41
3.2.2	Nanodiscs loaded with chlorambucil	52
3.2.3	Nanodiscs loaded with curcumin	54
3.2.4	Nanodiscs loaded with thioridazine	58
3.2.5	Nanodiscs loaded with novobiocin	60
3.2.6	Nanodiscs loaded with camptothecin	61
3.2.7	Nanodiscs loaded with tamoxifen	62
3.2.8	Nanodiscs loaded with clofazimine.....	63
3.2.9	Nanodiscs loaded with indomethacin	64
3.2.10	Nanodiscs loaded with fluorescein, chloroquine, oxymethazoline and rimantadine	65
3.3	Which drugs are incorporated?.....	68
3.4	SAXS investigation of drug loaded MLV and ULV	77
3.5	Summary	81
4	Chapter 4.....	83
4.1	Part I - Influence of lipid composition on drug incorporation	83
4.1.1	Introduction	83
4.1.2	Assemblies reconstituted with POPC: POPS	87
4.1.3	Assemblies reconstituted with 100% DLPC	91
4.1.4	Assemblies reconstituted with 100% DPPC	94
4.1.5	Assemblies reconstituted with POPC: DOPE PEG550	98
4.2	Part II – Influence of bilayer composition on ND reconstitution.....	103
4.2.1	Nanodiscs reconstituted with POPC: DOTAP	103

4.2.2	Nanodiscs reconstituted with block co-polymers	105
4.3	Summary	107
5	Chapter 5 - Modified nanodiscs for traceable cellular delivery	109
5.1	Introduction	109
5.2	Sortase A mediated modification of the MSP	109
5.3	The transport of labelled nanodiscs into mammalian cells	113
5.4	Summary	118
6	Chapter 6 - Conclusions and future work	119
6.1	Development of drug loaded ND systems	119
6.1.1	Changes in cargo composition	119
6.1.2	Changes in bilayer domain	120
6.2	Traceable delivery and release of drug	122
7	Chapter 7 - Experimental materials and methods	124
7.1	Instrumentation and materials	124
7.2	Buffer solutions and media	125
7.2.1	Bacterial growth media	125
7.2.2	Protein purification buffers	126
7.2.3	Buffers for SDS-Polyacrylamide gel electrophoresis (SDS-PAGE)	126
7.2.4	ND and ND-drug assembly buffer	126
7.2.5	SEC chromatography and release studies buffer	127
7.3	Methods	127
7.3.1	Purification of DNA	127
7.3.2	Protein overexpression, purification and analysis	127
7.3.3	The reconstitution of nanodisc assemblies	130
7.3.4	The reconstitution of ND with block co-polymers	132
7.3.5	The reconstitution of drug loaded nanodiscs assemblies	132

7.3.6	Analysis of MSP1D1 and of empty and drug loaded ND	133
7.3.7	The reconstitution of drug loaded MLV and ULV and their analysis by SAXS	139
7.3.8	Sortase mediated ligation of MSP1D1 with a fluorescent probe.....	140
8	Chapter 8 - Appendix.....	143
9	Chapter 9 - References.....	152

1 Chapter 1 - Introduction

In this introduction chapter, the broad category of self-assembled structures, with applications in nanomedicine, will be outlined. There are several excellent reviews summarising the emerging field of nanomedicine^{1, 2} and the vast pool of nanoscale systems engineered for its application. In the last decade, the huge potential benefits of these system' application in nanomedicine have attracted the interest of researchers,^{3, 4} leading to an increasingly fast and diversified progress of such research. With this in mind, a thorough review is difficult to attain and, more so, beyond the scope of this chapter. The following discussion will focus particularly on drug delivery systems, specifically designed and engineered for hydrophobic drugs. In addition, the lipid based discoidal systems, named nanodiscs, their design and emerging applications will be introduced.

1.1 The importance of nanotechnology

Nanotechnology is the branch of technology that involves the design, engineering and characterisation of man-made, novel materials by controlling their shape and size at the nanometer scale. Typically, this nanometer scale is described to be in the range of less than 100 nanometers.^{5, 6} The concepts of this technology stirred the interest of many researchers because the difference from macro scale to nanoscale might have an impact on the properties of materials. For example, the high surface area to mass ratio found in nanoscale materials could lead to their reactivity being enhanced.²

The concepts and ideas behind nanotechnology have been amongst us for some time. The possibility to examine and manipulate atoms and molecules individually was first mentioned by the 'father of nanotechnology', physicist Richard Feynman, in 1959. However, the development of nanotechnologies has only bloomed over the past decade as more innovative tools are being created in order to facilitate an accurate examination of small molecules. This ability to thoroughly understand and accurately tailor the fundamental properties of all materials - man-made or natural - at the nanoscale, will eventually impact all engineered materials, regardless of their applications. With the help of nanotechnology, many areas of research will greatly improve.

1.2 The field of nanomedicine

Over the recent years, advances in nanotechnology, materials science and biotechnology have come together to give rise to the state-of-the-art field of nanomedicine.⁷ Due to its key ability in using engineered nanostructures for diagnosis and treatment of disease, nanomedicine is considered a promising field in improving the quality of life. Advances in nanoparticle engineering, as well as the importance of nanoparticle characteristics such as size, shape and surface properties for biological interactions, are creating new opportunities for the development of nanomaterials for nanomedicine applications.

Nanomaterials used in medicine have numerous advantages such as controlling the biodistribution of drugs by changing the nanoparticle properties, enhancing the therapeutic index of the cargo drug resulting in a decrease in drug's toxicity and side effects or effectively escape removal by the reticuloendothelial system.^{8, 9} In addition, nanomaterials can systemically deliver hydrophobic compounds *via* active targeting specific cells with the help of highly selective ligands attached on to their surface, or passive targeting to sites through the enhanced permeability and retention effect (EPR).¹⁰ More so, the circulation half-life of nanoparticles could be extended by creating a stealth coating, thereby reinforcing this EPR effect to passively deliver drug molecules. Furthermore, upon delivery of drugs, the nanoparticles can use various mechanisms to release the cargo either slowly or under controlled conditions. For example, drug can diffuse out of the nanoparticle, drug can escape the carrier under swelling conditions (influenced by the rate of water diffusing in and the size of the cross-linked network which makes up the carrier), or it can be released as a response to an internal or external stimuli (such as temperature, pH or ionic strength).¹¹

In order to engineer new nanomaterials for such applications, the basic design principles and their formation have to be understood. Self-assembly can be used to create nanoparticles with multiple functionalities, the process of which will be outlined, in more detail, in the following section.

1.3 The principles behind self-assembled structures

Self-assembly can be defined as the spontaneous and reversible organisation of molecular units into thermodynamically stable and ordered structures through non-covalent interactions.¹² The weak nature of these interactions is responsible for the flexibility of the structure. Thus, self-assembly is the main strategy that biological systems use to build-up complex molecular assemblies. Many of these complex biological structures have evolved with the help of specific non-covalent interactions, such as hydrogen bonds and electrostatic interactions, which promoted the spontaneous organization between the components.

The self-assembly process starts when an entropic loss is balanced by an enthalpic gain. Hence, the ordered state forms as the system approaches equilibrium, reducing its free energy.¹³ For example, in the case of amphiphilic molecules - consisting of a hydrophilic head group and a hydrophobic tail - the unfavourable entropy is balanced by the presence of a driving force, which stimulates the spontaneous self-association of molecules. This driving force is the hydrophobic effect – the tendency of hydrophobic tails to exclude water molecules by self-aggregating and forming water free cores shielded by the hydrophilic head groups. As a result of this self-organisation, the tension, at the interface, between apolar tails and water is reduced.¹⁴ However, once the self-association of molecules has started, the molecules must arrange themselves into the most favourable structure. This favourable arrangement is determined by molecular geometry. In order to analyse the geometrical packing of the molecules, a dimensionless packing parameter is introduced. This parameter is determined by the optimum head group area, the volume of the tail and the maximum effective length to which the tail can extend to.

$$v_c/a_0 l_c$$

The dimensionless packing parameter; v_c is the volume of hydrocarbon chains, a_0 is the optimal head group area per molecule and l_c is the critical chain length – the maximum effective length to which they can extend

The aggregate of molecules will assemble into the most favourable shape, influenced by the packing parameter. For example, under the category of

amphiphilic molecules two types of molecules may be found: surfactants, which form micelles of different geometrical packing (spherical – packing parameter $< 1/3$, rod-like – cylindrical ($1/3 < \text{packing parameter} < 1/2$) or inverted hexagonal (packing parameter > 1) - and cubic) (Figure 1.1), and lipids (discussed in a later section - packing parameter ~ 1), that possess larger hydrophobic tails compared to their hydrophilic head group and, as such, form bilayer structures. These amphiphilic molecules are examples of self-assembled structures that follow a nucleated self-assembly process.

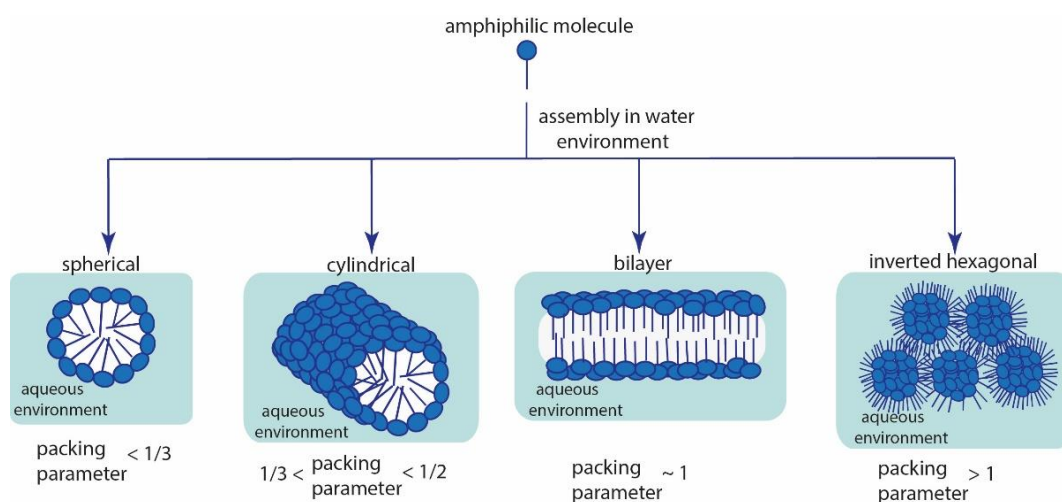


Figure 1.1 - Cartoon representation of surfactants assembly in water environment into micellar structures

In nucleated self-assembly, the average aggregate size in solution depends on the concentration of the substance in solution. This size distribution at equilibrium is entropically driven, meaning that, at low concentrations, the entropic dissociation is too strong to allow the formation of assemblies. As a result, the formation of the initial aggregates takes place only above a certain concentration, called critical micelle concentration, CMC. The system balances the loss of entropy by limiting the growth of the aggregates and by causing a vast distribution of sizes. Therefore, after reaching CMC, self-assembled aggregates and free amphiphilic molecules will coexist simultaneously in solution.

The molecular architecture of an amphiphilic molecule plays an important role in defining its CMC, in such that, the longer the hydrophobic tail of the molecule the smaller its CMC. Examples of these self-assembled molecules can be found

in nature, in abundance, as they are essential in creating a living, functional structure. Among the most significant self-assembly process found in biological systems is the formation of cellular membranes from phospholipids, the hydrophobic tails of which cluster together under the hydrophobic effect.

Taking inspiration from biological systems, self-assembly has become an important tool in designing and controlling the pattern organisation of building blocks. Quite possibly, using this fundamental process has enabled scientists to work towards a versatile solution with multiple functionalities. This is the case of drug delivery carriers, where research has bloomed in the past years, due to the way self-assembly has brought together efficient tools for creating and tailoring materials to suite specific needs.¹⁵⁻¹⁸ Advantages of such materials range from improved solubilisation and drug availability, to controlled drug release, reduced toxicity and prevention of uptake by the reticuloendothelial system. Whatever the enhancements these self-assembled nanomaterials bring to the cargo, which will be discussed in Section 1.5, firstly the challenges faced by poorly water soluble drugs need to be understood.

1.4 Poorly water soluble (hydrophobic) drugs and their challenges

The word 'hydrophobic' is derived from the Greek Hydro, meaning water, and Phobos, meaning fear. Hydrophobicity is the physical property of a nonpolar molecule to avoid a mass of water, predominantly due to the water-water hydrogen bonding being stronger than the intermolecular attraction between nonpolar molecules.^{19, 20} The degree of hydrophobicity is affected by how soluble the nonpolar molecule is in both immiscible phases, e.g. water and oil. This difference in solubility, at equilibrium, written as a ratio, is called the partition coefficient (P), commonly found as its logarithm (Log P).²¹

$$\log P_{\text{nonpolar solv/wat}} = \log \left(\frac{[\text{solute}]_{\text{nonpolar solv}}^{\text{un-ionized}}}{[\text{solute}]_{\text{water}}^{\text{un-ionized}}} \right)$$

Equation 1.1 Equation of the partition coefficient, written as its logarithm

Despite the fact that the hydrophobic small molecules used in our studies (discussed in Chapter 3) were first chosen based on a variety of Log P - from 3 to 8 – most of these molecules are charged at physiological pH, making the values for Log P unreliable. Therefore, the water solubility of these molecules was also taken into account. The water solubility of a drug is an important property that has high influence in the absorption and bioavailability of the drug. Poorly water soluble (hydrophobic) drugs tend to have a high toxicity because they are retained longer, have a wider distribution within the body and are challenging to formulate.²²

In recent years, the number of new drug candidates with poor water solubility has increased, reaching 70% of all drug discoveries.²³ In order to improve the poor solubility of drugs and minimise their side effects, researchers have employed particle technologies, varying from size reduction techniques to formulation of drug-cyclodextrin complexes and drug delivery systems *via* top-down (deconstructing large structures into small pieces, for a better understanding of the structure, such as milling) or bottom-up approaches (building molecule by molecule, such as self-assembly). These methods of enhancing drug solubility are very well highlighted in recent reviews.²⁴⁻²⁶ In the following subchapters, our focus will be on discussing nano-sized materials for the incorporation and delivery of poorly water soluble drugs, their advantages and limitations, as well as suggestions for improving these systems.

1.5 Self-assembled materials as nanocarriers for poorly water soluble drugs

In the last few decades, a new generation of nanomaterials (Figure 1.2) has been investigated for their potential applications in drug delivery and imaging.²⁷⁻³⁰ The rationale behind their investigation is that these materials have distinct functional and structural properties when scaled down in the nanometer range. For example, nanomaterials can transport high-dose therapeutic cargos as a result of their high surface area to volume ratio.

Another important aspect of these synthetic nanosystems is their biocompatibility. The uptake of these nanocarriers by undesired systems can

lead to toxic side effects. This problem can be prevented either by coating the surface of nanoparticles with a hydrophilic polymer, to protect them from opsonisation³¹ (adsorption of opsonin proteins on the surface of nanoparticles in order to be easily recognised by phagocytes), or by forming the nanoparticles from block co-polymers or lipids with hydrophilic and hydrophobic domains.

The size and shape of nanocarriers are also important factors in controlling the life time of nanoparticle systems. The size should be smaller than 500 nm to escape the fixed macrophages but larger than 8 nm to avoid rapid kidney clearance; the particle shape can have an effect on cellular internalisation and can also affect the transport and alignment of the particle once inside the cell.^{32, 33} For example, it has been shown that anisotropic particles, such as discs, can undergo cellular uptake at a much slower rate than isotropic particles (spheres).³⁴

The benefits of using these nanomaterials are enhanced by their increased solubility and *in vivo* stability, the possibility of being used in both active and passive targeting, and their contribution to simultaneously lessen the side effects of their cargo and improve its biocompatibility. Other advantages of using nanocarriers include prolonged circulation time, done by controlling their size and surface characteristics, enhanced intracellular penetration, and stimuli-sensitivity that allows nanocarriers to release the drug.³⁵ All these reasons are behind the belief that, with the help of nanomaterials, the area of nanomedicine will revolutionise the treatment of many diseases.

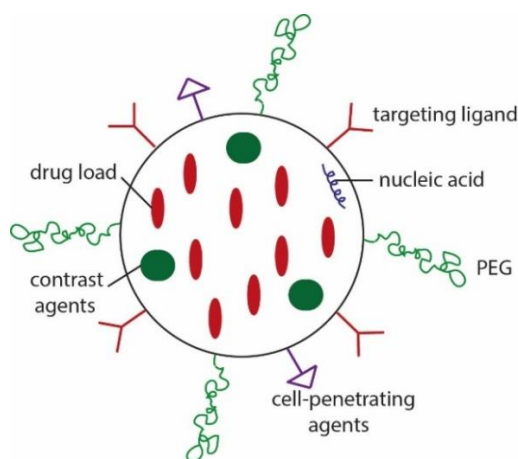


Figure 1.2 – Cartoon representation of multifunctional pharmaceutical nanocarrier

1.5.1 Theranostic nanocarriers

Theranostic nanocarriers are nanosystems designed as a biocompatible and biodegradable system for both imaging and therapeutic applications.³⁶ The components are strategically combined, due to their optical and structural functionalities, in order to create a nanosystem with enhanced delivery outcomes.

In order to provide a suitable platform, theranostic nanocarriers are ideally designed with characteristics which include selective accumulation in tumour, high loading and efficient release of drugs, imaging contrast and increased circulation lifetime. The resulting nanocarriers are, simultaneously, capable of diagnosis, drug delivery and monitoring of therapeutic response.

Several types of nanosystems have already been employed as theranostic nanocarriers, including gold nanocarriers,³⁷ polymer based nanocarriers,³⁸ quantum dots³⁹ and silica nanocarriers (Figure 1.3). For example, nanoparticles consisting of a hydrophobic Fe₃O₄ inner core grafted with poly (tert-butyl acrylate), and a mesoporous silica shell have been developed for bimodal imaging (magnetic resonance imaging/ near-infrared fluorescence) and the targeted delivery of paclitaxel.³⁹ The silica shell was modified with transferrin and near-infrared fluorescent dye. Their results successfully demonstrated that the paclitaxel loaded nanoparticles cluster selectively in tumour tissues, and exhibit a higher cell cytotoxicity than free drug.

Despite the growing interest of researchers in engineering various types of theranostic nanocarriers, there are still difficulties, which need to be addressed, in developing a biocompatible, highly specific tumour targeting nanosystem.

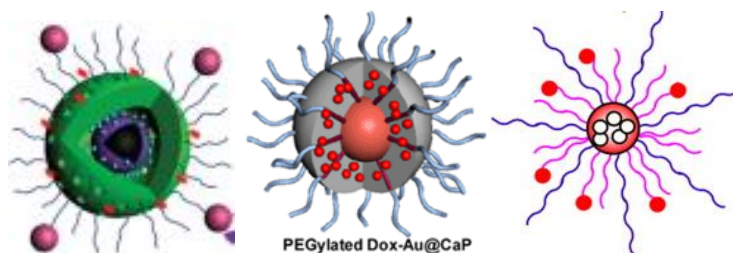


Figure 1.3 Schematic illustration of the self-assembly process of, from left to right, nanocarriers composed of Fe_3O_4 inner core with poly (tert-butyl acrylate) on the surface, and a mesoporous silica shell,³⁹ Doxorubicin incorporated into PEGylated gold nanoparticles, coated with a layer of calcium phosphate³⁷, Pluronic P105-doxorubicin conjugate (red) and Pluronic F127 (blue) micelles loaded with paclitaxel⁴⁰

1.5.2 Drug delivery systems

Self-assembled nanomaterials applied as drug delivery systems are nano-sized particles or systems that can be designed with different shapes and from a variety of materials including polymers (nanoparticles, micelles, or dendrimers), lipids (liposomes or solid lipid nanoparticles), viruses (viral nanoparticles), and hybrid structures. For example, polymer-based drug carriers may have the structure of capsules (nanoparticle shape), amphiphilic core/shell (micelle shape), or hyper-branched macromolecules (dendrimers); liposomes are colloidal structures composed of lipid bilayers and have a spherical shape; hybrid nanocarriers have a spherical structure, with an amphiphilic core/shell composed of hydrophobic polymer, lipid and hydrophilic polymer.

1.5.2.1 Amphiphilic block co-polymers nanocarriers

Over the past years, researchers have developed nano-encapsulation systems that can satisfy most of the required attributes. Self-assembled polymeric systems, composed of block co-polymers, have emerged as promising drug nanocarriers for the delivery of chemotherapeutic agents, due to their versatility. For instance, the chemical and physical properties of the polymeric structure could be easily adjusted just by selecting different monomers or polymerisation degrees.⁴¹

The structure of these amphiphilic micelles consists of a hydrophobic core and a hydrophilic shell (Figure 1.4). The hydrophobic part of the co-polymer non-

covalently associates, through hydrophobic interactions, with the hydrophobic drug, forming a tightly packed core. The hydrophilic part acts as a protective layer between the aqueous phase and the hydrophobic core and stabilises the system.

The incorporation of hydrophobic drugs into amphiphilic polymer nanocarriers can be done by several different methods (during the formation of nanocarriers, incubated with formed nanocarriers or chemically conjugated).⁴² However, the loading efficiency may be influenced significantly by them. For example, Shen *et al.* incorporated doxorubicin to light responsive spiropyran-poly (2-methacryloyloxyethyl phosphorylcholine) micelles by adding the drug to already formed micelles.⁴³ After removing the excess drug by dialysis, the drug loading content was determined to be 5.7%. The release profile of doxorubicin was established by diffusion of drug molecules from the nanocarriers, over a period of time. The study showed that only 20% of doxorubicin was released in 24 h, in the absence of UV irradiation. Whereas, the drug amount released increased to 50% when the micelles were UV irradiated, likely because the disassembly of micelles was photochemically triggered.

Another example of incorporating doxorubicin into a self-assembled system was developed by Zhai and his group.⁴⁴ In this study, drug carriers based on amphiphilic block co-polyphosphates with different hydrophobic block lengths were used. Doxorubicin was preloaded to the polymeric nanocarriers, suspended in dimethylformamide – added during the polymeric micelles formation. The solvent and free doxorubicin were subsequently removed by dialysis against phosphate buffer. The drug loading content was calculated to be up to 3.5 wt%, depending on the length of the hydrophobic block used. Apart from their established biocompatibility and biodegradability, these drug-loaded micelles have improved drug release behaviour with an initial burst release and a subsequent slower constant release. The release profile reached a maximum of 25% drug released, in 80 h, from the micelles assembled with the shortest block. In addition, the systems' toxicity, attributed to solvent residue, may be enhanced.

Furthermore, the drug loading efficiency was not only influenced by the incorporation method, but also by the balance of hydrophobic and hydrophilic parts within the amphiphilic polymer. In this case the polymer with the longest hydrophobic block had the highest incorporation efficiency. Similar results were also shown by Tran *et al.* for the incorporation of doxorubicin into polynorbornene-cholesterol/ poly(ethylene glycol) nanocarriers.⁴⁵

The long circulating time of co-polymer nanocarriers is considered an advantage for stably retaining the loaded drug molecules in the blood stream. However, the drug loading efficiency is greatly dependent on the compatibility between drug and polymer blocks and the balance between the hydrophobic and hydrophilic segments. More so, little is known about the interactions of polymeric nanocarriers with biological systems. Further investigation is required to overcome the above limitations of nanocarriers based on block co-polymers.

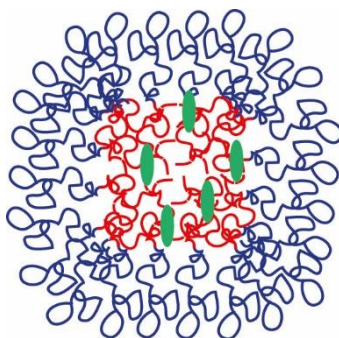


Figure 1.4 Cartoon representation of an amphiphilic block co-polymers nanocarrier; the hydrophilic polymer is represented in blue, the hydrophobic polymer, in red and the hydrophobic drug molecule, in green

1.5.2.2 *Virus-based carriers*

Virus based particles are the genome-free components of native viruses. The particles possess caged structures with a hollow interior, and consist of self-assembled virus protein subunits.⁴⁶ Due to their use, in nature, as containers for the delivery of molecules to specific cells and tissues, virus-like carriers have attracted the attention of many researchers, as potential vehicles for drug delivery.⁴⁷⁻⁴⁹

Virus like particles can be produced in living hosts, and therefore can provide three platforms - interior, exterior, and subunit interface – for genetic and chemical functionalisation. These features, along with their non-toxic biodegradability and precise shape and size, makes virus like carriers ideal for drug delivery. For instance, in their study, Zeng *et al.* showed that, after diffusion through the particles' pores, doxorubicin was entrapped into the cucumber mosaic virus particles by association with the native RNA.⁴⁸ After removing free drug *via* sucrose gradient centrifugation, the encapsulation efficiency of doxorubicin loaded in the particles was calculated at 14%. Virus like particles derived from plant viruses, such as cucumber mosaic virus⁴⁸ and cowpea mosaic virus⁵⁰, have been widely studied as cargo carriers for the delivery of drug molecules. However, their poor blood circulation limits their applicability.

Nanocarriers derived from animal viruses have also been researched as delivery vehicles because of their low immunogenicity and low toxicity. In literature, researchers have reported the encapsulation of paclitaxel, inside particles of adenovirus⁴⁹ or human JC polyomavirus,⁵¹ and their subsequent release in the target cells.

The multitude of encapsulation methods - coupling to the carrier in order to form a prodrug, loading *via* disulphide bonds, disassembly and reassembly of the carrier - and the relatively high encapsulation efficiency have proven virus like particles to be a suitable platform for drug entrapment. However, effective delivery of drugs depends also on other factors, such as the rate of cellular uptake or release kinetics. For example, Ren *et al.* has shown that, when compared to free doxorubicin, drug loaded virus like particles exhibited a similar or less effective cytotoxicity.⁵² In contrast, when same drug was covalently attached to cowpea mosaic virus, the complex showed enhanced cytotoxicity, despite a time-delayed drug release.⁵⁰ This inconsistent efficacy of drug encapsulation suggests that further investigation is required to find the optimum conditions.

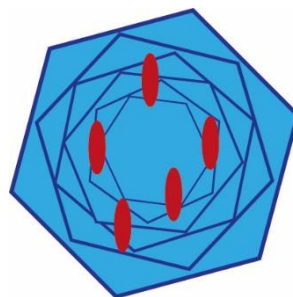


Figure 1.5 Cartoon representation of a drug loaded virus-like carrier

1.5.2.3 Lipid-based nanocarriers

Lipid based nanocarriers are biocompatible vesicles, with a closed bilayer structure surrounding an aqueous core (Figure 1.6). Over the past decades, lipid nanocarriers have been extensively used for the encapsulation of drug molecules - either inside the aqueous core or within the enclosed hydrophobic environment of the lipid bilayer – with the purpose of improving the drugs' pharmacokinetic profile and biodistribution.^{32, 53} Once inside, the nanocarrier protects the encapsulated drug molecules from external environment, avoiding degradation, improving the biodistribution and enhancing the drugs' efficiency. Furthermore, the membrane like environment of lipid nanocarriers can have a positive input on tasks such as delivery into cells. As a result of this intense study of lipids, a new class of therapeutics with improved drug delivery, and low cytotoxicity and immunogenicity, has already been developed into clinically approved products, such as Abelcet®, AmBisome®, and Visudyne®, for the delivery of amphotericin B and verteporfin.⁵⁴

The advantages of liposome nanocarriers rely upon its versatility when tailoring the physicochemical properties of the systems, regardless of the stage the formulation process is at. For example, bilayer thickness and phase transition temperature can be controlled by the length of the hydrocarbon chain. These properties can also be adjusted for improved drug release. For instance, the antiarrhythmic drug amiodarone showed prolonged release profile, lacking an initial burst, and high loading efficiency when encapsulated into lipid nanocapsules.¹⁷ However, despite its adaptability, tailoring the properties of liposomal carriers is not the only contributor to an enhanced efficiency of drug encapsulation. Drug properties, such as Log P or molecular weight, may be

important factors in determining the loading efficiency within the liposomal bilayer domain.

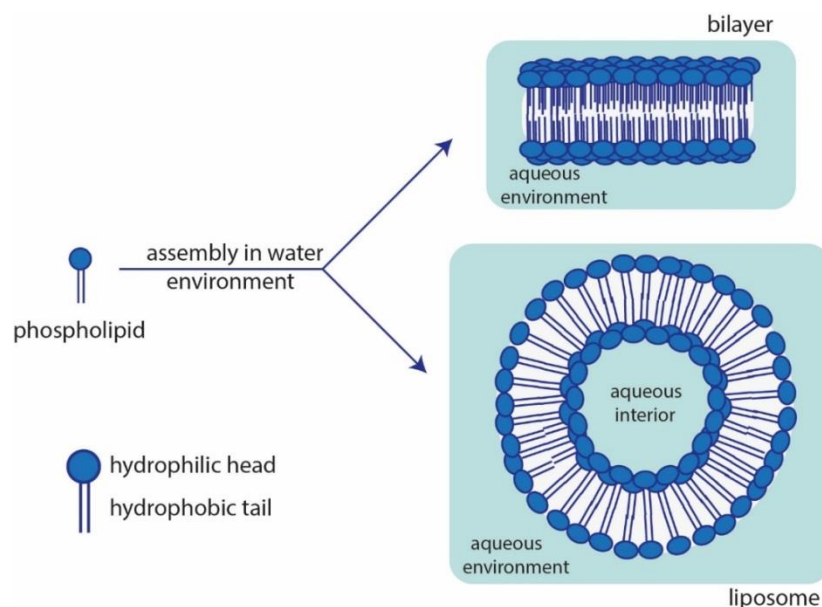


Figure 1.6 Cartoon representation of phospholipids assembling in water environment

1.5.2.4 Hybrid nanocarriers

Hybrid nanoparticles are core/shell structures which exhibit a combination of complimentary characteristics from both components, polymer and lipids.⁵⁵ The particles are typically composed of a hydrophobic polymeric core, surrounded by a shell, constituted from an inner lipid layer and an outer PEGylated lipid layer (Figure 1.7). Drug molecules can be encapsulated inside the polymeric core, while the shell acts as a protective layer, conferring biocompatibility to the sequestered molecules. The PEGylated outer layer functions as a ‘stealth’ coating, providing steric stabilisation and extending the circulation time of the complex.

Among the benefits of lipid-polymer hybrid nanoparticles the stability during storage, its high structural integrity and prolonged drug release due to the core/shell structure, are the most prominent.⁵⁶ Zhang *et al.* designed, in the late 2000s, a lipid-polymer hybrid nanoparticle system with tuneable size and surface charge, high drug loading yield, good cellular targeting ability and sustained drug release profile. These hybrid nanoparticles were formed from a

hydrophobic polymeric core, a hydrophilic polymeric shell and a lipid monolayer at the interface of the core and the shell.⁵⁷

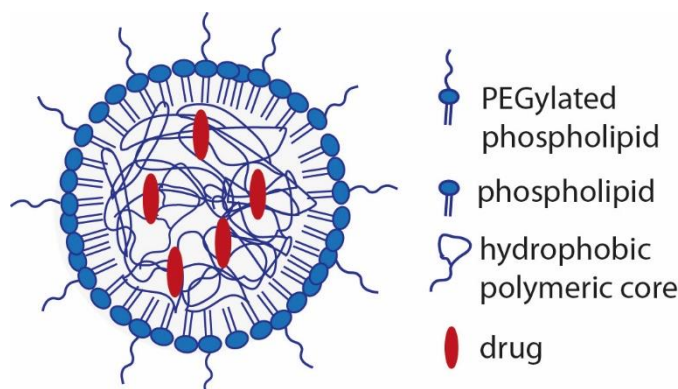


Figure 1.7 Cartoon representation of the lipid-polymer hybrid nanocarrier

The hybrid nanocarriers, however, may have limitations, such as wide size distribution, depending on the preparation method (nanoprecipitation or emulsification–solvent–evaporation). More so, despite their enhanced characteristics, the research of hybrid nanocarriers *in vivo* is still in its incipient stage.⁵⁸

Although nanoparticles offer many advantages as drug carriers, these systems still have many limitations such as content leakage and instability during storage, instability in circulation or poor bioavailability. In addition to the possible toxicity of nanoparticles, some of the materials used to constitute these systems may have toxic effects and therefore may not be viable for developing therapeutic products.⁵⁹ Furthermore, the distribution of nanocarriers within the body has to be understood, as well as their biodegradation and excretion routes. Last but not least, designing more efficient methods for the encapsulation of drugs coupled with activated release while tailoring the surface shape and stability of the nanosystem may become another barrier in developing these advanced drug delivery systems.

1.6 Nanodisc systems

Disc-shaped micelles are a group of amphiphilic structures that follow the self-assembly process. Because of their geometrical packing, phospholipids form the basic component for these nanostructures. Phospholipids are a class of

lipids that represent a major component of all cell membranes.⁶⁰ Due of their hydrophilic head and hydrophobic tail, when exposed to water, phospholipids tend to organize into a two-layered sheet with all of their tails pointing toward the center of the sheet (Figure 1.6). The center contains almost no water and excludes hydrophilic molecules, making them ideal for secluding hydrophobic small molecules. Most phospholipids contain a diglyceride, a phosphate group and a simple organic molecule such as choline (Figure 1.8).

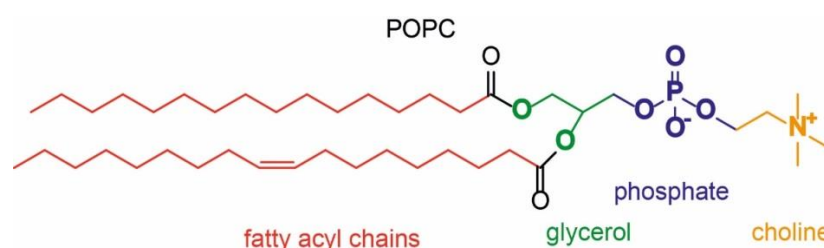


Figure 1.8 Structure of POPC (1-palmitoyl-2-oleoyl-*sn*-glycero-3-phosphocholine)

To stop these phospholipids from assembling into systems such as liposomes, a second component is introduced. This second component consists of either another phospholipid or a scaffold protein, adding to the formation of a versatile platform for investigating the dynamics and structure of amphiphilic molecules. The work described in the following subsections attempts to introduce these two self-assembled nanostructures, with similar shape, composition and applications, but distinct limitations.

1.6.1 Lipid discs – bicelles

One example of structures that adopts the disc-shape morphology are bicelles (Figure 1.9). Bicelles are generally composed of long-chain (12 to 18 carbons) and short-chain (6 to 8 carbons) phospholipids. The bilayer region is formed by the long-chain lipids and surrounded at the edge by the short-chain lipids, protecting the hydrocarbon tails from water molecules. Most commonly used phospholipids in the formation of bicelles are 1,2-dimyristoyl-*sn*-glycero-3-phosphocholine (DMPC) and 1, 2-diheptanoyl-*sn*-glycero-3-phosphocholine (DHPC).

The size of bicelles is controlled by the ratio between long-chain and short-chain lipids. If the ratio is over three, the bicelles are large and magnetically oriented.⁶¹

In addition, the bicelles have an adaptable morphology, characteristic with changes in lipid composition and temperature.⁶² More so, the long term stability of bicelles is limited by the hydrolysis of the ester bonds connecting the saturated chains and the headgroup, therefore it is strongly dependent of pH changes. One method to stabilise lipid bicelles discs is the addition of a PEGylated lipid. In a recent study, Liu *et al.* demonstrated that, by inclusion of PEGylated lipids along the edge of the bicelles, the structures are stabilised and the formation of multilamellar vesicles is inhibited.⁶³

Many recent studies have showed the advantages of using bicelles in NMR investigations of membrane proteins^{61, 64, 65} - due to their spontaneous self-orientation when exposed to a magnetic field – or in studies of partition, transport and delivery of hydrophobic drugs⁶⁶ – because the inside of bicelles is water free. However, their poor stability, pH, temperature and concentration dependence makes them ineffective in terms of providing an efficient controlled delivery system.⁶⁷

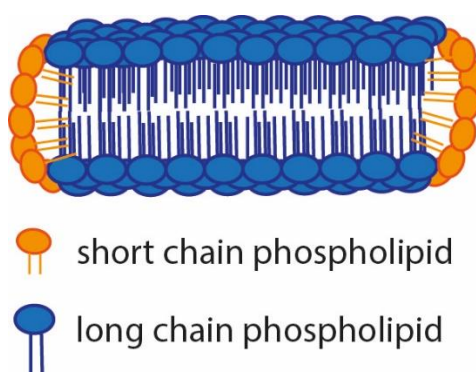


Figure 1.9 Cartoon representation of disc-shaped micelles (bicelles)

1.6.2 HDL inspired discs

Another example of disc-shaped amphiphilic nanostructures is the nanodisc (ND). As in the case of bicelles, the basic components that form the bulk of the disc-shaped bilayer are phospholipids. The second component added to the nanostructure is an amphipathic membrane scaffold protein (MSP) derived from Apolipoprotein A1 (ApoA-I), and lacking the globular N-terminal domain. ApoA-I is the predominant constituent of high density lipoproteins (HDL), which have an important role in reverse cholesterol transport⁶⁸ (Figure 1.10). The N-terminal helix 44–65 and the C-terminal helix 210–241 of ApoA-I have an affinity to

initially bind to the hydrocarbon chains of phospholipids whenever in their presence,⁶⁹ making this specific scaffold protein ideal for using as a protein belt. The helical conformation of ApoA-I promotes interactions between its hydrophobic face and phospholipids, while the hydrophilic side forms interactions with the aqueous phase. This amphipathic α -helices formation is driven by the 22-mer repeats identified in the structure of ApoA-I.⁷⁰

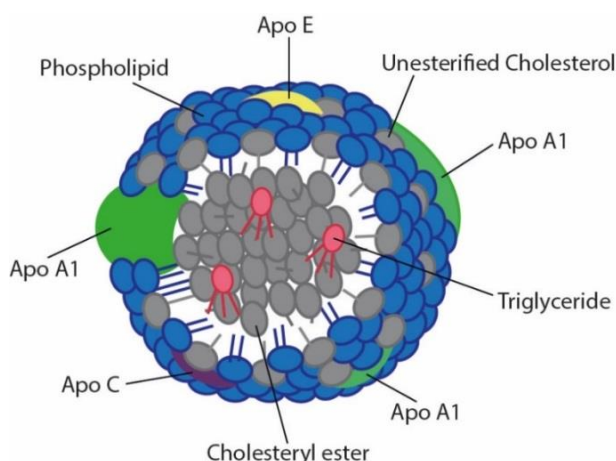


Figure 1.10 Cartoon representation of high density lipoproteins

Designed for the first time by Sligar's group,⁷¹ ND are nanoscale noncovalent assemblies whose hydrophobic edge of the phospholipid bilayer is stabilized by two or more copies of MSP, called the protein 'belt'. Their size ranges from 9.7 to 12 nm, depending on the scaffold protein used in the reconstitution. Therefore, the small size of nanodiscs is considered a major advantage.

One such model of a lipid/protein disc with a cylindrical lipid bilayer in the center and two helical protein molecules around the lipid is illustrated in Figure 1.11. Nanodiscs are relatively monodisperse, if a correct ratio of MSP to phospholipid is used. The scaffold protein interacts with the hydrophobic fatty acyl chains of phospholipids at the edge of the disk, conferring stability and, at the same time, water solubility to the ND.

ND are formed using a process that takes place when the detergent added to the self-assembling mixture, is removed, by dialysis or adsorption to hydrophobic beads. Simultaneously, the assembly process between MSP and phospholipids starts, arranging them into a discoidal bilayer. Their formation

process, along with design changes adapted for hydrophobic drug incorporation will be further discussed in the results chapters.

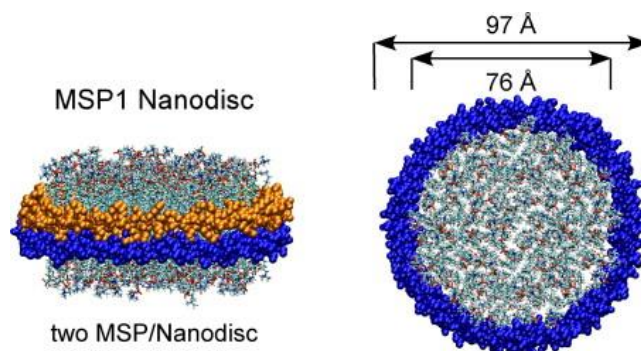


Figure 1.11 Bayburt's illustration of the ND structure based on theoretical simulations using coarse grain and whole-atom molecular dynamics and solution X-ray scattering⁷²

Subsequent to their design, optimum formulation and stability studies, the researchers have observed that the “native like” lipid bilayer portion of the ND provides an environment capable of solubilising and sequestering hydrophobic molecules.⁷³ Therefore, they can serve as ‘model membranes’ for characterising embedded proteins or as carriers for the delivery of drugs.

1.6.2.1 *Changes in ND structure*

The nanodisc system, earlier mentioned, was developed, in the early 2000s, in order to study the phase transition behaviour of the incorporated lipids. The membrane scaffold proteins first used were MSP1 and MSP2. The sequence of MSP1 contained 200 amino acids, designed with a histidine tag and a Factor X recognition site. MSP2 was a genetic fusion of two MSP1, using a glycine–threonine linker. To form the nanodiscs, each MSP was self-assembled with DPPC or POPC, in order to find the optimum conditions for the formation of homogeneous populations of nanodiscs.⁷¹ The phase behaviour of the nanodiscs demonstrated that the incorporated phospholipids retain the basic thermodynamic properties of a lipid bilayer. This behaviour resembled that of a cellular membrane and provided an excellent platform for studying insoluble membrane proteins in soluble systems,⁷⁴ such as cytochrome P450,⁷⁵ bacteriorhodopsin,⁷⁶ bacterial chemoreceptors⁷⁷ and G-protein coupled

receptors (GPC).⁷⁸ Examples of these nanodiscs systems will be further summarised.

The nanodisc system designed with MSP1 was further researched by Bayburt *et al.*, for the self-assembling of bacteriorhodopsin, as a model protein containing seven-transmembrane segments.⁷⁶ The result was found to provide a soluble and monodisperse structure. MSP1 was again used alongside POPC in the assembly of nanoscale phospholipid bilayer system with the purpose of incorporating the β (2)-adrenergic receptor; the first GPC receptor assembled into a nanodisc. The resulting compound allowed antagonists, agonists and G proteins to access the physiologically intracellular and extracellular faces of the receptor⁷⁹ (Figure 1.12).

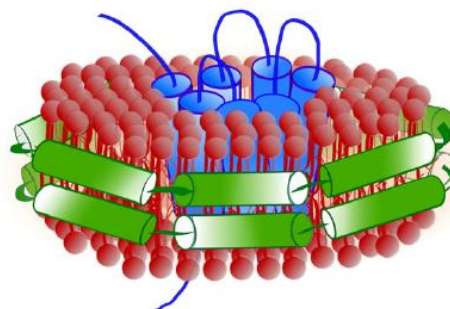


Figure 1.12 GPC receptor embedded in a nanodisc system⁷⁹

Following the design and production of the engineered scaffold proteins, Sligar's research group, in collaboration with Denisov, have demonstrated the influence of N-terminal residues in membrane scaffold protein and its overall length, in forming the nanodiscs and controlling their size.⁸⁰ Their study found that, for the formation of nanodiscs, the first 20-22 amino acids of the scaffold protein are not required. More so, the histidine tag engineered at the N-terminal is not involved in the self-assembly process between scaffold protein and phospholipids.

One of the newly generated scaffold protein was MSP1D1. This protein was obtained from MSP1 *via* the deletion of the first 11 N-terminal amino acids. One study in which MSP1D1 self-assembled with phospholipids to form ND was for the immobilisation of cytochrome P450.⁸¹ The protein embedded into the ND system was investigated by Nath *et al.* using single-molecule fluorescence

spectroscopy. By using total internal reflection fluorescence microscopy (TIRFM), fluorescence correlation spectroscopy (FCS) and Förster resonance energy transfer (FRET), they demonstrated that the developed ND system successfully immobilised single membrane proteins without covalent modification.

MSP1D2, derived from MSP1 *via* the removal of the first 22 N-terminal amino acids, was also used as scaffold protein in self-assembled ND, for a better understanding of the electron transfer between Nicotinamide adenine dinucleotide phosphate (NADPH) and cytochrome P450. The study involved the characterisation of cytochrome P450 reductase (CPR) embedded into ND.⁸² Using spectro-potentiometry, Das *et al.* researched the electrochemical behaviour of this reductase when in a membrane environment, and observed changes in the redox potentials of the di-flavin domains, which deliver electrons, towards more positive values. These changes led to the possible conclusion that the lipid environment of the ND affected the redox potential of the inserted CPR.

Other scaffold proteins were engineered from MSP1 *via* insertion of additional amphipathic helices into the core MSP sequence.⁸⁰ These extended proteins, called MSP1E1, MSP1E2, and MSP1E3, had one, two or three extra 22-mer amphipathic helices added to the central part of the MSP1 sequence, respectively. Literature reveals that these engineered MSP have been employed in studies of chemoreceptor transmembrane signalling,⁷⁷ catalytic activity of ATP-binding cassette transporters⁸³ or solubilisation of integral membrane proteins.⁸⁴

These ND systems, assembled with various ApoA1⁸⁵ or MSP of tailored lengths^{86, 87} were primarily reconstituted as model membranes to functionally and structurally characterise membrane proteins. However, the lipid environment of the ND could sequester an assortment of hydrophobic molecules. With this in mind, researchers have conducted preliminary studies of nanodisc complexes formulated with various types of hydrophobic drugs, in order to show their predilection for sequestering small hydrophobic drug molecules.

One such study was done by Nelson *et al.* to test the efficiency of incorporated amphotericin B, used as an antifungal drug.⁸⁸ The group designed a system based on nanodiscs-associated Amphotericin B (AMB), in the assembly of which recombinant human ApoA-I was used as the protein belt. In addition, they demonstrated the ND-drug systems' enhanced effects at a lower dosage frequency, produced by a possible altered clearance time. The group also observed no significant differences in the cytokine response assayed between AMB-ND treatment groups and those treated with phosphate buffer or empty ND.

Another example of complex based on integrating all-*trans* retinoic acid (ATRA) into a nanodisc assembled with recombinant human ApoA-I was developed by Redmond *et al.*⁷³ Their purpose was to design a potentially useful vehicle for solubilisation and *in vivo* delivery of ATRA. The resulted system effectively induced apoptosis in cultured hepato-carcinoma cells. Their group demonstrated that the properties of ATRA were unaffected and its bioavailability was enhanced by incorporation into ND compared to free ATRA. Similar results have been shown by Buehler *et al.* The group developed a drug delivery system using a vault-binding lipoprotein complex that formed a lipid bilayer nanodisc. The resulted engineered vaults loaded with ATRA showed enhanced cytotoxicity against the hepatocellular carcinoma cell line HepG2.⁸⁹

The multitude of engineered ApoA-I and MSP found in literature and mentioned above, had the initial purpose of optimising and creating monodisperse, stable ND assemblies. This was done for a better, subsequent usage in characterising integral membrane proteins. The protein belt only interacts with the hydrophobic edge of the lipid bilayer. The stable model membrane, thus created, is the main interactor with the embedded molecule to be characterised.

ND systems have been assembled with various phospholipid compositions. Initially, this was investigated following concerns regarding which lipids facilitate the formation of stable, monodisperse ND.^{71, 86} However, later studies have investigated different lipid compositions, depending on the incorporated system that required characterisation. For example, DPPC and DMPC, lipids with high transition temperature, were used in providing an understanding of the phase

transitions lipids are susceptible to, when assembled in a nanoscale, enclosed structure.⁹⁰ In other studies, anionic lipids were used in the formulation of ND, either for the characterisation of clotting proteins, which have affinity towards assembly in membranes rich in anionic lipids,⁹¹ or to determine the redox potential of cytochrome P450.⁸²

These nanoscale structures because of their disc-shaped structure, with a lipid bilayer surrounded by a protein belt have advantages over liposomes in terms of smaller size, increased stability due to the protein belt. In addition, nanodiscs can be prepared with controlled size and stoichiometry and have access to both sides of the phospholipid bilayer domain. Thus the nanodisc system provides an innovative platform for understanding membrane protein functions as well as creating a water-free environment for targeted delivery of various hydrophobic agents protecting the inside content during circulation in the body. They have promising affinities for surface modifications such as polymer coating to prolong circulation half-life or functionalization with ligands to achieve targeting to specific cells or tissues. Furthermore, the ND systems promise substantially fewer side effects than current drugs, while enhancing efficacy and are expected to bring an improvement in patient life quality.

1.7 Outline of the project

The research of the project was aimed at investigating the encapsulation and release kinetics of poorly water soluble drugs from self-assembled nanosystems. As discussed in the previous section, researchers have already shown the potential of nanodiscs in providing a membrane like environment for incorporating membrane proteins, or even hydrophobic small molecules. However, the need for a simple approach to systematically study the relation between physical parameters related to loading and release of poorly water soluble drugs from ND systems, still exists.

The main objective of the project was to formulate an optimised ND system for further incorporating and releasing a range of hydrophobic small molecules, with the aim of finding common criteria for creating an effective nanosystem for delivery into mammalian cells. Hydrophobic drug molecules tend to be superficially characterised when incorporated into a delivery system, as the primary focus usually turns towards the systems' performance in cellular uptake compared to free drug. Therefore, after the initial optimisation of ND assembly, the research was focused on investigating a combination of strategies for incorporating twelve hydrophobic drugs (Figure 1.13). For the nanodiscs reconstitution, two strategies have been studied, the first comprises of adding the MSP to a mixture of lipid and detergent micelles, and second strategy involves adding MSP stabilised in Na cholate micelles to a dried lipid film. Loading the drug molecules into the ND systems was studied by using two strategies, the drugs were added either passively, under overnight shaking conditions, to a solution of ND (post-incorporation), or by loading the drug during the reconstitution of ND (pre-incorporation). In Chapter 3 is discussed the work conducted for reaching this goal.

The second objective was to vary the lipid composition within the ND, and observe the efficiency of incorporating and releasing two of the selected drugs. Charged lipids, small chain lipids, PEGylated lipids and lipids with high transition temperature were investigated for the reconstitution of empty and drug loaded ND. Subsequent drug loading capacity and release kinetics were also studied.

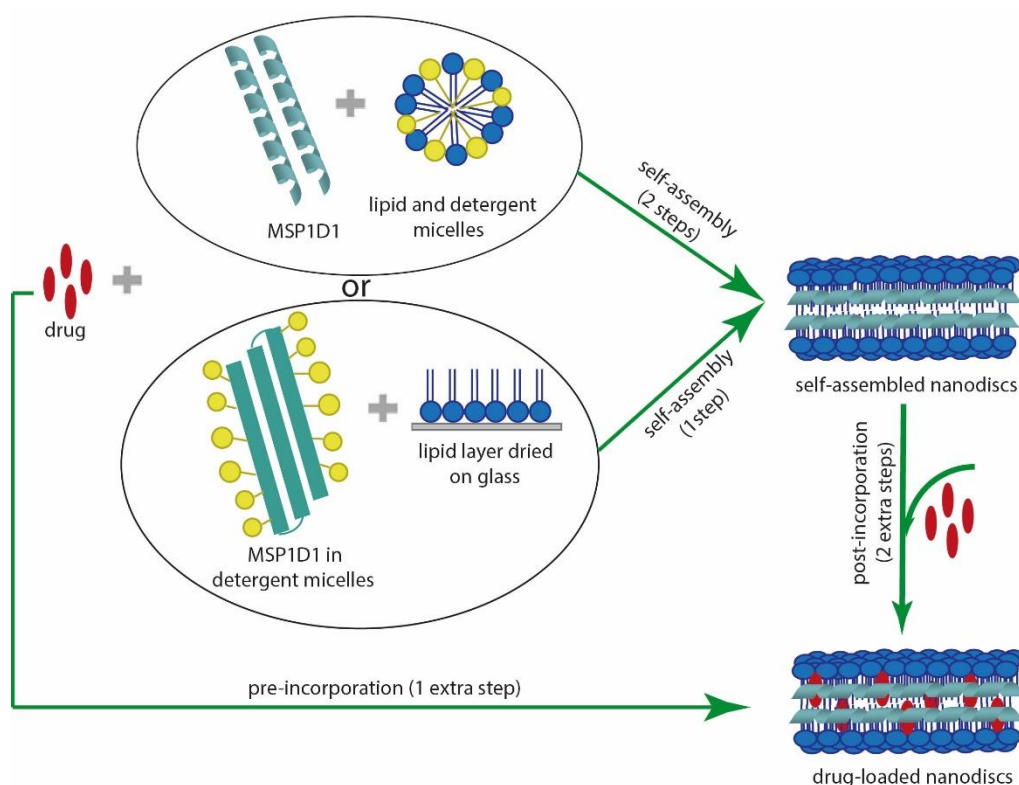


Figure 1.13 Incorporation of hydrophobic small molecules into ND systems

The final objective was to site-specifically modify the scaffold protein for *in vitro* imaging during cell studies, by using the Sortase A mediated ligation (Figure 1.14). The labelling of MSP while in the ND formation and the presence of incorporated drug molecules were investigated. Subsequent delivery of the fluorescein modified ND-drug system into mammalian cells was studied.

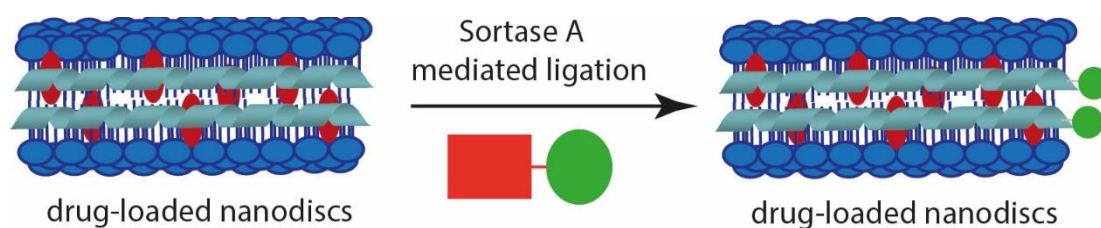


Figure 1.14 Strategy for modifying the ND systems with fluorescein using Sortase A mediated ligation; the labelling process has been done also on empty ND

2 Chapter 2 - Assembly and characterisation of POPC nanodiscs

2.1 Introduction

Due to their geometrical packing, phospholipids form the basic component of the amphiphilic structures investigated. Previous studies⁷¹ have identified POPC, a zwitterionic phospholipid (Figure 2.1), as a suitable building block for creating nanodisc assemblies, therefore POPC was utilised in initial efforts to reconstitute the nanoscale structures. In order to stop phospholipids from assembling into liposomes, MSP1D1, an amphipathic membrane scaffold protein, was introduced as a second component. This scaffold protein was derived from MSP1 by removing the first eleven N-terminal amino acids. This chapter describes the development of such nanoscale assemblies using SDS-PAGE electrophoresis, size exclusion chromatography (SEC), dynamic light scattering (DLS) and circular dichroism (CD).

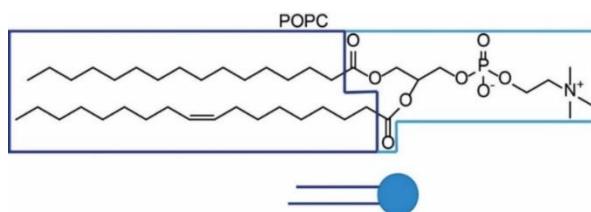


Figure 2.1 The structure of POPC

2.2 MSP expression and purification

The first step in formulating ND assemblies was to produce the protein. The pMSP1D1 plasmid was purchased in DH5 α strain and following inoculation, this was transformed into *E. coli* cells. The His₆ tagged MSP protein was expressed in TB (Terrific Broth) using *E. coli* cells (Figure 8.1, Figure 8.2). The scaffold protein expressed in TB medium followed the method of Sligar *et al.*⁷¹ This consisted of inducing the cells with IPTG when an OD₆₀₀ of 2.5 was reached and reducing the temperature of the incubation from 37 °C to 28 °C after induction.

After protein expression, the cells were harvested and lysed. The scaffold protein released in the supernatant was purified on a Ni column at 4 °C. The histidine residues in the His₆ tag of MSP binds to nickel ions on the resin, thus

enabling separation from impurities and other proteins expressed alongside MSP1D1. For better solubilisation of MSP, sodium cholate (40 mM) was added in the elution buffer.

Above its CMC of 14 mM, the cholate detergent forms micelles, which act as a protective coating for the scaffold protein (Figure 2.2). In an aqueous environment, this coating is formed by the hydrophobic tail of sodium cholate, which undergo hydrophobic interactions with the exposed amino acids of MSP1D1, and the hydrophilic head group of the detergent forms hydrogen bonds with the water molecules.

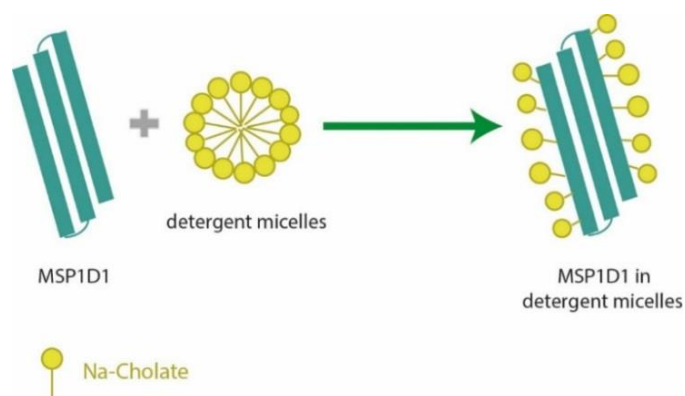


Figure 2.2 Cartoon representation of the sodium cholate micelles forming a protective coating for MSP

The investigation of MSP1D1 was conducted by SDS-PAGE electrophoresis and MS (mass spectroscopy) with the purpose of confirming its expression and purity. However, these techniques are using conditions which lead to the denaturing of the analysed protein, and therefore are causing the MSP to unfold to its monomeric structure. As a result, it is difficult to determine if the protein has an oligomeric structure after being isolated from the Ni column. Therefore, other techniques – SEC and DLS – were also adopted as methods of characterisation to confirm the size of the purified MSP.

The MSP1D1 was further purified by SEC. A set of calibrants with different molecular weights (MW), which can be found in Chapter 7, were run through the column. The analysis helped identify the oligomeric and monomeric states from exceedingly aggregated protein, and estimate their apparent mass.

Following purification by SEC, DLS was used to confirm the size of MSP in solution.

SDS-PAGE electrophoresis was performed to test the expression and purity of the MSP. When compared with the protein standards showed in lane 1, the MSP migrated on the SDS-PAGE gel to around 25 kDa, confirming its expected mass of 24.6 kDa. The SDS-PAGE gel of the expressed MSP during (lanes 2 to 5) and after the purification process at 4 °C (lanes 6 and 7) indicated that the MSP was well expressed in TB medium (Figure 2.3). This can be attributed to the use of a controlled promoter for induction (0.1 mM IPTG), which drove the expression of MSP. Additionally, it is presumed that lowering the temperature after induction, from 37 °C to 28 °C, may facilitate the correct folding of the protein. The SDS-PAGE gel also indicated negligible MSP loss during the purification process (lanes 2-5). The purity of MSP1D1 expressed by *E. coli* was evaluated and confirmed by mass spectroscopy (MS) (Figure 2.3). The protein mass calculated from the measurements was 24,663 Da (expected MW = 24,662 Da).

The analysis by SEC of MSP, overexpressed in TB medium, confirmed the absence of large aggregates, which might interfere with nanodiscs formation. However, protein oligomers, with an apparent MW of 175 kDa and 80 kDa, can be observed in Figure 2.4, A. These oligomers were probably formed due to most scaffold protein in solution consisting of heterogeneous agglomerates. MSP1D1 is derived from ApoA-I, therefore a reason behind the formation of these oligomers could be due to the temperature dependent self-association property ApoA-I possesses.⁹²

Unfiltered samples of pure MSP collected in fractions eluted between 12 mL and 19 mL after the SEC analysis, were characterised by size distribution using DLS. The results showed formation of pure oligomer scaffold protein with a diameter of around 2 nm and a population of heterogeneous aggregates with a diameter of 6.5 nm (Figure 2.4, B).

The overexpression of protein was performed in two media with the aim of optimising and increasing the protein yield. MSP1D1 was also overexpressed

in Auto Induction media (AIM), however in this instance low levels of scaffold protein, in its monomeric state, were present after expression and purification. Comparing results obtained *via* SDS-PAGE and SEC, it could be deduced that the optimum conditions were decreasing the temperature during the purification process. This was done to avoid aggregation of the MSP. In addition, TB medium had a better yield in expressing MSP1D1 - which has a tendency to oligomerise – and therefore, was chosen to continue the production of protein in bacteria.

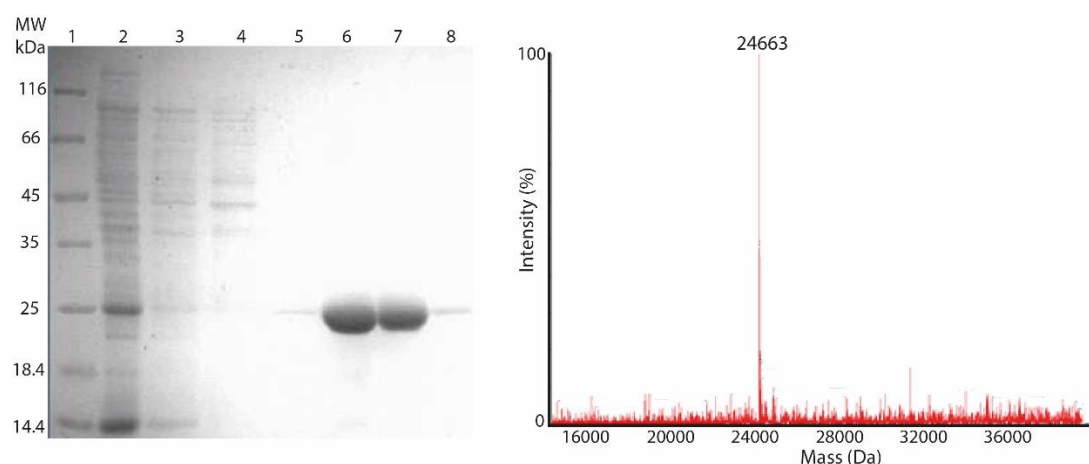


Figure 2.3 12% SDS PAGE of MSP purified on Ni column: 1 - Marker; 2 – Flow through; 3 – 1st wash; 4 – 2nd wash; 5 – 3rd wash; 6 – 8: eluted MSP with sodium cholate; Mass spectrum of monomeric MSP in acid after SEC analysis; MW of 24,663 Da (expected MW = 24,662 Da)

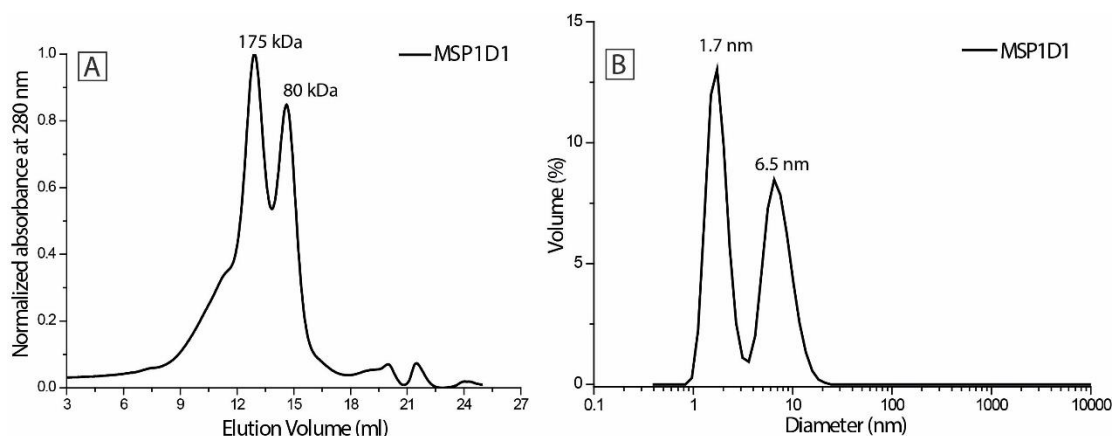


Figure 2.4 A - SEC chromatogram and B - DLS of pure MSP in elution buffer

2.3 The reconstitution of POPC nanodisc assemblies

2.3.1 Original method of reconstitution

Nanodiscs are formed following Sligar *et al.* method of reconstitution - named method A (Chapter 7), as schematically shown in Figure 2.5. The scaffold protein is added to a mixture of lipid and detergent micelles. Subsequently, the detergent is removed by adsorption to hydrophobic bio-beads (adsorbent beads composed of a large number of cross-linked microspheres used for adsorbing molecules from aqueous solutions). Simultaneously the self-assembly, *via* H bonding and hydrophobic interactions, between MSP and POPC starts, arranging them into a disc-shaped nanostructure.

In order to reconstitute monodisperse ND with an exact molar ratio of MSP to POPC, an accurate concentration of both constituents was determined. The pure MSP concentration was calculated using the absorbance measured at 280 nm and it was found to be between 1 and 3.2 mg/mL. Assay of total phosphorus was used to estimate the total amount of phospholipids to be added in the assembly process of ND (Chapter 7). The calculated concentrations were further used to reconstitute ND assemblies.

The subsequent SEC analysis of ND showed no void volume peak except for a trace with the same retention time as Alcohol dehydrogenase, used as a MW standard for column calibration (Figure 2.6). The ND was found to have an apparent MW of 150 kDa.

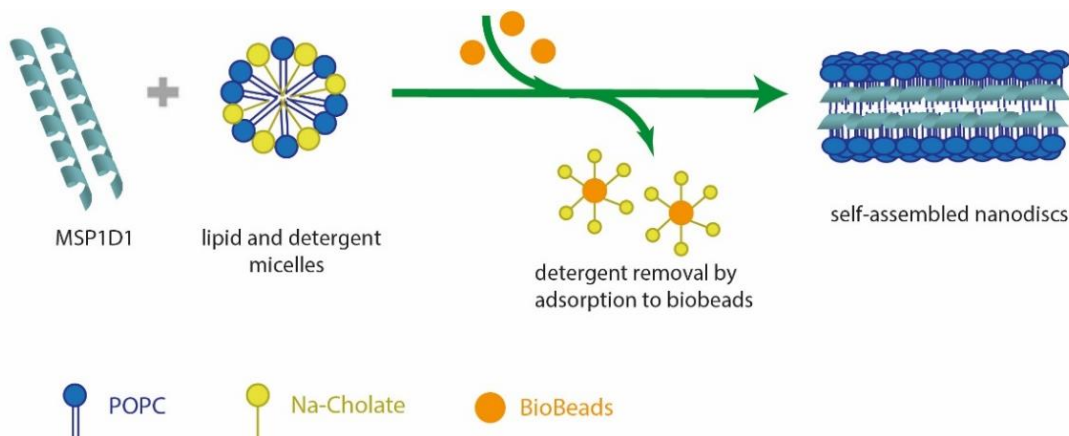


Figure 2.5 Schematic representation of the POPC ND reconstitution process based on the method developed by Sligar (method A)

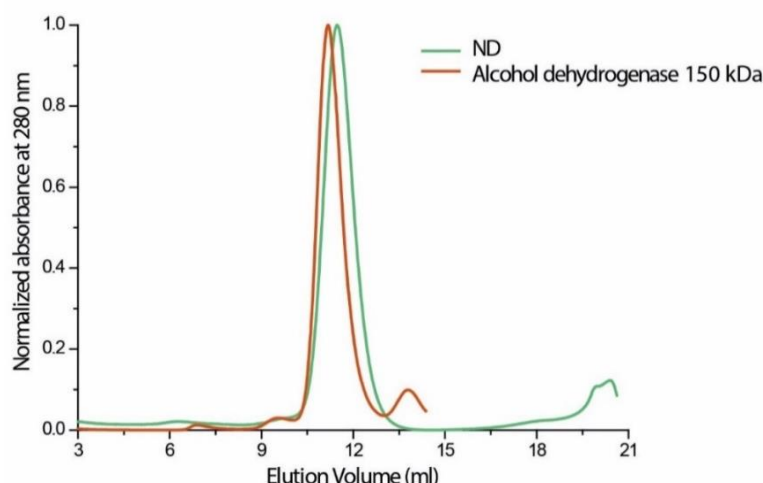


Figure 2.6 SEC chromatogram of ND assemblies; the assembly has approximately the same retention time as Alcohol dehydrogenase (AD) indicating an apparent MW of 150 kDa

2.3.2 Improved method of reconstitution

Nanodiscs were reconstituted successfully by initially following Sligar's method of assembly. However, occasional increase in room temperature affected the formation of POPC and detergent micelles, thus altering the formation of monodisperse ND. To avoid such situations an adapted method – method B – was employed. Because detergent, at a concentration above its CMC, was already present in the pure MSP solution (for stability purposes), in this new method one step of the reconstitution was avoided. Instead of mixing MSP to already formed POPC and detergent micelles, MSP stabilised in Na cholate micelles was added to a dried POPC film (Figure 2.7). Subsequently, upon addition of bio-beads and removal of cholate detergent, the self-assembly between MSP and POPC started, arranging them in a disc-shaped bilayer.

The analysis by SEC of newly reconstituted ND was carried out to check the formation of ND assemblies and to dismiss the development of other aggregates. Previous SEC experiments of the scaffold protein had suggested the formation of oligomeric forms of the protein in solution. However, when the MSP in detergent micelles is added to the POPC layer, it arranges as a protein belt around the hydrophobic edge of the POPC bilayer, and together they assemble into ND structures (Figure 2.8). ND were found to have the same elution volume as Alcohol dehydrogenase, suggesting an apparent MW of

approximately 150 kDa (138 kDa, apparent mass calculated with the equation generated by the calibration curve found in Chapter 7) (Figure 2.9). The apparent size and diameter of 10 nm (Figure 2.10), as expected from previous studies⁸⁰ is associated with two or more MSP and 126 lipids per nanodisc. Lipid concentration in these samples was measured using a total phosphorus assay.

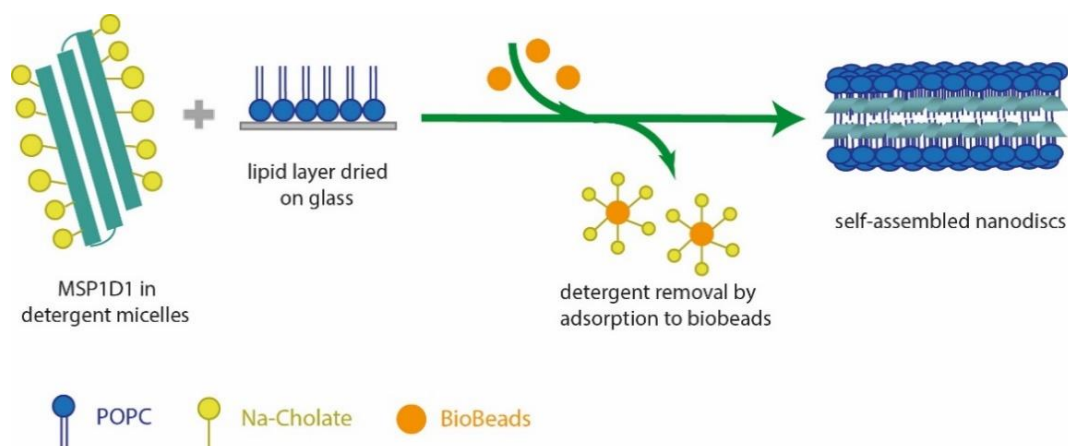


Figure 2.7 Schematic representation of the POPC ND reconstitution process using the shorter assembly protocol (method B)

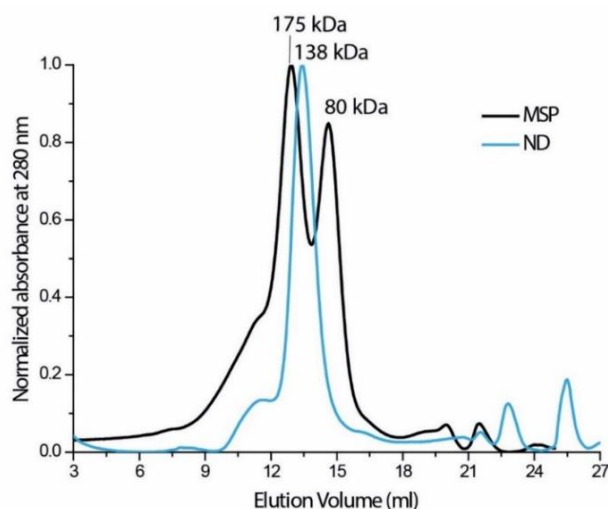


Figure 2.8 SEC chromatograms of ND sample in 20 mM Tris, 0.1 M NaCl and MSP in elution buffer

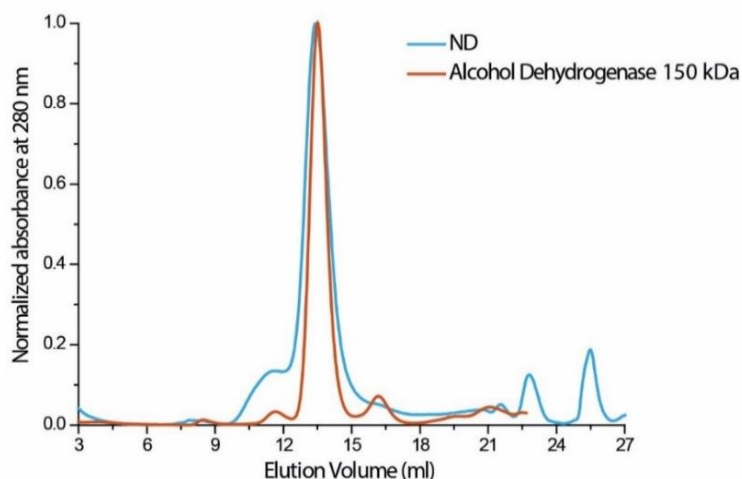


Figure 2.9 SEC chromatogram of ND reconstituted using method B; the assembly has the same retention time as AD

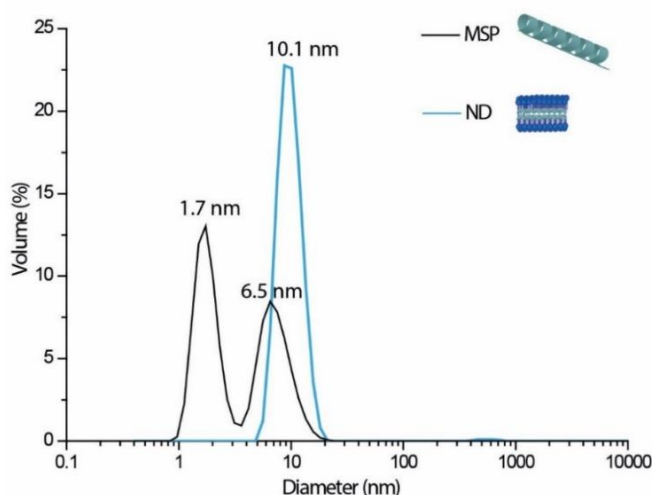


Figure 2.10 DLS measurements of MSP in elution buffer and reconstituted ND using method B

2.3.3 Circular dichroism (CD)

CD spectroscopy was used to observe how the secondary structure of the scaffold protein changes when interacting with other molecules such as lipids. The CD measurements were conducted by Mr. Nasir Khan on an APP Chriscan CD spectropolarimeter, part of the Astbury Centre for Structural Molecular Biology facilities.

The secondary structure of the scaffold protein alone and when in the presence of POPC was investigated. In Figure 2.11, the negative peaks at 210 nm and 225 nm⁹³ and the positive peak at 195 nm specific to α helix conformation⁹⁴ are present in the ND system. Furthermore, a prominent increase in peak intensity

detected for all three peaks (195 nm, 210 nm and 225 nm) demonstrated an increase in α helix content from MSP alone to ND assemblies. This rise is probably caused by lipid-protein interactions within the ND, as the lipid free scaffold protein consists mostly of heterogeneous aggregates⁹⁵.

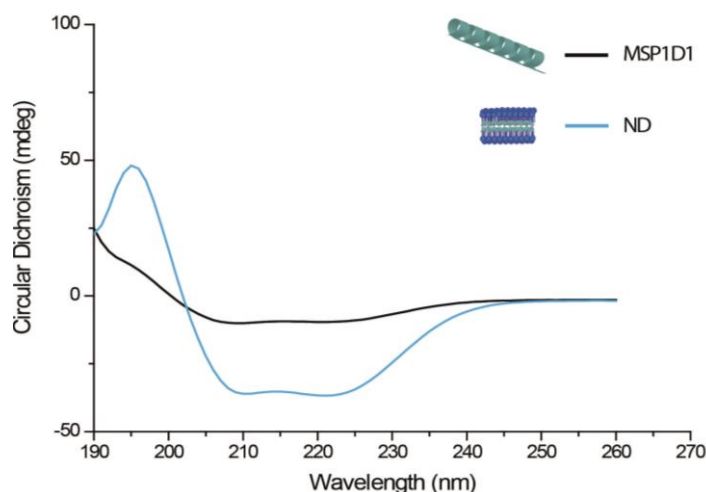


Figure 2.11 Circular dichroism of MSP in elution buffer and ND; the peaks specific to α helix conformation are at 195 nm, 210 nm and 225 nm

2.4 Summary

MSP was expressed in AIM and TB media and purified at room temperature and 4 °C with the purpose of finding the optimum environment for protein production. Decreasing the temperature during purification process was the key factor in avoiding MSP aggregation. Nevertheless, TB medium had a better yield in expressing the insoluble protein and was further chosen to continue protein overexpression in *E. coli* cells. Protein overexpression and purity were confirmed by SDS-PAGE electrophoresis and MS analysis. The presence of oligomeric structures and their size were observed by SEC and DLS techniques.

Following MSP overexpression and purification, the ND assemblies were reconstituted. The protocol for ND assembly was adapted to add pure MSP stabilized in Na cholate micelles to a layer of POPC. The ND thus reconstituted were found to have an apparent molecular weight of approximately 150 kDa, which was associated with two or more MSP and 126 lipids per nanodisc.

A combination of SEC and DLS used to characterise the ND assemblies has demonstrated the influence of MSP aggregation on the reconstitution and MW of the ND. CD measurements have shown changes in α helix content of the scaffold protein during formation of protein belt around the phospholipid bilayer.

3 Chapter 3 - Incorporation of poorly water soluble drugs into ND

Poorly water-soluble (hydrophobic) drugs tend to have high toxicity, wider distribution within the body and are often extensively metabolised.²² These side effects can be minimised by using self-assembled nanocarriers to transport such hydrophobic drugs. This can protect the cargo during circulation, enhance the drugs' bioavailability and decrease the side effects that unincorporated drugs inherently possess.

The nanoscale size and particle geometry of the previously reconstituted stable ND may provide a suitable environment for targeted delivery of poorly water-soluble molecules. However, as shown in Chapter 1, little is known about the capacity of these ND assemblies to load and release hydrophobic small molecules. In order to show their function as drug carrier, a series of hydrophobic drugs were incorporated into ND. This chapter will discuss the loading, release and interactions between the drug molecules and the phospholipid domain of the ND.

3.1 The poorly water soluble small molecules

The hydrophobic molecules studied for loading and release from ND assemblies vary from high to low hydrophobicity, have planar or bulky structures, different physicochemical properties and pharmacology indications (Tables 3.8 to 3.12).

It was hypothesised that all the selected hydrophobic drug molecules have favourable properties for loading into ND and therefore were investigated to generate design rules for drug loading into ND and the optimum conditions for incorporation and release from the self-assembled nanostructures. Firstly, different methods for reconstituting drug loaded ND were investigated, in order to find the optimum approach. If the incorporation was successful and the best route for reconstituting loaded ND was chosen, then the question concerning how many molecules were incorporated per ND would arise. To assess the drug load per ND, three methods of characterisation were selected. The drug molecules could then be separated into groups based on their loading

capability. Once the drug incorporation was optimised and calculated, the rate of drug release from ND and the interactions between drug molecules and the phospholipid bilayer were investigated.

3.2 Finding the optimum approach for drug loading within ND

The optimum approach for loading the hydrophobic drugs into ND was found by investigating four routes: two methods of reconstituting ND assemblies were used, and for each method, the drug was incorporated *via* two pathways. In the previous chapter we have demonstrated the successful reconstitution of monodisperse ND using 1:65 as the molar ratio between MSP and POPC. However, in these experiments, other molar ratios were also used, 1:50 and 1:30, in order to accurately determine the optimum incorporation conditions.

One method of reconstituting ND was achieved by following Sligar's method of assembly - method A. This has been shown in a number of studies to be an efficient drug carrier for loading hydrophobic small molecules.^{88, 96} However, with the aim of decreasing the formulating steps and overall time and due to occasional increases in room temperature affected the formation of POPC and detergent micelles, the adapted method - method B - was employed.

Method 1 of incorporating drug molecules into ND – postloading

Initially, to incorporate the hydrophobic molecules within the reconstituted ND, the drugs were added passively, under overnight shaking conditions, to a solution of stable ND assemblies (Figure 3.1 and Figure 3.2). This method of incorporation will be referred to as postloading or post-incorporation method. Studies conducted by Luo *et al.*⁹⁷ and Song *et al.*⁹⁸ showed successful passive drug encapsulation into carrier systems, such as co-polymer micelles and lipid-based nanospheres, and release of camptothecin and chlorambucil, respectively.

As a starting point, ND were reconstituted before attempting to incorporate the hydrophobic drugs. For this, either method A or method B of reconstitution was employed. To the solution of reconstituted ND, the drugs, in power form, were

added and left overnight at 4 °C, with gentle shaking. The unincorporated drug was then eliminated by centrifugation or, more efficiently, by SEC partition.

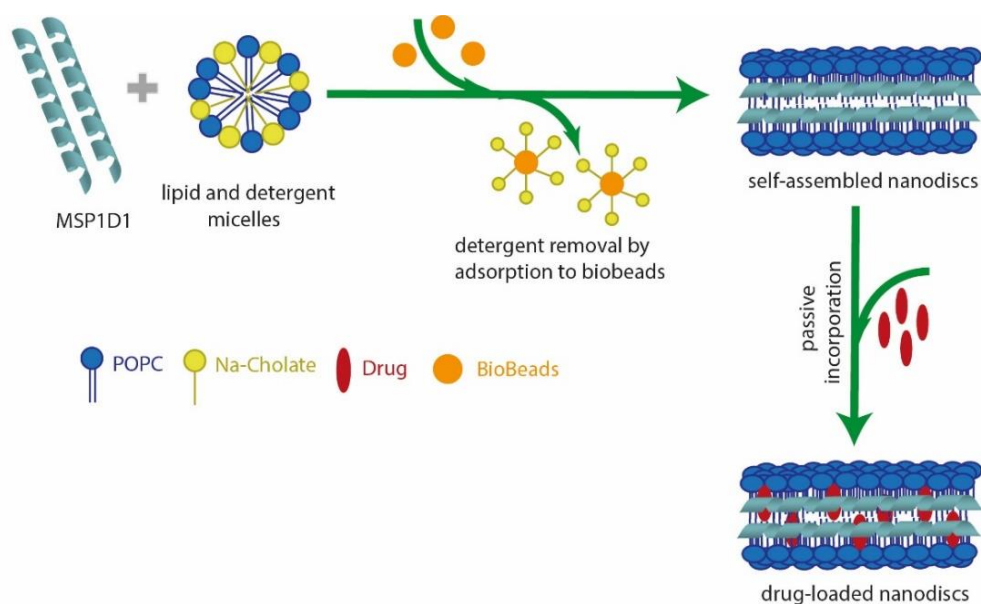


Figure 3.1 Schematic representation of the POPC ND reconstitution process, using method A, followed by postloading the drug into ND assemblies

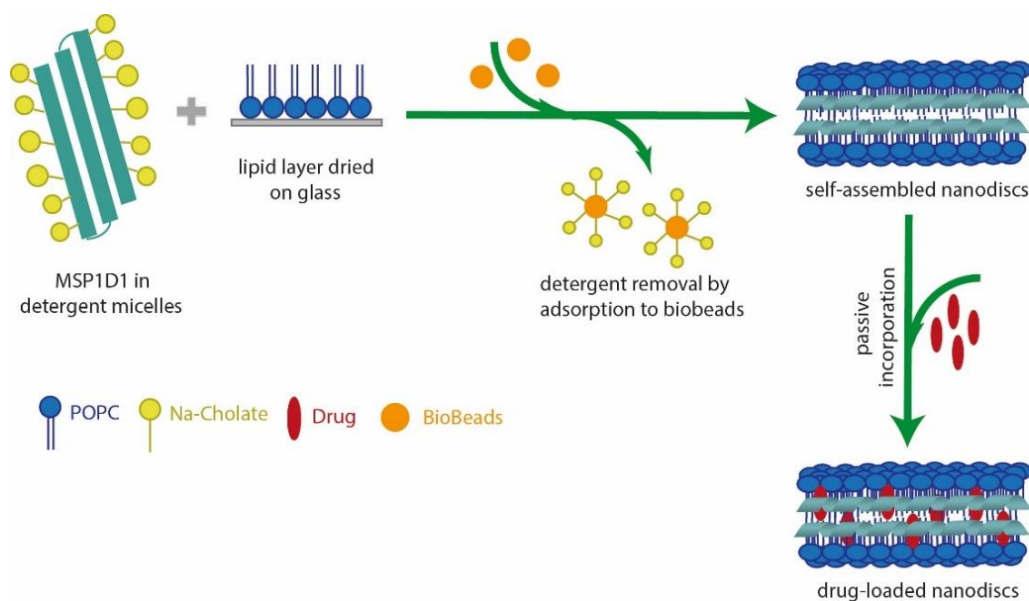


Figure 3.2 Schematic representation of the POPC ND reconstitution process, using method B, followed by postloading the hydrophobic molecules into ND assemblies

Method 2 of incorporating drug molecules into ND – preloading

The second drug incorporation method applied involved loading the drug molecules during the reconstitution of ND assemblies. The method of incorporation will be referred to as preloading or pre-incorporation method. This incorporation technique was often seen in literature where studies shown good loading efficiency and sustained release of drugs such as amphotericin B, curcumin and camptothecin.⁹⁹⁻¹⁰¹

The drug molecules were dissolved in chloroform and dried with POPC into a thin film, in which the drug molecules were trapped between the hydrocarbon chains. Subsequently, following the two methods of ND reconstitution, the drug molecules were incorporated into lipid/MSP and detergent micelles (Figure 3.3, Figure 3.4). After detergent removal *via* adsorption to bio-beads, the assembly process between MSP, POPC and drug molecules started arranging them into a discoidal bilayer, with the drug molecules, presumably, loaded into the phospholipid domain.

A series of methods were applied to investigate the efficiency of the loading process, the loading capacity and drug release kinetics and how these are affected by the structural and physical properties of the loaded hydrophobic drugs. First technique, SEC, was used to confirm drug loading and to examine the influence hydrophobic molecules incorporation has on the size of the assemblies, which could further be used to calculate an apparent MW. Subsequently, the ND assemblies with loaded drug molecules were separate on the SEC column from unincorporated drug molecules. The chromatograms, at 280 nm (protein absorbance) and at drug's absorbance are of empty ND and different ND-drug assemblies (the drug's absorbance could be found in Chapter 7, Table 7.2). A CD experiment was conducted, in parallel, to study the change in secondary structure of the scaffold protein when amiodarone and curcumin were pre-incorporated to ND. Subsequently, filtered ND and drug-loaded ND samples collected after SEC partition were characterised by size distribution. These experiments were carried out to analyse the effect that drug loading has on the diameter of the systems. After separating the ND containing drug molecules from unincorporated drug by SEC, UV-spectroscopy and High

Performance Liquid Chromatography (HPLC) were chosen to identify the most advantageous way to analyse how many drug molecules were loaded within the ND assemblies. Spectrophotometric measurements of ND and ND-drug assemblies were performed in the 200-600 nm wavelength range. HPLC experiments were conducted at 280 nm and drug's absorbance wavelength. For both methods, the nanostructures were dried under vacuum and disassembled by resuspension in TFE (2,2,2-Trifluoroethanol). Experiments of drug release were performed with the successful loaded and poorly loaded drug molecules (loaded using method B of reconstitution). This allowed observations on the rate of drug release from the systems.

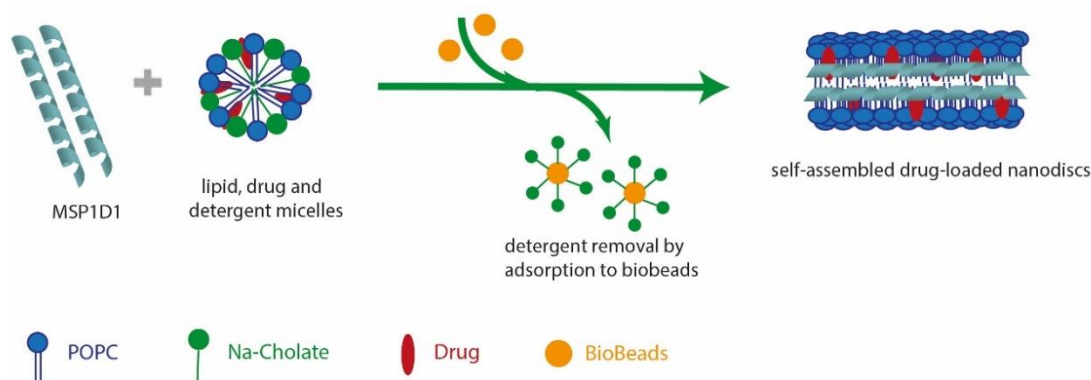


Figure 3.3 Schematic representation of the assembly of drug loaded ND; the drug molecules were preloaded to ND assemblies using method A of reconstitution

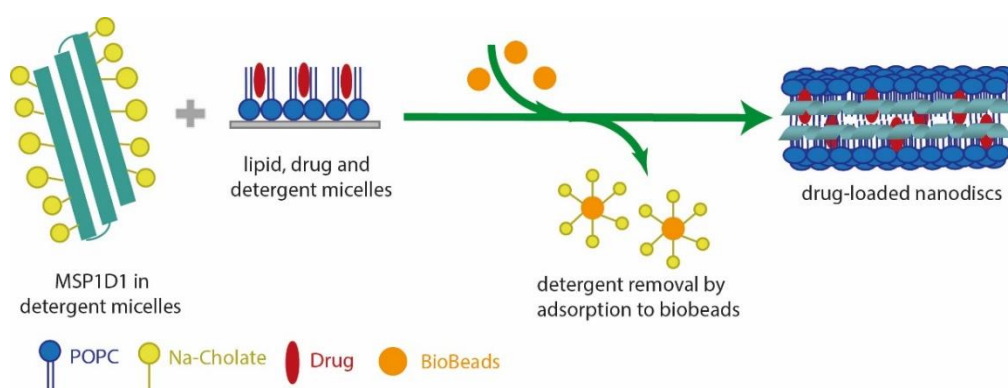


Figure 3.4 Schematic representation of the assembly of drug loaded ND; the drug molecules were preloaded to ND assemblies using method B of reconstitution

3.2.1 Nanodiscs loaded with amiodarone

Amiodarone (AMD) is an antiarrhythmic drug, frequently used in clinics to decrease heart rate and increase vascular resistance.¹⁰² Despite its preferred usage, amiodarone has a low water solubility (4.76 µg/mL), is extensively metabolised in the liver and its high toxicity can generate dangerous side effects.

3.2.1.1 Analysis by size-exclusion chromatography

Amiodarone showed successful loading within the ND for both methods of incorporation and reconstitution of ND. This was demonstrated by the single peak present at the elution time of ND. At a molar ratio of 1:30 MSP to POPC and a postloading reconstitution, the SEC chromatogram showed, in addition to the ND peak at 11 mL, a smaller peak at 20.5 mL probably corresponding to unincorporated amiodarone (Figure 3.5, A).

When the molar ratio changed to 1:65 MSP to POPC, regardless of the reconstitution approach, a slight difference in elution time could be observed for the ND with loaded amiodarone (Figure 3.5, B and C). The faster elution time indicated an increase in the apparent MW resulted, presumably, from the agglomeration of amiodarone at the water phospholipid head group interface rather than loading within the phospholipid domain of the ND (230 kDa MW for ND AMD from 140 kDa MW for empty ND).

Comparatively, when amiodarone was preloaded to ND at a 1:65 MSP to POPC molar ratio, using method A, the elution times of ND AMD and ND were almost identical (Figure 3.6, A). Furthermore, the chromatogram of ND AMD showed a small shoulder attached to the peak corresponding to ND. A possible explanation could be that the loading of amiodarone generated instability during ND formation, which resulted in the reconstitution of polydisperse ND AMD assemblies.

The chromatogram of ND AMD formed following method B of reconstitution, where, the drug was preloaded to assemblies, showed a single narrow peak at the elution time specific to ND (apparent MW of 111 kDa), (Figure 3.6, B).

Incorporation of poorly water soluble drugs into nanodiscs

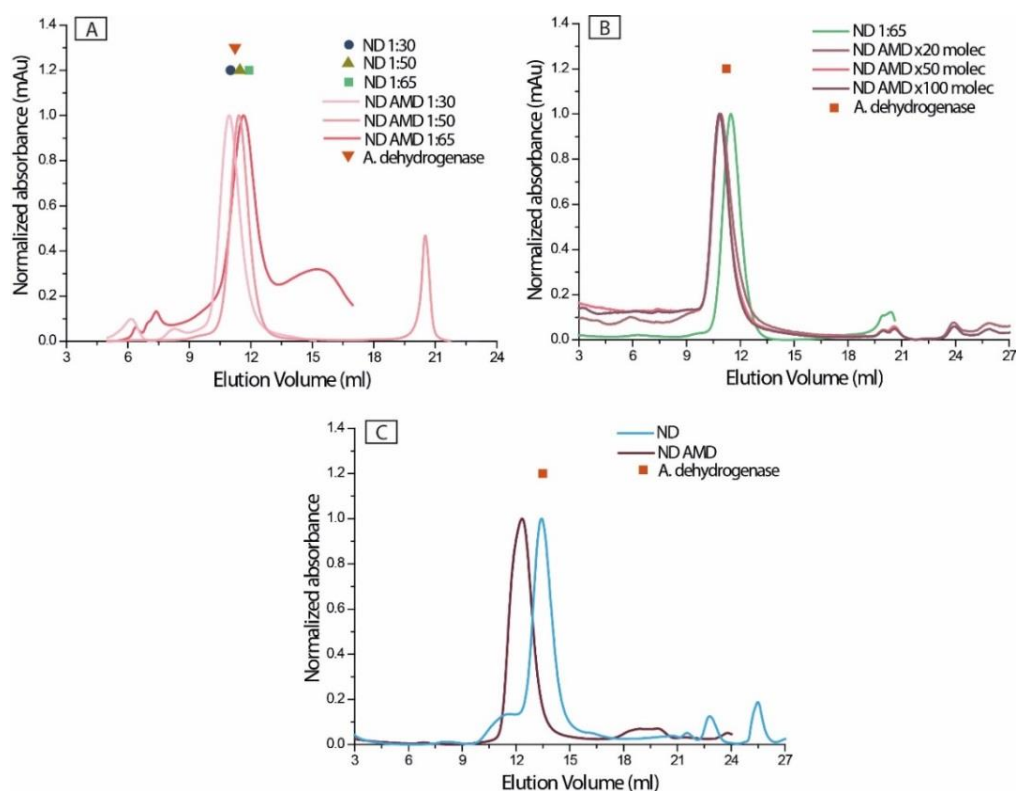


Figure 3.5 SEC chromatograms of ND AMD, ND and the elution time of AD: A - ND reconstituted with 1:30, 1:50 and 1:65 molar ratio using method A; B – ND reconstituted with 1:65 molar ratio using method A; AMD was added in three different quantities; C - ND reconstituted with 1:65 molar ratio using method B; AMD was postloaded to ND; ND and AD were measured at 280 nm, ND AMD were measured at 242 nm

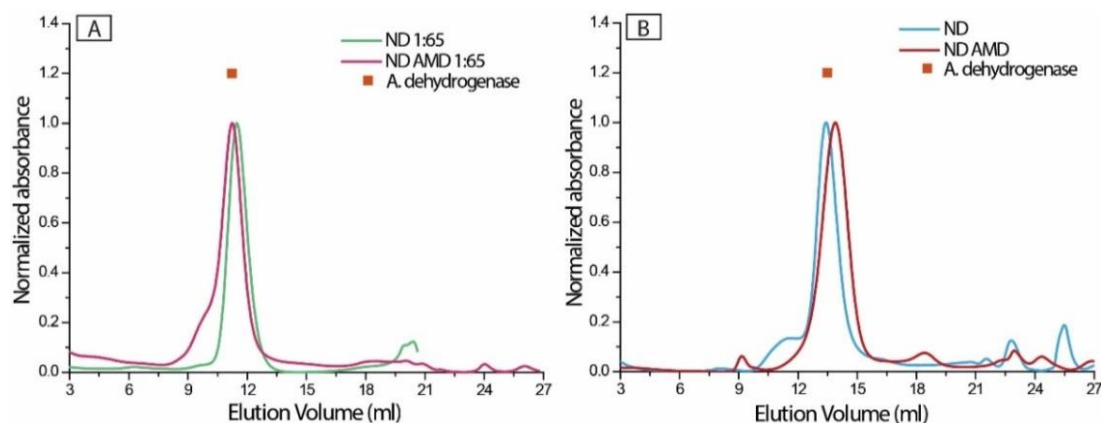


Figure 3.6 SEC chromatograms of ND AMD, ND and the elution time of AD: A - ND reconstituted using method A; B - ND reconstituted using method B; for all ND AMD assemblies, AMD was preloaded to ND (1:65 molar ratio); ND and AD were measured at 280 nm, ND AMD were measured at 242 nm

3.2.1.2 Analysis by dynamic light scattering

It was determined that stable nanodiscs and nanodiscs with loaded amiodarone were formed with distinct diameters (Figure 3.7). The variation in diameter was dependent on the drug loading method and the protein to POPC ratio used for the ND-drug reconstitution.

When amiodarone was preloaded to ND, an increase in ND AMD size was observed, from 10.1 nm, the diameter of empty ND, to 11.7 nm. On the other hand, when amiodarone was postloaded to ND, the drug did not alter the diameter (10.1 nm) of the ND reconstituted with 1:50 and 1:65 MSP to POPC. It was found that, for ND reconstituted with 1:30 MSP to POPC, large aggregates with a diameter of 615.1 nm were formed, as well as smaller ND AMD with a diameter of 4.84 nm, presumably as a result of aggregation over time.

Conclusively, the results have shown negligible increase in the diameter of the system when amiodarone was loaded within the phospholipid domain of ND. This lack of a significant difference in particle size between empty and loaded carriers was also described in the study conducted, by Lamprecht *et al.*,¹⁷ on the incorporation of amiodarone into lipid nanocapsules.

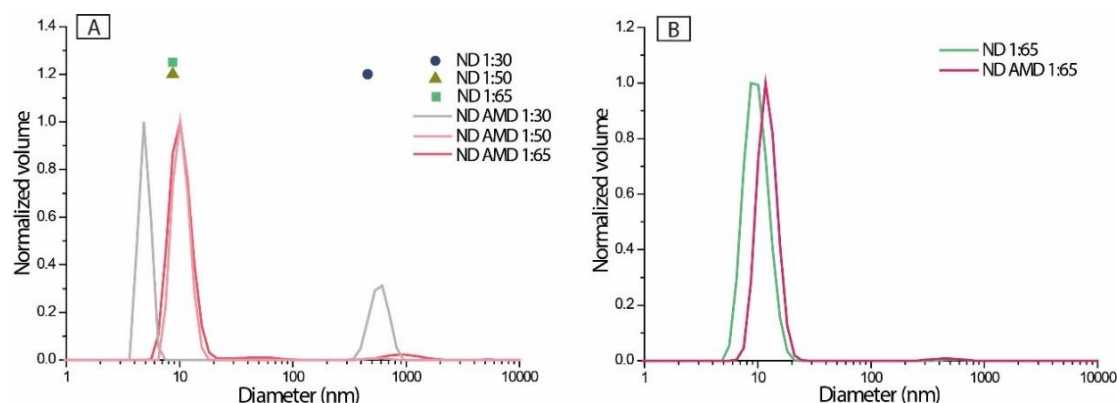


Figure 3.7 DLS of A – AMD postloaded to ND reconstituted with 1:30, 1:50 and 1:65 molar ratio; B - AMD preloaded to ND reconstituted with 1:65 molar ratio; assemblies were reconstituted using method A

3.2.1.3 Analysis of the amiodarone load

3.2.1.3.1 UV spectrophotometry

For the analysis of amiodarone load, two methods of calculation were employed. The UV spectra of ND AMD have shown increased absorbance compared to the spectra of empty ND (Figure 3.8). However, the methods were chosen because the UV absorbance of MSP might interfere with the absorbance of the drugs that were incorporated within stabilised ND. First method is based on measuring and equating the POPC concentrations in empty and drug loaded ND. Firstly, the absorbance of MSP in ND-drug is calculated by relating it to the POPC concentration. This was done based on the assumption that, by equating the POPC concentration, the MSP concentration remains the same. More explicitly, if the concentration of POPC in empty ND is 3.6 mM, then the absorbance, at the specific wavelength, for MSP in those empty ND is 0.25 Au. Knowing these values, we can subsequently calculate the absorbance of MSP in ND-drug at a certain POPC concentration. Following this, the difference in absorbance between theoretically empty ND and ND with loaded drug is given by the loaded drug (Table 3.1).

	Calculated drug concentration (mM)	Calculated molecules of drug loaded per ND
ND AMD ¹	0.8	19
ND AMD ²	3.75 ± 1.7	81 ± 63

Table 3.1 Calculated drug concentrations and number of AMD molecules loaded per ND; AMD was postloaded to ND reconstituted with ¹1:50 and ²1:65, using method A; repeat measurements were conducted only for ND AMD²

Subsequent to the calculations, nothing conclusive could be drawn for ND AMD reconstituted with 1:65, as the standard deviation was too big. However, for the assemblies reconstituted with 1:50, the number of amiodarone incorporated per ND was found to be 19.

In the second method used, a matrix was applied to calculate the amount of amiodarone incorporated per ND (Eq. 3.1). This method, independent of POPC concentration, involved calculating the MSP and amiodarone concentrations

from the absorbance of each sample at drug and MSP wavelength and the inverse matrix of their extinction coefficient in TFE, at the specific wavelength. From the measured spectra of each drug and MSP, their extinction coefficient was calculated with the Beer-Lambert Law (Eq. 7.1) (Table 3.2). The extinction coefficients were also calculated for each sample in methanol and hexane – data not shown.

$$C = M^{-1} A$$

Equation 3.1 Equation showing the relationship between MSP and drug concentrations, their extinction coefficient and absorbance at a given wavelength

Where:

$$C = \begin{pmatrix} C_{MSP} \\ C_{drug} \end{pmatrix},$$

$$M = \begin{pmatrix} \varepsilon_{MSP,x} & \varepsilon_{drug,x} \\ \varepsilon_{MSP,280} & \varepsilon_{drug,280} \end{pmatrix},$$

$$A = \begin{pmatrix} A_x \\ A_{280} \end{pmatrix},$$

x = wavelength for drug absorbance.

	ε in TFE at 242 nm (mol ⁻¹ cm ⁻¹)	ε in TFE at 280 nm (mol ⁻¹ cm ⁻¹)
AMD	18391.05	2581.2
MSP	27281.02	24790.15

Table 3.2 Extinction coefficient values calculated, with the Beer-Lambert Law, for AMD and MSP suspended in TFE; the extinction coefficient was calculated based on the absorbance at the specific wavelength

Using the matrix equation and the extinction coefficients from Table 3.2, the molecules of amiodarone loaded per ND were calculated (Table 3.3). For the assemblies using post-incorporation method and reconstituted with 1:50 and 1:65 molar ratios (method A), the number of amiodarone incorporated was found to be identical. An addition of 2 molecules incorporated per ND was seen when amiodarone was preloaded to ND. Presumably, the energy required for amiodarone clusters to break the water cages surrounding them and diffuse inside the hydrophobic domain of the ND is too high, therefore less molecules will be incorporated into ND using postloading¹⁰³.

Sample	Calculated MSP concentration (mM)	Calculated drug concentration (mM)	Calculated number of drug loaded molecules
ND AMD ¹	0.23	1.08	9
ND AMD ²	0.14	0.63	9
ND AMD ³	0.37	2.13	11

Table 3.3 Calculated MSP and drug concentrations, and molecules of AMD loaded per ND; method A was used; ¹AMD was postloaded to ND reconstituted with 1:50; ²AMD was postloaded to ND reconstituted with 1:65; ³AMD was preloaded to ND reconstituted with 1:65

Assessing the number of small molecules loaded per ND by UV-spectroscopy resulted in an overestimation of MSP concentration which in turn led to underestimating the molecules of drug incorporated. This inaccuracy and inconsistency of the results combined with the noisy data collected from the UV analysis caused us to consider another method for loading evaluation. Therefore, the use of HPLC analysis was explored further in the investigation of the loading efficiency.

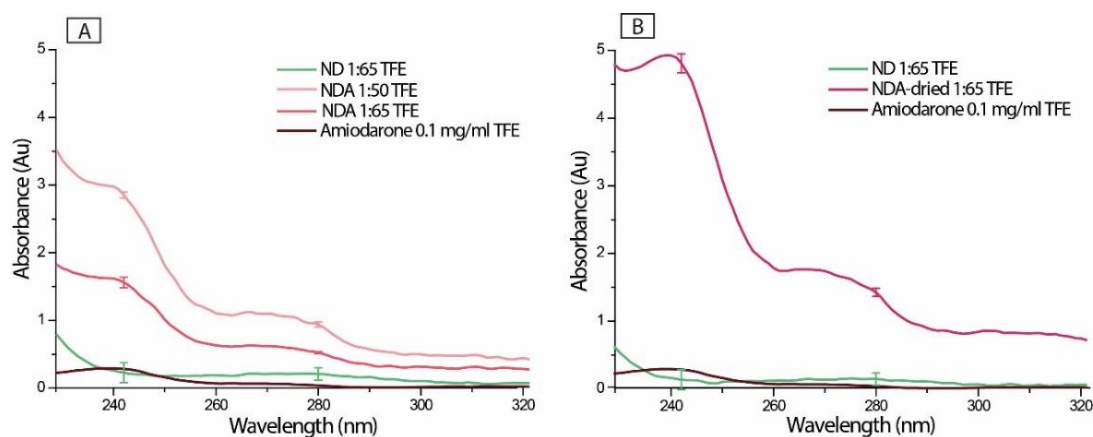


Figure 3.8 UV spectras of ND AMD resuspended in TFE: A – AMD was postloaded to ND using method A; B – AMD was preloaded to ND using method A; the analysis was conducted at 242 nm

3.2.1.3.2 High performance liquid chromatography

Similarly to analysis by UV spectroscopy, for the investigation using HPLC, amiodarone loaded ND were disassembled by resuspension in TFE. This was done to facilitate a better separation from the scaffold protein and produce an accurate evaluation of the amount of drug incorporated. Once the components of the disassembled structure were separated on the HPLC column and analysed at protein and drug absorbance, the amount of both MSP and drug in the system could be quantified.

An example of HPLC chromatograms of ND AMD, preloaded using method B of reconstitution, could be seen in Figure 3.9. In the amiodarone loaded ND, the peaks of MSP and drug were visible at different elution times; comparable to the peaks of MSP alone and drug in TFE visible on the diagram inserted in the chromatogram. This separation gave an elution time for each component and with the help of generated calibration curves (Figure 8.3, Figure 8.4) the concentration in mg/mL of MSP and amiodarone in assemblies could be calculated. HPLC analysis was also performed on amiodarone postloaded within ND using method B of reconstitution and on amiodarone preloaded to ND using method A.

It was found that, for amiodarone post-incorporated to ND formed with 1:65 MSP to POPC molar ratio, 9.5 ± 2 molecules of drug were loaded per ND. When a lower molar ratio was used to reconstitute ND (1:50) the amount of amiodarone incorporated was reduced to 5.8 ± 2.5 molecules per ND (Table 3.4). When amiodarone was preloaded to ND, the amount of drug incorporated per ND was greater – 10 ± 6.8 molecules per ND. These results have led to the belief that the loading efficiency was affected by the use of different methods for loading drug molecules.

Additionally, the concentration of ND was calculated based on the calibration curve of MSP and the amount of lipids in each sample was determined with phosphorous assay. The ND AMD assemblies had a ND concentration of 48.8 ± 26 μ M and 100 ± 22 POPC. In this instance, the number of POPC per

ND fluctuated considerably probably as a consequence of different exposure times in the presence of hydrophobic bio-beads during ND reconstitution.

Sample	Measured number of POPC per ND <i>via</i> phosphorous assay	Calculated final concentration of ND <i>via</i> HPLC (μM)	Calculated number of AMD loaded per ND <i>via</i> HPLC
ND AMD ¹	nc	31.8 ± 25	10 ± 6.8
ND AMD ²	99	63.4	5.8 ± 2.5
ND AMD ³	100 ± 22	48.8 ± 26	9.5 ± 2

Table 3.4 Measured number of POPC per ND, calculated concentrations of ND and amount of AMD loaded per ND; ¹AMD was preloaded to ND reconstituted with 1:65; ²AMD was postloaded to ND reconstituted with 1:50; ³AMD was postloaded to ND reconstituted with 1:65; method B of reconstitution; nc – not calculated

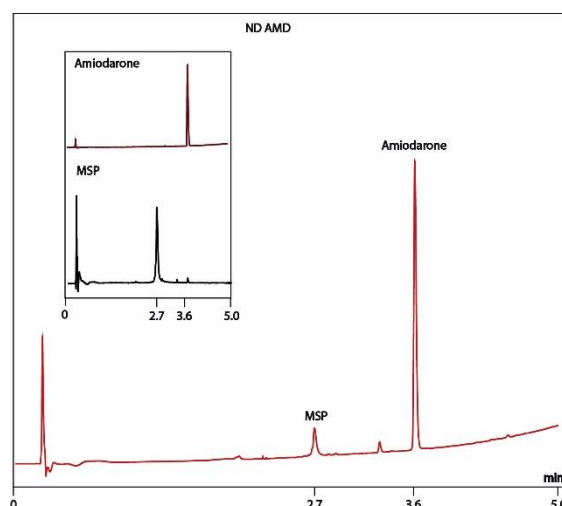


Figure 3.9 HPLC chromatograms of ND AMD measured at 242 nm; the inside chromatograms are an example of AMD and MSP with a known concentration measured at 242 nm and 280 nm, respectively; AMD was preloaded to ND, using method B

3.2.1.4 Analysis by circular dichroism

The negative peaks at 210 nm and 225 nm and the positive peak at 195 nm specific to α helix conformation⁹⁴ are present in the ND systems with incorporated amiodarone (Figure 3.10). Furthermore, a shift of the positive peak from 195 nm to 192 nm was detected from empty ND assemblies to amiodarone loaded ND. The increase can be attributed to the drug molecules loaded into the systems. These observations led to the similar belief, demonstrated by Nguyen *et al.*¹⁰⁴ In their study, of amphotericin B loaded DMPC nanodiscs, the

helical structure of the protein was not affected when drug molecules were incorporated into ND.

CD experiments were not conducted for all successfully loaded drug molecules. However, it was inferred that a similar result would be expected because of successful ND formation which would require the MSP to fold correctly around the lipid-drug domain.

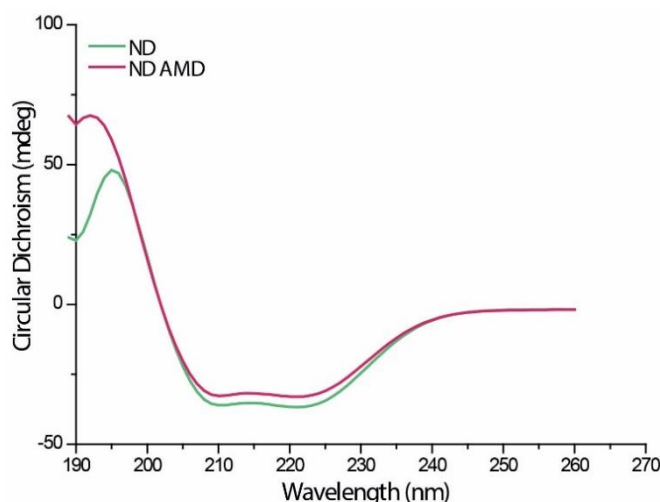


Figure 3.10 CD spectras of ND and ND AMD; AMD was postloaded to ND reconstituted with 1:65 ratio; the peaks specific to α helix conformation are at 195 nm, 210 nm and 225 nm

3.2.1.5 Release of poorly water soluble drugs upon dilution

Drug release experiments were performed on amiodarone loaded into ND reconstituted using method B. A dialysis assay against stirred Tris buffer at 37°C (Figure 3.11, A) was conducted by changing the equilibrium between loaded and unloaded amiodarone concentrations (Figure 3.11, B). Samples were taken at specific intervals and measured by UV at drug's absorbance. The release studies of all drug-loaded ND assemblies were performed in triplicate.

The fractional release of drug molecules (f_r) was then calculated using a first order rate equation (Eq. 3.2) and an exponential curve fitted to the drug release data. The exponential model with 1 parameter (Eq. 3.3, where k is the rate parameter) was fitted to describe how rapidly the process of drug release occurs. The half-life of the drug (Eq. 3.4, $t_{1/2}$ is the half-life) was calculated from the rate constant value for the drug release given after fitting the exponential

model. Half-life, $t_{1/2}$ values of drug molecules released from ND can be found in Table 3.8 to Table 3.12.

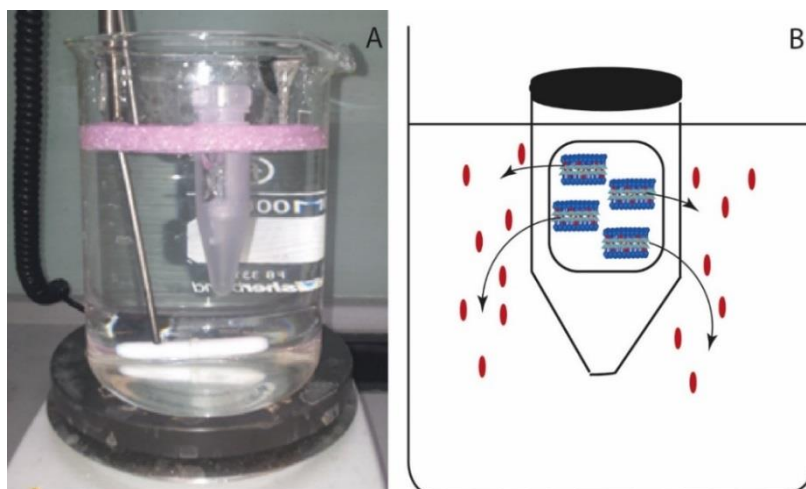


Figure 3.11 A - Representation of dialysis assay in buffer; B - Schematic representation of equilibrium changes between loaded and unloaded drug concentrations

$$f_r = \frac{\alpha_{t=0} - \alpha_t}{\alpha_{t=0} - \alpha_{empty}}$$

Equation 3.2 First order rate equation used for calculating the fractional release of drug molecules; $\alpha_{t=0}$ is the absorption of ND-drug at time, $t=0$; α_t is the absorption of ND-drug at specific time; α_{empty} is the absorption of empty ND at the wavelength of the loaded drug

$$f_r = 1 - e^{(-kt)}$$

Equation 3.3 The exponential model with 1 parameter fitted to the drug release data; k is the rate parameter

$$t_{1/2} = \frac{\ln(2)}{k}; \quad \Delta t_{1/2} = \frac{\Delta k}{k} \times t_{1/2}$$

Equation 3.4 The half-life of the drug and its standard deviation calculated from the rate constant value given for the drug release, after fitting the exponential model from Eq. 3.3

Most amiodarone molecules were released in 24 h with no initial burst observed (Figure 3.12). This can probably be attributed to all drug molecules being incorporated, as unloaded amiodarone was previously removed by SEC. Amiodarone preloaded to ND had a calculated $t_{1/2}$ of $5.4 \text{ h} \pm 0.67$ and its constant release was almost complete within 24 h (Figure 3.12, A). In literature,

the release of amiodarone from lipid nanocapsules was, likewise, described as not displaying an initial burst effect.¹⁷ Although the drug release at physiological pH was extended over a longer period of time compared to our findings.

When amiodarone was postloaded to ND assemblies, an exception was found. The first stage of amiodarone release showed a significant initial burst effect. This involved the release of more than 50% of the loaded drug in the first hour (Figure 3.12, B, dark red). The drug release reached a plateau after 2 h for the ND AMD reconstituted with 1:65 MSP to POPC. The $t_{1/2}$ of the drug, subsequently calculated from the rate parameter, was $0.62 \text{ h} \pm 0.14$.

In the case of amiodarone postloaded to ND formed with 1:50 MSP to POPC, after the initial burst, the drug was released constantly within 6 h (Figure 3.12, B, light red). The $t_{1/2}$ was calculated to be $0.88 \text{ h} \pm 0.03$. This notable burst effect could be the result of amiodarone accumulation near the phospholipid headgroups¹⁰⁵. Overall, dissociation of amiodarone loaded ND assemblies occurred with an apparent 100% release. The experiments carried out with free drug in the absence of ND showed that the equilibrium was achieved much quicker (data not shown).

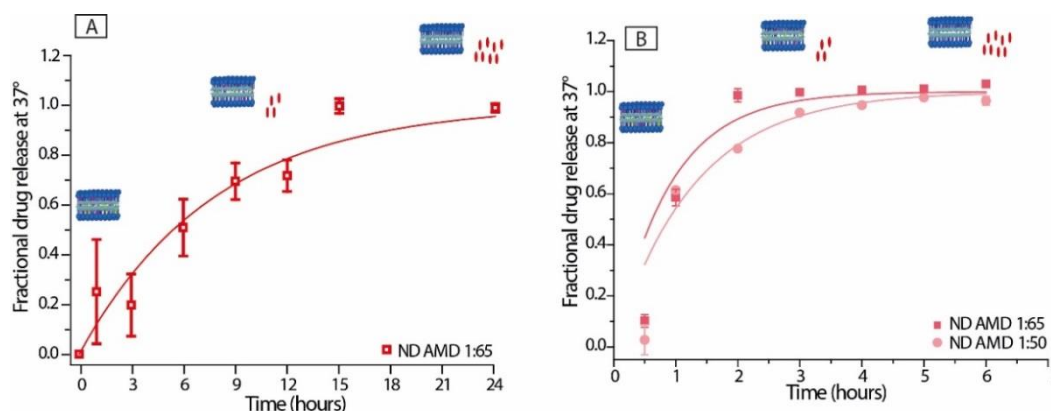


Figure 3.12 Fractional drug release at 37 °C for A – ND AMD, AMD preloaded to ND, and B – ND AMD, AMD postloaded to ND; the aliquots were measured at 242 nm; $t_{1/2}$ values were: A - $5.4 \text{ h} \pm 0.67$; B - $0.62 \text{ h} \pm 0.14$, for the ND reconstituted with 1:65, and $0.88 \text{ h} \pm 0.03$ for the ND reconstituted with 1:50; data is shown as the mean \pm SD

The techniques used to characterise ND AMD assemblies have demonstrated the influence drug incorporation has on the MW and size of the assemblies and on the secondary structure of the scaffold protein that forms the protein belt. In addition, SEC was further used to separate the ND-drug assemblies from unincorporated free drug molecules. This separation was completed for the better subsequent quantification of the amount of drug molecules loaded.

Following the thorough characterisation of amiodarone loaded ND, a series of drug molecules were also incorporated into ND. Their characterisation adopted a similar path to that of amiodarone loading.

3.2.2 Nanodiscs loaded with chlorambucil

Chlorambucil (CLB) is a known carcinogen with a higher water solubility than amiodarone (77.3 µg/mL), and it is used as antineoplastic agent for the treatment of various forms of cancer.

Method B of reconstituting ND with 1:65 MSP to POPC molar ratio proved successful and was straightforward to follow. Thus, for practical reasons, this approach was used for loading chlorambucil into ND.

The analysis by SEC, at 254 nm, of ND CLB showed that incorporation of chlorambucil gave contrasting results. The ND CLB assembled by postloading chlorambucil to ND, showed a peak, with small absorbance (Figure 3.13, A). Although of low intensity, this peak, eluted 0.5 mL faster than empty ND, confirmed the incorporation of chlorambucil. The apparent MW of these assemblies was 211 kDa. In addition, the SEC trace revealed two peaks with a retention time of 20 mL and 24 mL. The high absorbance observed for these peaks would imply that most drug molecules were eliminated as aggregates of various sizes (apparent MW between 1 and 6 kDa).

Contrary to postloading of drug, the chromatogram of ND CLB formed *via* preloading the drug, showed a single peak seen at the almost identical elution time of empty ND (Figure 3.13, B). Hence, chlorambucil was thought to have exhibit successful loading within the ND. The shoulder seen in the SEC trace resulted, probably, from the reconstitution of polydisperse ND CLB or

aggregation over time of the initially monodisperse ND CLB. In addition, the unincorporated chlorambucil was eliminated, around 24 mL, as two peak with small absorbance. The analysis by SEC has demonstrating clearly that the best route for incorporating chlorambucil into ND was by using the pre-incorporation method.

Subsequently to determining the best route for incorporating chlorambucil, HPLC was employed to calculate how many drug molecules were pre-incorporated per ND. The samples were prepared as in the case of amiodarone. An example of HPLC chromatogram of ND CLB could be seen in Figure 8.6. The amount of chlorambucil incorporated per ND was calculated at 6.5 ± 1.7 molecules per ND.

Due to the successful incorporation of a relatively high number of chlorambucil per ND, the rate of drug release was also investigated. Similar to amiodarone, most chlorambucil molecules were released in 24 h with no initial burst (Figure 3.14). The equilibrium between the concentrations of loaded and free chlorambucil was achieved after 15 h, with only 80% of the drug being release into the buffer. The low release profile was observed to be similar with the literature value.⁴² In the recent study, Rao *et al.* showed that, in mild acidic conditions, only 71% of chlorambucil was released from self-assembled norbornene based triblock co-polymers. A reasonable hypothesis for the system to reach equilibrium below 100% can be correlated to a high solubility in water, but a more favourable interaction within the organic phase. Hence the moderate log P value of 3.8. The $t_{1/2}$ for chlorambucil calculated from the rate constant was $5.8 \text{ h} \pm 0.48$. An improvement of $t_{1/2}$ value was observed, as the current literature indicates the circulation $t_{1/2}$ of free drug is 1.5 h.¹⁰⁶

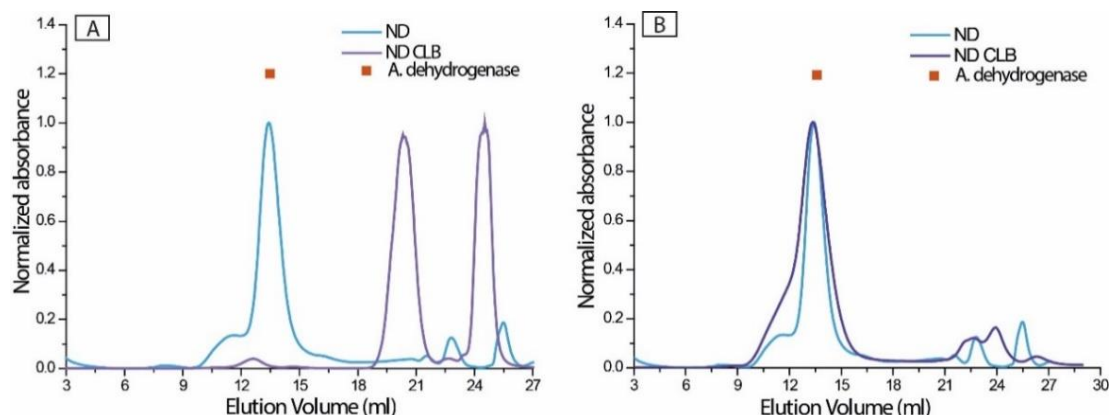


Figure 3.13 SEC chromatograms of ND CLB, ND and the elution time of AD: A - CLB was postloaded to ND; B - CLB was preloaded to ND; reconstitution using method B; ND and AD were measured at 280 nm, ND CLB were measured at 254 nm

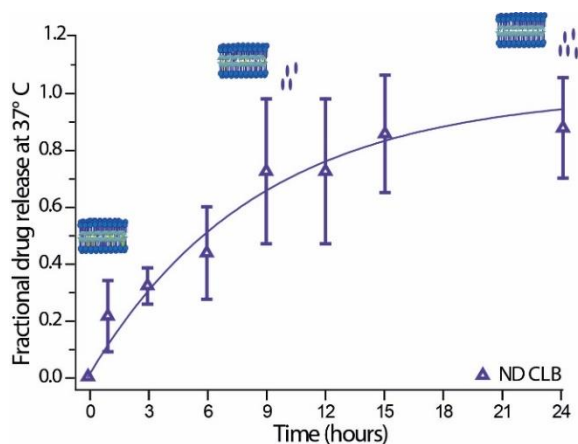


Figure 3.14 Fractional drug release at 37 °C for ND CLB, CLB was preloaded to ND; the aliquots were measured at 254 nm; $t_{1/2}$ value was 5.8 h \pm 0.48; data is shown as the mean \pm SD

3.2.3 Nanodiscs loaded with curcumin

Curcumin (CCM), the principal curcuminoid of turmeric, because of its bright yellow colour, is used as food colouring. A recent study also showed increased fluorescence of curcumin when associated with amyloid- β oligomers which could lead to novel therapies in combating Alzheimer disease.¹⁰⁷ Regardless of the potential therapeutic effect, curcumin displays poor absorption, rapid metabolism and low water solubility. Curcumin has a lower water solubility than amiodarone, and previous studies have demonstrated its encapsulation into PEGylated liposomes¹⁸ or even ApoA-I nanodiscs.¹⁰⁰ Therefore, curcumin incorporation (pre- and post-) was investigated by applying method A.

On the analysis of ND CCM by SEC formulated *via* postloading the drug, a narrow peak was present at the elution time of ND (Figure 3.15, A). This was observed for both molar ratios involved in the reconstitution process. However 1:50 ND CCM showed, in addition to the ND peak a peak at a later elution time, possibly corresponding to unloaded curcumin. The analysis of ND with preloaded curcumin, revealed a wider peak, which could indicate a broader size distribution of ND CCM (Figure 3.15, B).

Alongside amiodarone, curcumin was the second drug for which size distribution and changes in the secondary structure of MSP were analysed in order to determine the impact of curcumin incorporation (Figure 8.7 and Figure 8.8). The observations supported the conclusions drawn after SEC analysis and had similar outcomes as amiodarone incorporation – minimal difference in size and unaltered helical structure of MSP, between empty and loaded ND. Similar size distribution was also described in literature by Kupetz *et al.*,¹⁰⁸ on the incorporation of curcumin into lipid nanoemulsions.

These observations suggested the successful formation of ND assemblies, however further investigation was needed to determine if curcumin was loaded into ND. Using UV spectroscopy (Figure 8.9), the number of curcumin molecules postincorporated per ND was determined. This method of evaluating the number of drug molecules loaded per ND appeared most promising for calculating curcumin incorporation. Applying the method of equating POPC concentrations, the calculations showed a higher amount incorporated for the assemblies reconstituted with 1:50 molar ratio. This led to the loading of 10 molecules of curcumin per ND compared to 2 molecules, for the assemblies formed with 1:65 molar ratio. The difference in molecules loaded implied that there was more space for the drug molecules to be incorporated, as a consequence of the phospholipid packing within the bilayer being less compact.

	Calculated drug concentration (mM)	Calculated molecules of drug loaded per ND
ND CCM ¹	0.43	10
ND CCM ²	0.08 ± 0.07	2 ± 1.8

Table 3.5 Calculated CCM concentrations and number of molecules loaded per ND; ¹CCM was postloaded to ND (1:50 molar ratio); ²CCM was postloaded to ND (1:65 molar ratio); reconstituted using method A

To verify the accuracy of these calculations the matrix equation was also employed. With its help, and knowing the extinction coefficients (Table 3.6), the molecules of curcumin loaded per ND were calculated (Table 3.7). The postloaded method using 1:50 ratio was again found to incorporate more curcumin per ND than the ratio of 1:65 - 4 molecules and 2 molecules, respectively. However, the curcumin preloaded to ND (1:65 ratio) provided the highest number of loaded molecules - 23 molecules per ND. These calculations suggested that, regardless of the reconstitution ratio between MSP and POPC, the method of preloading curcumin gave better results. An explanation could be that vast amount of energy would be required to break the water cages surrounding the curcumin molecules in order to diffuse them into the lipophilic environment of the ND. Comparatively, when curcumin is dried with a layer of lipids, upon resuspension in aqueous environment, less energy is required for rearranging the curcumin molecules and phospholipids into a bilayer formation.

	ε in TFE at 430 nm (mol ⁻¹ cm ⁻¹)	ε in TFE at 280 nm (mol ⁻¹ cm ⁻¹)
CCM	14403.46	626.24
MSP	1779.20	24790.15

Table 3.6 Extinction coefficient values calculated, with Beer-Lambert law, for CCM and the MSP suspended in TFE; the extinction coefficient was calculated based on the absorbance at the specific wavelength

Sample	Calculated MSP concentration (mM)	Calculated drug concentration (mM)	Calculated molecules of drug loaded
ND CCM ¹	0.19	0.39	4
ND CCM ²	0.082	0.086	2
ND CCM ³	0.011	0.013	23

Table 3.7 Calculated MSP and drug concentrations, and molecules of CCM loaded per ND; ¹CCM was postloaded to ND (1:50 molar ratio); ²CCM was postloaded to ND (1:65 molar ratio); ³CCM was preloaded to ND (1:65 molar ratio); method A of reconstitution

Observing the rate of curcumin release led to contradictory conclusions compared to amiodarone and chlorambucil. Here, the release of curcumin (1:65 reconstitution ratio) was rapid, reaching 80% after 6 h ($t_{1/2} = 7.4 \text{ h} \pm 0.4$) (Figure 3.16, light brown). More so, a 20% burst release was observed after 30 min for ND CCM reconstituted with 1:50 ratio (Figure 3.16, dark yellow). This initial burst was followed by a slower loss that did not exceed 40% of curcumin release (overall release time was 6 h; $t_{1/2} = 3.9 \text{ h} \pm 1.3$). In the literature, for curcumin loaded PEGylated hybrid liposomes, a similar drug release profile was described as a sustained release of 35% curcumin within 24 h, however lacking the initial burst.¹⁸ The method of postloading the drug within ND contributed to curcumin weakly binding to the phospholipid headgroups. Hence, the presence of a burst effect could be the result of rapid release of curcumin accumulated near the ND surface.

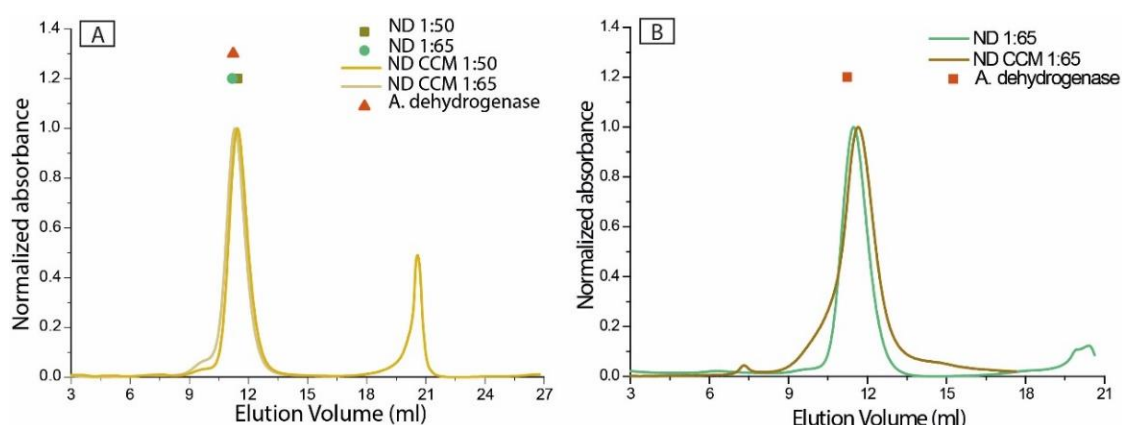


Figure 3.15 SEC chromatograms of ND CCM, ND and the elution time of AD: A - CCM was postloaded to ND reconstituted with 1:50 and 1:65 molar ratio; B - CCM was preloaded to ND reconstituted with 1:65 molar ratio; for all assemblies, method A was followed; samples were measured at 280 nm

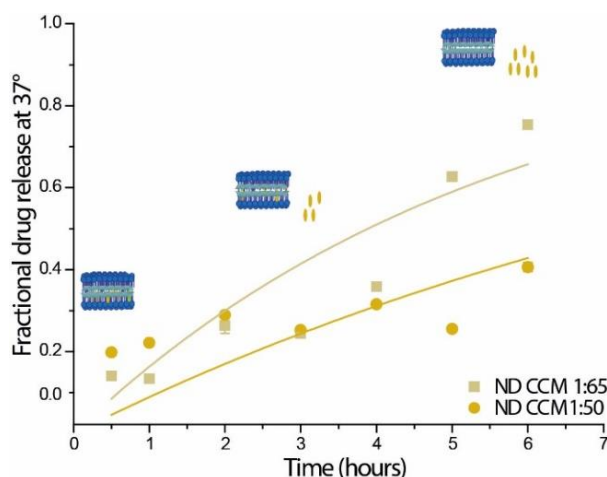


Figure 3.16 Fractional CCM release at 37 °C from ND; CCM was postloaded to ND; the aliquots were measured at 430 nm; $t_{1/2}$ values were $7.4 \text{ h} \pm 0.4$ for the ND reconstituted with 1:65, and $3.9 \text{ h} \pm 1.3$ for the ND reconstituted with 1:50; data is shown as the mean \pm SD

3.2.4 Nanodiscs loaded with thioridazine

Thioridazine (TRD), a phenothiazine antipsychotic drug with water solubility of $0.855 \mu\text{g/mL}$, is indicated for the treatment of schizophrenia. Thioridazine was another drug candidate used to investigate loading and release from ND systems. When thioridazine was postloaded to ND, the SEC trace displayed multiple peaks, indicating a vast size distribution (Figure 3.17, A). The most prominent peak coincided with a slight increase in MW, which confirmed the drug loading. Additionally, the presence of aggregates in the void volume supported the belief that thioridazine postincorporated led to instability in the ND systems. This instability was also seen to depend on the number of thioridazine added during reconstitution of ND with preloaded thioridazine (Figure 3.17, B). However, its earlier elution time – comparative to drug postloaded ND – suggested the possibility that more thioridazine molecules may be incorporated per ND. The unincorporated drug was detected as peaks eluted at later times.

Despite the inability to quantify the number of thioridazine content per ND *via* HPLC, due to the difficulty in separating the components (Figure 8.10), but with encouragements from the SEC results, the rate of drug release preloaded into ND was investigated. Similar to the release of amiodarone and chlorambucil preloaded to ND, thioridazine was released over a period of 24 h, at a rate

proportional to its concentration in ND - $t_{1/2}$ was $3 \text{ h} \pm 0.33$ (Figure 3.18). Subsequently, the absence of an initial burst observed on the release profile was in good agreement with literature findings.¹⁰⁹ Although, the release of thioridazine from ND reached an apparent completion, compared to only 60% of thioridazine being released from the polymeric micelles. A reason behind the difference in drug released could be based on the higher volume of release media used for the drug loaded ND assemblies; hence the buffer had a greater capacity for solubilising the free drug.

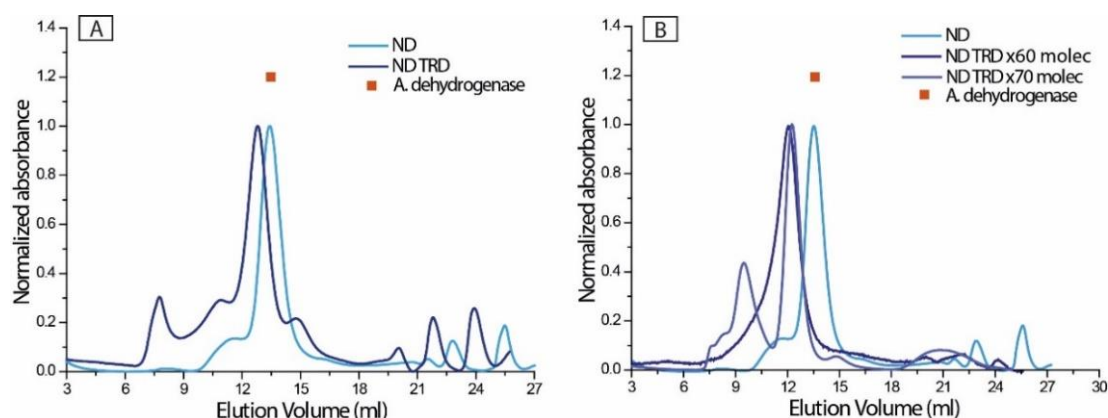


Figure 3.17 SEC chromatograms of ND, ND TRD and the elution time of AD: A - TRD was postloaded to ND; B - TRD was preloaded to ND; reconstituted with method B; ND and AD were measured at 280 nm, ND TRD was measured at 262 nm

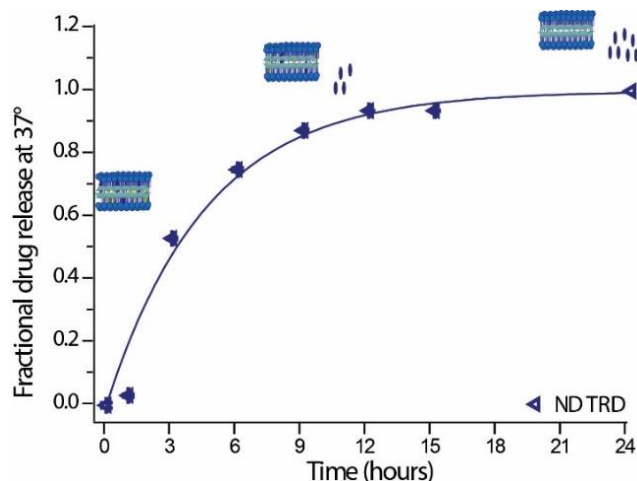


Figure 3.18 Fractional TRD release at 37 °C from ND; TRD was preloaded to ND; the aliquots were measured at 262 nm; $t_{1/2}$ was $3 \text{ h} \pm 0.33$; data is shown as the mean \pm SD

3.2.5 Nanodiscs loaded with novobiocin

Novobiocin (NVB) is an aromatic compound with antibiotic properties. Novobiocin has a similar MW to amiodarone but higher water solubility (9.66 $\mu\text{g/mL}$) and a voluminous structure. The drug was incorporated to ND *via* postloading and preloading method and an investigation was conducted into the efficiency of loading and release from ND. The reconstitution experiments conducted for novobiocin postloaded to ND were performed by project student Noha Abou El Magd.

The analysis of novobiocin preloaded and postloaded to ND, *via* SEC, produced narrow peaks, that coincided with the trace characteristic to ND, and confirmed the drug loading (Figure 3.19, A). However, polydispersity within the sample was observed for novobiocin preloaded to ND, generated, probably, either by overtime aggregation or by interactions between drug molecules and the lipid bilayer (Figure 3.19, B). The release rate of preloaded novobiocin further investigated has demonstrated that release did not go to completion within 24 h - $t_{1/2}$ was $9.8 \text{ h} \pm 0.9$ (Figure 3.20, A). Due to its low incorporation rate into ND (2 molecules loaded per ND; determined by HPLC - Figure 8.12), log P and the predicted solubility, it can be deduced that the drug has neither a preference for the aqueous or organic phase. Although the drug exhibited poor loading within ND, this prolonged release could allow the delivery of novobiocin to the site of action without significant drug loss.

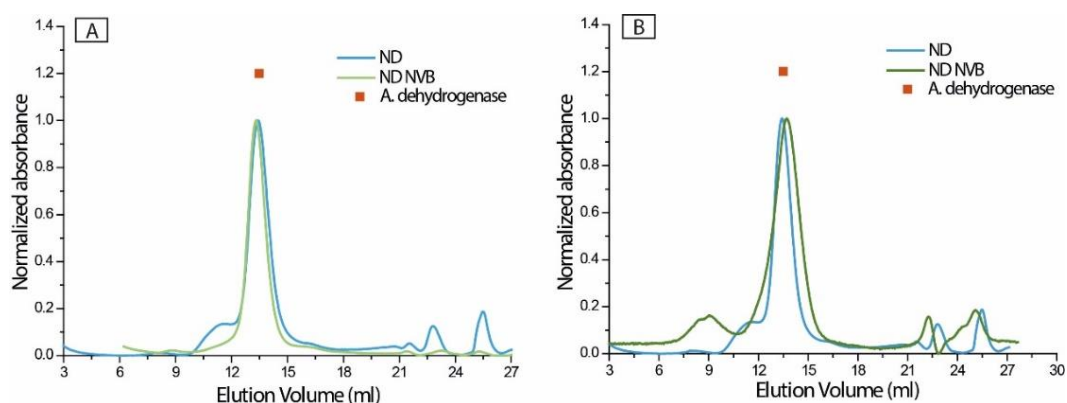


Figure 3.19 SEC chromatograms of ND, ND NVB and the elution time of AD: A - NVB was postloaded to ND; B - NVB was preloaded to ND; assemblies reconstituted using method B; ND and AD were measured at 280 nm, ND NVB were measured at 324 nm

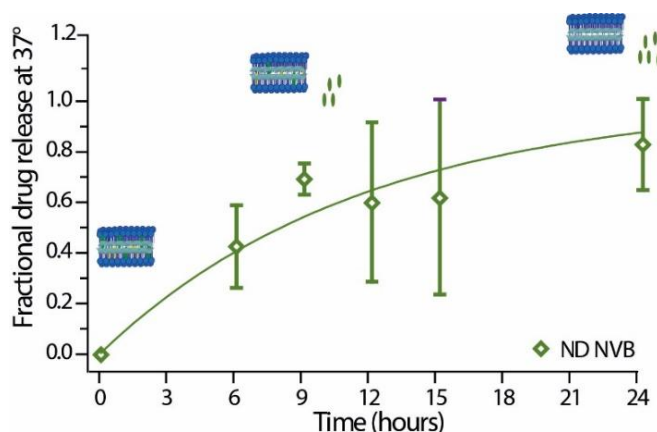


Figure 3.20 Fractional NVB release at 37 °C from ND NVB; NVB was preloaded to ND; the aliquots were measured at 324 nm; $t_{1/2}$ value is 9.8 h \pm 0.9; data is shown as the mean \pm SD

3.2.6 Nanodiscs loaded with camptothecin

Camptothecin (CPT) is a heterocyclic compound investigated for the treatment of cancer. Although its anticancer activity was demonstrated in preliminary clinical trials, camptothecin is also known for its adverse side effects and low water solubility (0.511 mg/mL).

The ND CPT analysis by SEC revealed an increase in the apparent MW presumably caused by camptothecin incorporation into ND (238 kDa the MW of ND CPT) (Figure 3.21). However, the majority of unincorporated camptothecin eluted later as a single peak. These conclusions as well as the later calculated loaded drug per ND *via* HPLC (0.24 molecules per ND, Figure 8.14) suggested a low incorporation efficiency. Despite the poor incorporation of camptothecin into ND, an apparent 100% drug release was observed. The equilibrium between concentrations of loaded and free camptothecin was achieved within 24 h - $t_{1/2}$ was 13.8 h \pm 3.2 (Figure 3.22, B). Drug exhibited a gradual sustained release pattern and no initial burst. This could potentially be associated with total drug incorporation, despite only 0.24 molecules of camptothecin being loaded per ND.

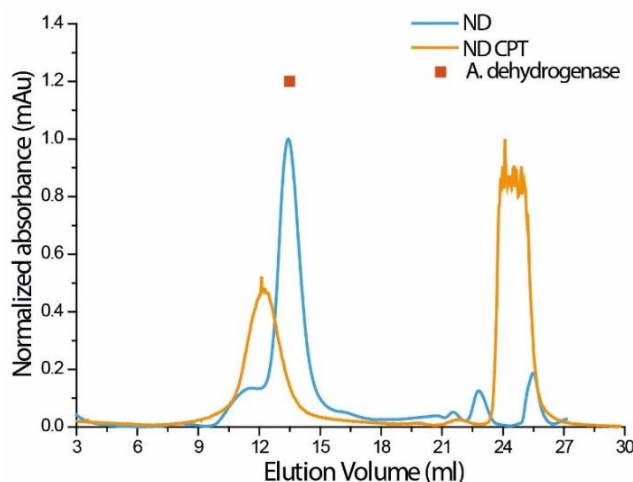


Figure 3.21 SEC chromatograms of ND, ND CPT and the elution time of AD; CPT was preloaded to ND, reconstituted *via* method B; ND and AD were measured at 280 nm, ND CPT was measured at 218 nm

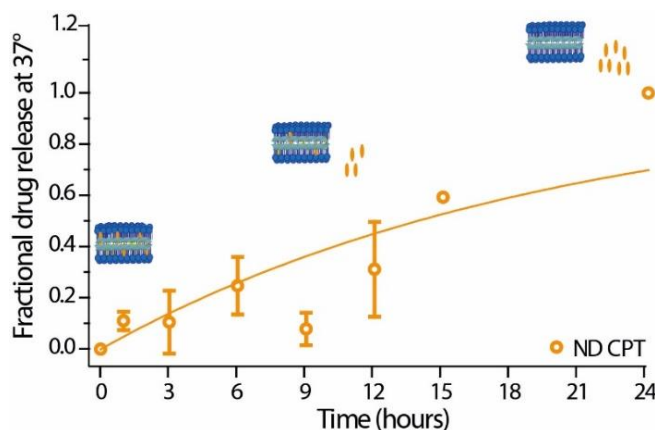


Figure 3.22 Fractional CPT release at 37 °C from ND; CPT was preloaded to ND; the aliquots were measured at 218 nm; $t_{1/2}$ was 13.8 h \pm 3.2; data is shown as the mean \pm SD

3.2.7 Nanodiscs loaded with tamoxifen

Tamoxifen (TMX) is a nonsteroidal agent that binds to estrogen receptors, with relevance in the treatment of metastatic breast cancer. Tamoxifen is extensively metabolised and has a water solubility value of 1.02 $\mu\text{g/mL}$.

On the SEC chromatogram of tamoxifen preincorporated to ND, the formation of ND assemblies and clusters of unincorporated drug was observed (Figure 3.23). The absorbance used (277 nm) – close to MSP absorbance (280 nm) – might suggest the reconstitution of either empty ND or drug loaded ND with poor incorporation efficiency. This possibility was emphasised by the

low amount of tamoxifen per ND further calculated from HPLC (Figure 8.16) – 0.4 molecules per ND. Due to its poor incorporation and the previous inconclusive observations on the release of novobiocin and camptothecin - with similar poor incorporation – it was decided not to examine the rate of tamoxifen release from ND.

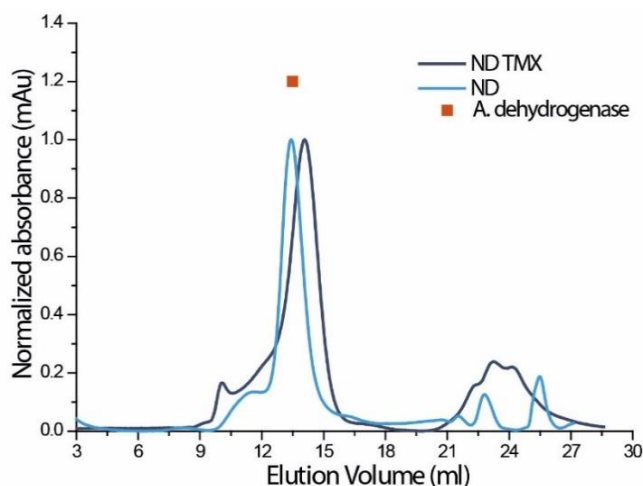


Figure 3.23 SEC chromatograms of ND, ND TMX and the elution time of AD; TMX was preloaded to ND, reconstituted *via* method B; ND and AD were measured at 280 nm, ND TMX was measured at 277 nm

3.2.8 Nanodiscs loaded with clofazimine

Clofazimine (CLF), a riminophenazine dye, has similar water solubility to amiodarone (1.51 $\mu\text{g/mL}$) and is used for the treatment of leprosy. Therefore, clofazimine was a suitable candidate for loading and release from ND systems.

After clofazimine was postloaded to ND using method B of reconstitution, analysis *via* SEC indicated an increase in the apparent MW caused by clofazimine incorporation (306 kDa MW of ND CLF) (Figure 3.24). The reason for the difference in apparent MW could be associated with clofazimine molecules attaching to the surface of ND and creating an enlarged particle. HPLC analysis and subsequent calculations revealed 4 molecules of clofazimine incorporated per ND (Figure 8.17).

Although the initial investigation showed successful formation of ND, separation problems on SEC occurred when ND CLF were analysed. Visible red traces of free clofazimine were observed on the top filter of the gel filtration column. In

order to not contaminate other ND-drug samples, the investigation of ND CLF was interrupted.

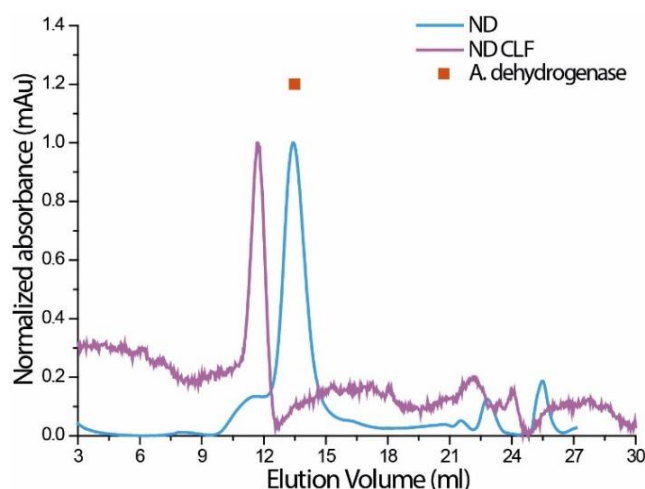


Figure 3.24 SEC chromatograms of ND, ND CLF and the elution time of AD; CLF was preloaded to ND and reconstituted *via* method B; ND and AD were measured at 280 nm, ND CLF was measured at 486 nm

3.2.9 Nanodiscs loaded with indomethacin

Indomethacin (IND) is an anti-inflammatory agent for which the water solubility can be varied with temperature.¹¹⁰ When indomethacin was preloaded into ND, the SEC chromatogram showed the peak characteristic to drug loaded ND, corresponding to an apparent MW calculated at 252 kDa (Figure 3.25). A trail with high absorbance was observed at a later retention volume. This was attributed to aggregates of unincorporated indomethacin. The observation concluded was that probably ND was solubilising very little indomethacin. However, the subsequent inefficiency to quantify the number of molecules per ND *via* HPLC (Figure 8.18) made the investigation inaccessible. Therefore, observation on the release rate was further interrupted.

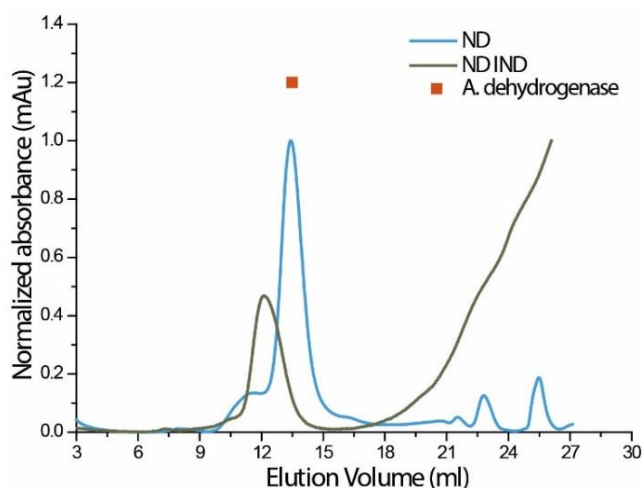


Figure 3.25 SEC chromatograms of ND, ND IND and the elution time of AD; IND was preloaded to ND, reconstituted *via* method B; ND and AD were measured at 280 nm, ND IND was measured at 318 nm

3.2.10 Nanodiscs loaded with fluorescein, chloroquine, oxymethazoline and rimantadine

Fluorescein (FLC) is a synthetic organic compound used as a fluorescent tracer for many applications. Chloroquine (CLQ) is an aminoquinoline derivate with water solubility of 17.5 $\mu\text{g/mL}$, used as anti-malarial drug. Oxymethazoline (OXM) is a 260 Da compound from phenylpropanes class, mainly used for the treatment of nasal congestions. Rimantadine (RMD), a cyclic amine with 9.15 $\mu\text{g/mL}$ water solubility, is a synthetic antiviral drug which acts by disrupting the membrane.

After analysing the ND-drug systems by SEC, these drugs were grouped because of their unsuccessful incorporation into the ND system. For example, the chromatograms of fluorescein postloaded to ND, regardless of the molar ratio of reconstitution, indicated that despite ND formation, little fluorescein was loaded into ND. Most unincorporated fluorescein eluted as aggregates of free drug (Figure 3.26).

In the case of chloroquine, the incorporation within ND displayed similar outcomes – absence of drug loaded ND peak (Figure 3.27, A and C). However, the chromatograms analysed at 280 nm, revealed that ND assemblies were formed (data not shown), demonstrating that the drug incorporation process did not affect the formation of empty ND. Only the preloaded chloroquine-ND *via*

method B suggested the formation of drug loaded ND (Figure 3.27, B). The increase in apparent MW might have been caused by chloroquine incorporation (292 kDa the MW of ND CLQ). Presumably, chloroquine molecules bind weakly to the POPC head groups, and partially pack between the hydrocarbon chains of the phospholipid domain. A low incorporation efficiency is suggested by the height of ND peak compared to the peaks associated with polydisperse aggregates of POPC, chloroquine and oligomeric protein, and unloaded free chloroquine.

The SEC analysis found that oxymethazoline postincorporated to ND led to the formation of ND-drug with an apparent MW of 272 kDa and of aggregates composed of oxymethazoline, POPC and MSP in different proportions – from void volume aggregates to clusters of free drug (Figure 3.28, A). The SEC chromatogram of oxymethazoline preloaded to ND, revealed that the majority of drug was eliminated as free drug molecules (Figure 3.28, B). The peak characteristic to ND was seen eluted, but the relatively low absorbance indicated that only a small quantity of oxymethazoline was incorporated into the assemblies.

For rimantadine preincorporated into ND, the investigation led to the belief that rimantadine loading generated deformations of the lipid bilayer within ND, contributing to the formation of aggregates. Nevertheless, the presence of the two peaks eluted later suggested few enlarged particle aggregates and smaller species, respectively (Figure 3.29).

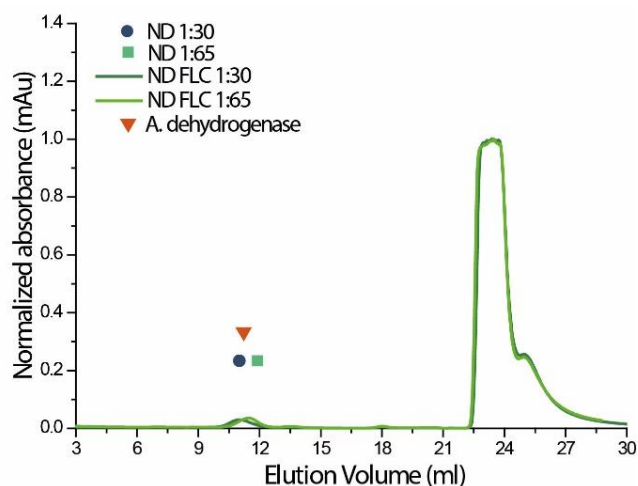


Figure 3.26 SEC chromatograms of ND, ND FLC and the elution time of AD; assemblies were reconstituted using method A and 1:30 and 1:65 molar ratios, FLC was postloaded to ND; all samples were measured at 280 nm

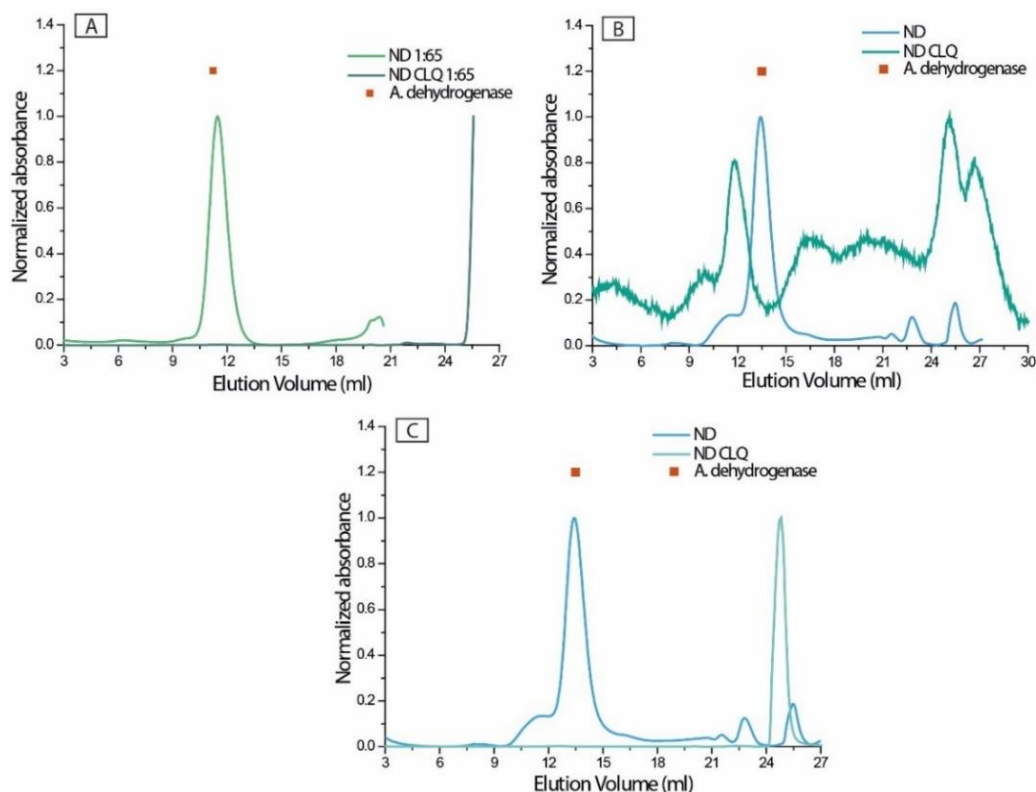


Figure 3.27 SEC chromatograms of ND CLQ, ND and the elution time of AD: A - assemblies were reconstituted with method A.; B and C - assemblies were reconstituted with method B; A and B – CLQ was preloaded to ND; C - CLQ was postloaded to ND; ND and AD were measured at 280 nm, ND CLQ was measured at 343 nm

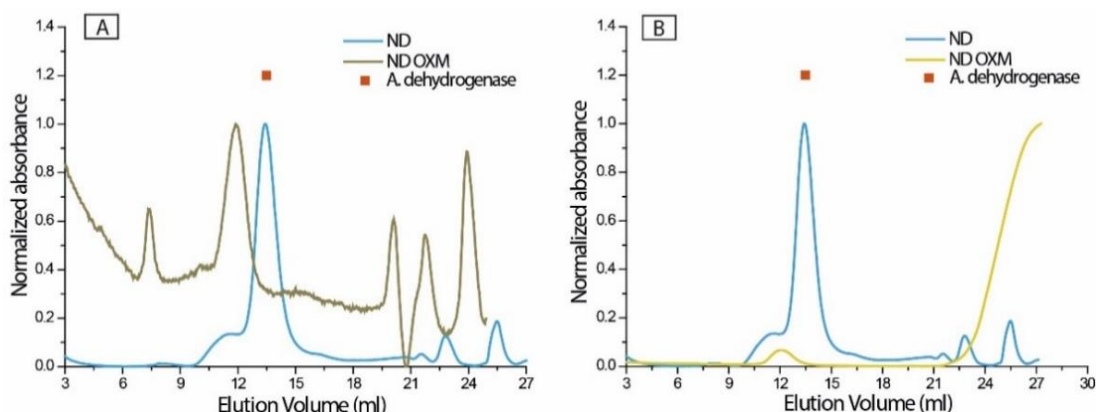


Figure 3.28 SEC chromatograms of ND, ND OXM and the elution time of AD: A - OXM was postloaded to ND; B - OXM was preloaded to ND; assemblies were reconstituted *via* method B; ND and AD were measured at 280 nm, ND OXM was measured at 315 nm

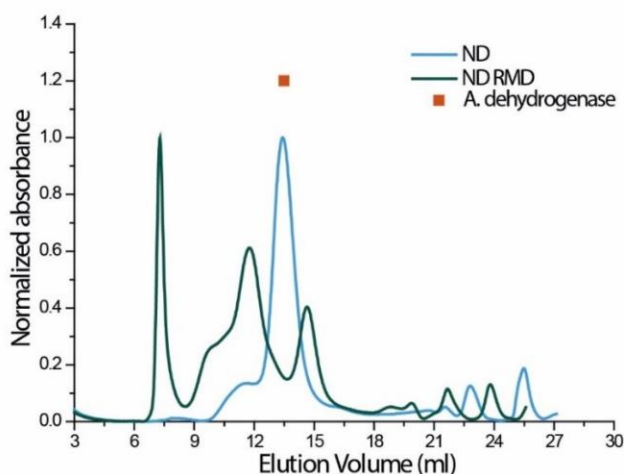


Figure 3.29 SEC chromatograms of ND, ND RMD and the elution time of AD; RMD was preloaded to ND; assemblies were reconstituted using method B; all samples were measured at 280 nm

3.3 Which drugs are incorporated?

The investigation of drug loaded ND assemblies on SEC was the first important step in dividing the hydrophobic drug molecules into groups of molecules with different selectivity towards loading into ND. The second divider was their subsequent analysis on HPLC, in order to calculate the number of molecules incorporated per ND. Following this classification, the release rate of drug molecules (chosen from three groups) was observed.

In the tables presented below, the hydrophobic small molecules have been separated into five different groups. Table 3.8 and Table 3.9 show six

hydrophobic molecules successfully loaded within ND. For the hydrophobic molecules represented in Table 3.9, the apparent number of molecules loaded could not be determined due to separation problems on SEC and HPLC. Table 3.10 shows three hydrophobic molecules with poor incorporation within the ND; all three tables contain the properties of the drugs analysed and their $t_{1/2}$ values. Table 3.11 and Table 3.12 show three hydrophobic molecules with unsuccessful loading into ND, their properties and the impact drug incorporation had over the formulation or disruption of ND assemblies, respectively.

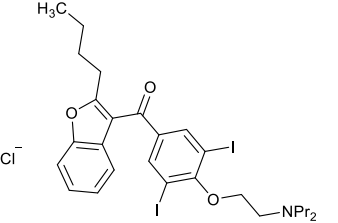
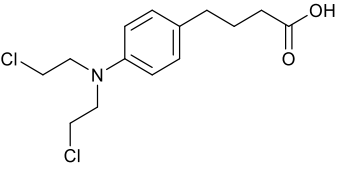
Drug	Structure	Log P	Isoelectric point	MW /gmol ⁻¹	Solubility in water/ g/L	Physiological charge	Apparent molecules of drug loaded	Half-life t _{1/2} value/ h
AMD		7.9	-	645.3	4.76×10 ⁻³	+1	10 ± 6.8 ¹ 5.8 ± 2.5 ² 9.5 ± 2 ³	5.4 ± 0.67 ¹ 0.88 ± 0.03 ² 0.6 ± 0.14 ³
CLB ¹		3.8	3.08	304.2	12.4	-1	6.5 ± 1.7	5.8 ± 0.48

Table 3.8: Table of hydrophobic molecules with successful loading within ND, their properties¹¹⁰ and results from incorporation and release from the ND systems; ¹drugs were preloaded to ND; ²drug were postloaded to ND reconstituted with 1:50; ³drug were postloaded to ND reconstituted with 1:65

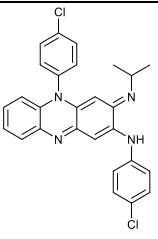
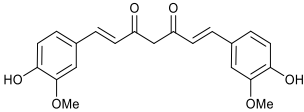
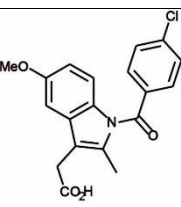
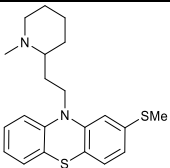
Drug	Structure	Log P	Isoelectric point	MW /gmol ⁻¹	Solubility in water /g/L	Physiological charge	Half-life t _{1/2} value/ h
CLF ^{3,i}		7.6	10.84	473.4	2.25×10 ⁻⁴	+1	-
CCM ⁱ		3.6	-	368.4	6×10 ⁻⁴ ¹¹¹	0	3.9 ± 1.3 ² 7.4 ± 0.4 ³
IND ^{1,ii}		4.2	0.77	357.8	9.37×10 ⁻⁴ at 25 °C	-1	-
TRD ^{1,ii}		5.9	-	370.5	3.36×10 ⁻⁵	+1	3 ± 0.33

Table 3.9 Table of hydrophobic molecules with successful loading within ND and their properties^{110, 112}; apparent molecules of drug loaded could not be determined due to separation problems on SECⁱ and HPLCⁱⁱ; ¹drugs were preloaded to ND; ²drug were postloaded to ND reconstituted with 1:50; ³drug were postloaded to ND reconstituted with 1:65

Drug	Structure	Log P	Isoelectric point	MW /gmol ⁻¹	Solubility in water /g/L	Physiological charge	Apparent molecules of drug loaded	Half-life t _{1/2} value/ h
NVB		4.1	1.92	612.6	9.66×10 ⁻³	-1	2	9.8 ± 0.9
TMX		7.1	-	371.5	1.76×10 ⁻⁴ at 25 °C	+1	0.4	-
CPT		2	7.39	348.3	5.11×10 ⁻¹	0	0.24	13.8 ± 3.2

Table 3.10 Table of hydrophobic molecules with poor loading within ND, with their properties¹¹⁰ and results from incorporation and release from the ND systems; all drugs were preloaded to ND

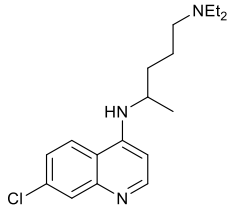
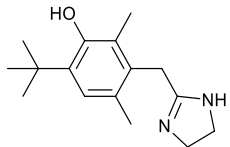
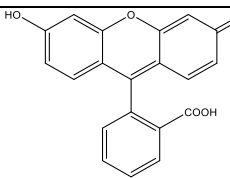
Drug	Structure	Log P	Isoelectric point	MW /gmol ⁻¹	Solubility in water g/L	Physiological charge
CLQ		4.3	-	515.9	1.06×10 ⁻⁴	+2
OXM		3.4	10.47	260.4	5.15×10 ⁻²	+1
FLC		3.88	2.4	332.3	0.0255	0

Table 3.11 Table of hydrophobic molecules with unsuccessful loading and their properties;¹¹⁰ all drugs were preloaded to ND; drug incorporation did not affect the formulation of ND assemblies

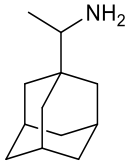
Drug	Structure	Log P	Isoelectric point	MW /gmol ⁻¹	Solubility in water/ g/L	Physiological charge
RMD		3.2	-	179.3	9.15×10 ⁻³	+1

Table 3.12 Table of hydrophobic molecules with unsuccessful loading and their properties;¹¹⁰ drug was preloaded to ND; drug incorporation disrupted the formulation of ND assemblies

The SEC and HPLC analyses showed that the ND systems had favourable results when loading amiodarone and chlorambucil. Amiodarone also exhibited much slower release from ND, when was preloaded using method B of reconstitution. An understanding of the selectivity of amiodarone and chlorambucil for preferential loading within the phospholipid domain can be associated with their log P and insolubility in water (Figure 3.30, Figure 3.31).

These are causing the phospholipids within the ND to bond the drug molecules primarily by hydrophobic interactions.

Other drugs such as tamoxifen, novobiocin and camptothecin, with similar log P and MW as amiodarone and chlorambucil (Figure 3.30, Figure 3.32), had a much lower preference to loading within ND. The reason as to why the molecules had poor incorporation can be that tamoxifen has a bulky rigid structure with three aromatic rings, which would give less flexibility when packing within the phospholipid domain. In the case of novobiocin, a presumable explanation would be that the drug interacts only with the head groups of POPC arranging itself on the surface of the bilayer. Although camptothecin has a long structure consisted of chains of cyclic and aromatic rings, it has a low hydrophobicity and comparatively high water solubility (Figure 3.31) making it less suitable to be packed between the lipid hydrocarbon chains.

Although showing successful incorporation, the apparent molecules of thioridazine, indomethacin, curcumin and clofazimine loaded could not be determined due to separation problems. Clofazimine and curcumin were difficult to work with because of solubility problems caused during the SEC experiments. As regards to thioridazine and indomethacin, the obstacle in quantifying the number of molecules incorporated was found during analysis *via* HPLC, as the elution time for drugs coincided with the elution time of MSP. Thioridazine had a relatively low half-life of $3 \text{ h} \pm 0.33$ for a molecule with such low water solubility and high log P. An apparent 100% release profile was also observed, probably associated with the high capacity of the buffer used to solubilise the free drug

The hydrophobic drugs, listed in Table 3.11 and Table 3.12 and having a Log P between 3 and 4.5, but a broad range of water solubility and MW, were proven unsuccessful after the samples were studied on SEC (Figure 3.30 to Figure 3.32, grey rotated triangles). This observation was reached from the small-scale or absence of a ND-drug peak at the elution time of ND, although empty ND formation was noticed. The experiments conducted with rimantadine showed the drug disassembled almost all the ND systems - a small peak present at ND

elution time compared to a much longer peak in the void volume. This result is unsurprising as rimantadine - an antiviral agent with bulky, non-planar molecular geometry – may be disrupting the POPC membrane and forming aggregates with the scaffold protein and POPC.

In the case of chloroquine and oxymethazoline empty ND were formed. Chloroquine had an unsuccessful rate of loading probably due to its compact structure and aromatic rings which makes it more rigid and therefore less likely for favourable packing within the lipid bilayer. The results arising from the unsuccessful loading of oxymethazoline were associated with the anchoring site being too small, leading to weak interactions with the head groups of phospholipids.

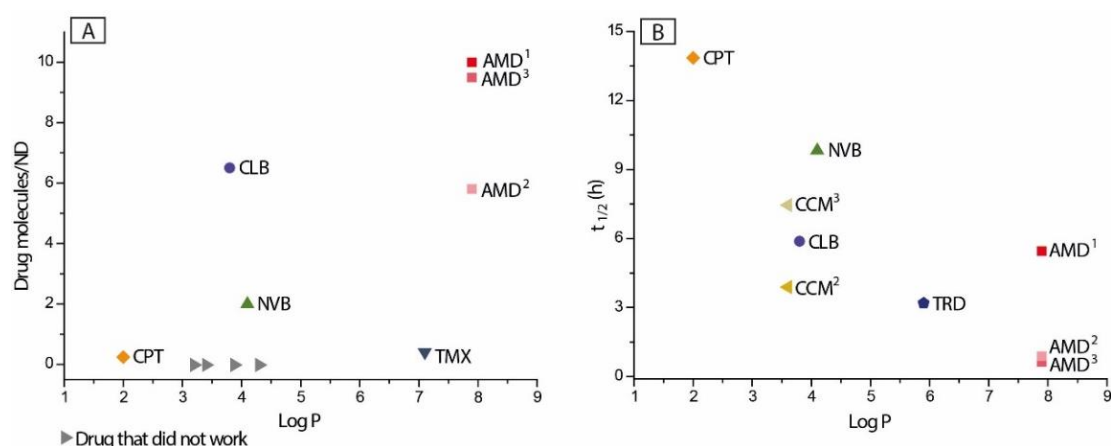


Figure 3.30 A - Relation between Log P of the hydrophobic drugs and the number of molecules incorporated per ND; B - Relation between Log P of the hydrophobic drugs and t_{1/2}; ¹ and unmarked drugs were preloaded to ND; ²drug were postloaded to ND reconstituted with 1:50; ³drug were postloaded to ND reconstituted with 1:65

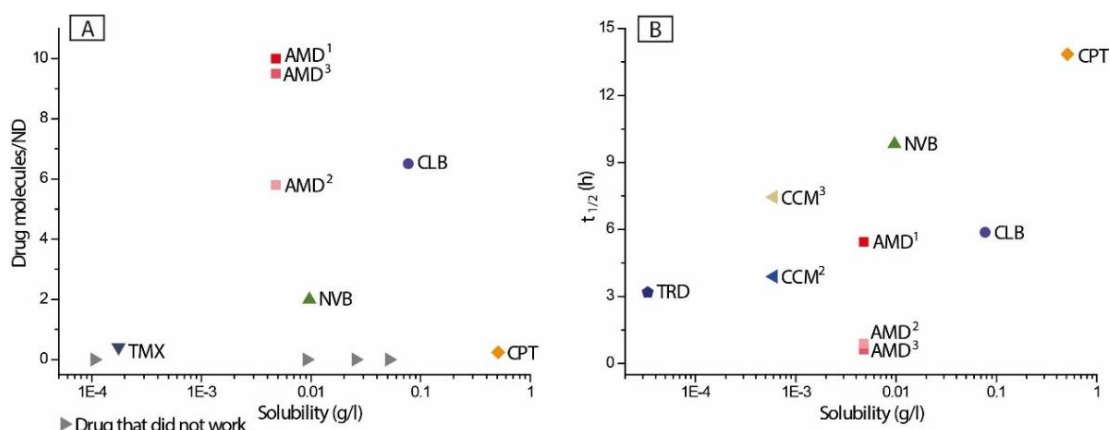


Figure 3.31 A - Relation between water solubility of the hydrophobic drugs and the number of molecules incorporated per ND; B - Relation between water solubility of the hydrophobic drugs and $t_{1/2}$; ¹ and unmarked drugs were preloaded to ND; ² drug were postloaded to ND reconstituted with 1:50; ³ drug were postloaded to ND reconstituted with 1:65

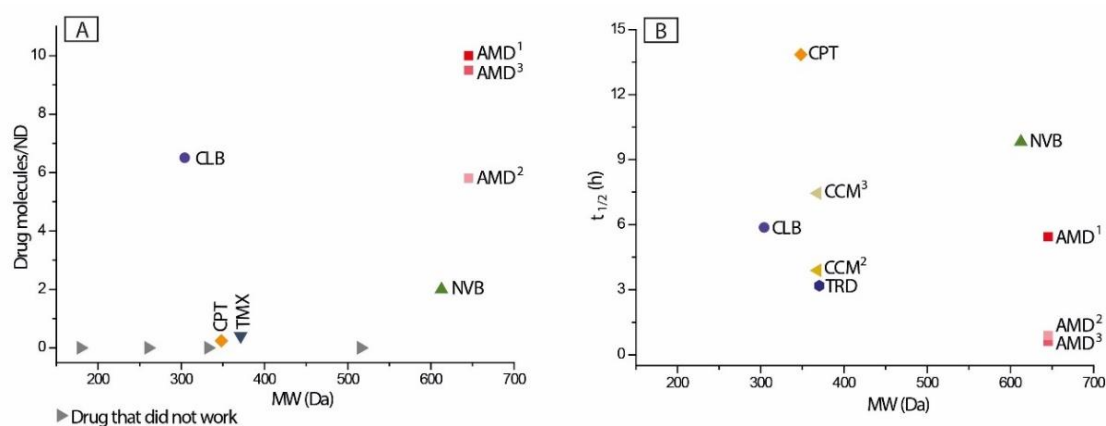


Figure 3.32 A - Relation between MW of the hydrophobic drugs and the number of molecules incorporated per ND; B - Relation between MW of the hydrophobic drugs and $t_{1/2}$; ¹ and unmarked drugs were preloaded to ND; ² drug were postloaded to NDs reconstituted with 1:50; ³ drug were postloaded to ND reconstituted with 1:65

It was difficult to establish simple criteria by which hydrophobic drug molecules with different physico-chemical properties would be incorporated and released from the ND assemblies. Many considerations had to be taken in account when incorporating the drug molecules into ND. Their loading capacity was not only determined by their insolubility in water and MW but also by the interactions with the hydrophilic head groups and hydrophobic hydrocarbon chains of the phospholipids within the ND. Additional investigations *via* SAXS analysis were

required for a better understanding of the interactions between drug molecules and the phospholipid domain of ND systems.

3.4 SAXS investigation of drug loaded MLV and ULV

For this investigation, the MSP component was removed from the systems as our previous experiments demonstrated no considerable interaction between the drugs and MSP. Thus, the ND were replaced with multilamellar vesicles of POPC, suspended in deionised water, and used to incorporate the drug molecules. The multilamellar vesicles (MLV) and unilamellar vesicles (ULV) were used as model membrane systems for the loading of amiodarone, chlorambucil, indomethacin, tamoxifen and rimantadine. Drug loaded systems were analysed by small angle X-ray scattering (SAXS) for a better understanding of the influence drug incorporation has on the model membranes. The measurements and subsequent analysis of the scattering patterns were done by Dr. Amin Dilmaghani, from School of Food Science and Nutrition, University of Leeds.

The collected data was fitted by applying the modified Caillé theory, previously described by Drasler *et al.*¹¹³ Examples of the obtained diffraction patterns for drug loaded POPC systems could be observed in Figure 3.33.

It is believed that amphiphilic molecules tend to partition at the lipid-water interface.¹¹⁴ Amiodarone, tamoxifen and rimantadine possess a positive physiological charge, due to the protonated amino group. The other two drugs investigated, chlorambucil and indomethacin, have a carboxyl group, that when deprotonated, gives a negative charge to the molecule. The fitting parameters subtracted after analysis of SAXS patterns have indicated that the ratio of ULV to MLV formation is affected by the physiological charge of the incorporated drugs. Subsequent to analysing the data, the ratio of ULV to MLV present in the sample, quantified by the fitting parameter N_{diff} (Table 3.13), was 1 for the model membrane system with positively charged drug molecules incorporated. This suggested that the presence of cationic drugs has led to the formation of a population composed entirely of ULV. Comparatively, when chlorambucil and indomethacin are incorporated into the model membrane, the formation of MLV

is observed. This was indicated by the values of N_{diff} being close to 0. More so, these conclusions are also indicated by the diffraction pattern of the POPC and drug loaded POPC systems (Figure 3.33). Two sharp peaks could be observed on the diffraction pattern of the samples containing the majority of MLV. In contrast, on the diffraction pattern of the samples consisting of ULV, the two peaks were replaced by a broad curve.

The electron density profile described by Gaussian distributions (Figure 3.34) was used to estimate the head group positions (z_H), and thus estimate the membrane thickness. When chlorambucil, indomethacin and amiodarone were incorporated into POPC systems, a decrease in the membrane thickness was observed. The decrease in membrane thickness could be related to the drug molecules disrupting the packing of the head group region due to partitioning close to the head group and water interface rather than near the hydrocarbon chains. However, the thickness of the POPC membrane was negligibly increased by the incorporation of tamoxifen and rimantadine. In addition, this perturbation of the membrane could be directly correlated with the efficiency of the drug loading within the phospholipid domain. For example, amiodarone loading, which led to the highest decrease in membrane thickness, was demonstrated to have the highest incorporation efficiency – 10 molecules per ND. Comparatively, lower decrease in membrane thickness generated by chlorambucil loading is associated with lesser number of drug molecules loaded per POPC domain – 6.5 molecules per ND. However, amiodarone and chlorambucil had similar release profiles, exhibiting no initial burst and having a half-life between 5 and 6 h, presumably demonstrating that the variation in membrane thickness did not affect the efficiency of their release.

In addition, POPC membrane fluctuations, given by the mean of inter-membrane distance, σ , were seen to increase by 29% when chlorambucil and indomethacin were incorporated into the bilayers. This has demonstrated that the incorporation of drug molecules into the POPC domain was correlated with an increase in membrane softness. The fluctuation of inter-membrane distance is obtained from the Caillé parameter, η , via the equation, described below.¹¹³:

$$\sigma = \sqrt{\eta} \times \frac{d}{\pi}$$

Equation 3.5 The relationship between Caillé parameter (η) and the mean fluctuation of inter-membrane distance (σ), d is the lamellar repeat distance (d -spacing in Table 3.13)

Fitting parameters	POPC	POPC CLB	POPC IND	POPC TMX	POPC RMD	POPC AMD
d-spacing/ nm	6.38	6.41	6.37	na	na	na
Number of layers	23	11	11	na	na	na
Caillé parameter, η	0.073	0.121	0.125	na	na	na
the mean fluctuation of inter-membrane distance, σ	0.55	0.71	0.72	na	na	na
The head group position, z_H / nm	1.83	1.76	1.79	1.85	1.84	1.67
Ndiff	0.0020	0.0071	0.074	1	1	1

Table 3.13 Table of fitted parameters subtracted after analysis of SAXS patterns, for empty POPC MLV, MLV loaded with CLB, IND, and ULV loaded with TMX, RMD and AMD; na – not applicable

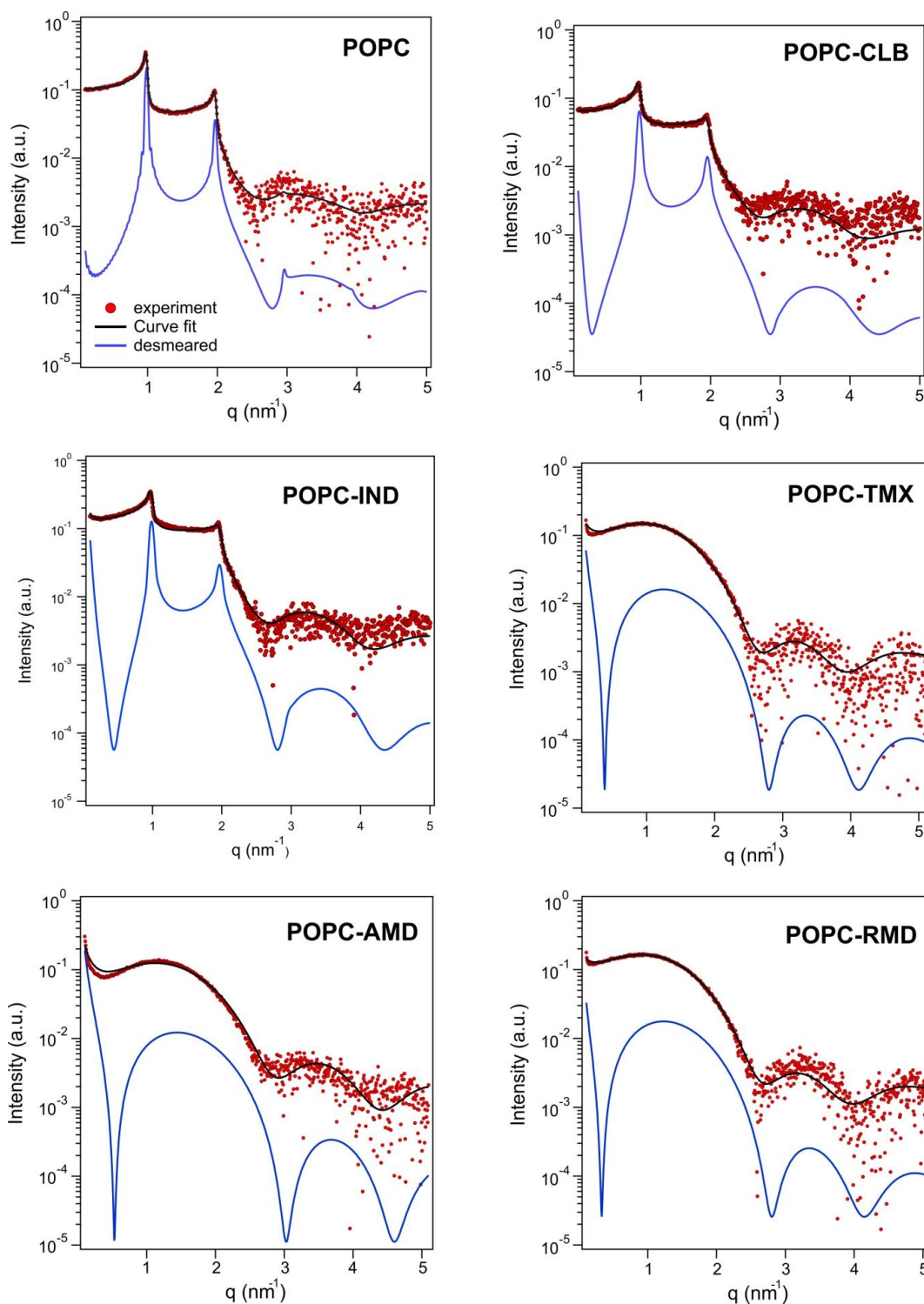


Figure 3.33 Diffraction pattern and corresponding fitting (black lines) and desmeared curves (blue lines). Data for POPC in deionized H_2O , POPC with CLB, IND, TMX, AMD and RMD; data was recorded at 25 °C

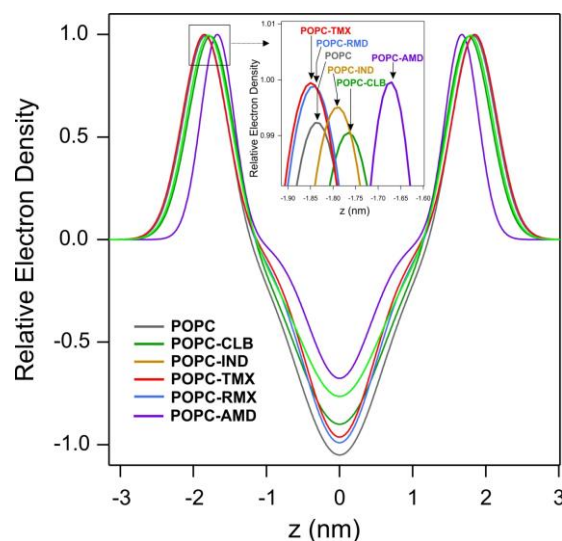


Figure 3.34 The electron density profile described by Gaussian distributions for empty POPC MLV, MLV loaded with CLB, IND, and ULV loaded with TMX, RMD and AMD

3.5 Summary

Because of favourable properties for loading into ND, twelve hydrophobic drug molecules were investigated. This was successfully done in order to generate the optimum conditions for incorporation and release, and to determine the impact their incorporation has on the size and structure of the ND systems.

The protocol for ND assembly was adapted to load the hydrophobic drugs into the systems arranging the components into a discoidal bilayer with the drug molecules loaded into the phospholipid domain. The optimised protocol showed an increase in drug incorporated per ND and a slower release rate.

Following the drug loading, a series of techniques used to characterise the ND-drug assemblies have demonstrated the influence drug incorporation has on the MW and size of the assemblies, and on the secondary structure of the scaffold protein that forms the protein belt.

Subsequently, an optimised method of characterisation, using HPLC, was developed to accurately determine the amount of hydrophobic small molecules loaded into ND. Consecutively, the drug molecules were separated into groups based on their loading capability and the rate of release from ND. The separation gave insights on the influence of drug properties on the incorporation and release from ND.

The analysis of SAXS patterns suggested that incorporation of amiodarone, rimantadine and tamoxifen (positive physiological charge) into POPC model membranes has led to the formation of ULV. Whereas, incorporating chlorambucil and indomethacin (negative physiological charge) into POPC model membranes resulted in MLV formation. The incorporation of chlorambucil and indomethacin has increased the fluctuation inter-membrane distance by around 30% and decreased the membrane thickness. For amiodarone and chlorambucil incorporation, this decrease in membrane thickness was seen to be correlated with the efficiency of drug loading within the POPC bilayer.

4 Chapter 4

4.1 Part I – Influence of lipid composition on drug incorporation

4.1.1 Introduction

Nanodiscs can be readily formed using POPC, and can be loaded with a variety of drugs. However, little is known about the effect of variation in lipid composition, either on ND formation or drug loading. In the following chapter the effect of lipid composition on the incorporation and release of amiodarone and chlorambucil from ND was investigated.

Amiodarone and chlorambucil molecules were incorporated into lipid, MSP and detergent micelles, following the method of preloading drug into ND reconstituted *via* method B. This method involved loading the drug molecules during the reconstitution of ND, as previously described in Chapter 3. Briefly, the drug molecules were dried with various lipid compositions (Table 4.1), into a thin film. Subsequently, by addition of MSP/detergent, the drug molecules incorporated into lipid, MSP and detergent micelles, were incubated at 4 °C. The exception was ND reconstituted with DPPC, for which the mixture was incubated at 42 °C. After detergent removal, the assembly process between the MSP, POPC and drug molecules started. The unincorporated drug was then eliminated by SEC analysis. A series of methods - SEC, DLS, HPLC and UV-spectroscopy – were applied to investigate the influence of lipid composition on the efficiency of the drug loading process and drug release kinetics.

Lipid composition within ND	Physical properties of the bilayer domain within ND
POPC ¹¹⁵	The surface has no net charge
POPS (up to 50%)	Alter the charge density
DLPC ¹¹⁶	Create thinner membrane like systems
DPPC ¹¹⁵	Form gel phase ND at room temperature
DOPE PEG550 ¹¹⁷ (10%)	Steric protection of the ND

Table 4.1 Table of lipid compositions and their properties within the ND

Four distinct lipid mixtures were considered, each used to supplement the POPC in the reconstitution of ND. The first mixture of phospholipids consisted of negatively charged phosphatidylserine and zwitterionic phosphatidylcholine. The presence of anionic 1-palmitoyl- 2-oleoyl-*sn*-glycero-3-phospho-L-serine (POPS) (Figure 4.1) in the bilayer could potentially create a more stable system. This could be due to the favourable electrostatic interactions between the positively charged residues present in MSP and the negatively charged PS head group of the lipid.¹¹⁸ In addition, the inter-nanodisc repulsion, given by the high net charge of ND, would likely prevent aggregation. The variation in lipid composition, with up to 100% POPS in reconstituted ND, was frequently studied in literature by groups of researchers, describing the positive effect these anionic lipids have on binding membrane-associated signalling molecules to the bilayer surface.^{87, 91, 119}

The second mixture of phospholipids used to reconstitute ND was by adding to the zwitterionic phosphatidylcholine, a PEGylated phosphoethanolamine. In order to facilitate the reconstitution of ND with a favourable lipid distribution and no other large conglomerates,¹²⁰ 10% PEGylated 1,2 – dioleoyl - *sn*-glycero- 3 – phosphoethanolamine - N - [methoxy (polyethylene glycol) - 550] (DOPE PEG550) was used (Figure 4.1). The incorporation of PEG into lipid structures was often used by researchers to protect the lipid surface by creating a steric barrier, and increase the blood circulation time of the carrier. Additionally, it was demonstrated by Johansson *et al.* that the distribution of drug molecules at the water/membrane interface reaches equilibrium regardless of the PEGylated lipid composition in the membrane.¹²¹

The first lipid composition to replace POPC entirely was another zwitterionic phosphatidylcholine lipid. In this case, the lipid, 1, 2-dilauroyl-*sn*-glycero-3-phosphocholine (DLPC), has smaller, saturated hydrocarbon chains (Figure 4.1). The presence of DLPC in the bilayer would create thinner bilayer that could potentially favour the incorporation of drugs with small MW. Additionally, the preloading of positively and negatively charged drug molecules could influence the favourable packing within the bilayer, leading to the reconstitution of stable and monodisperse assemblies. In literature, researchers have often used, in their studies, ND reconstituted with DLPC to investigate membrane proteins.^{122, 123}

To reconstitute the assemblies, the POPC composition was, again, replaced with another zwitterionic phosphatidylcholine lipid. Here, the lipid, 1,2-dipalmitoyl-*sn*-glycero-3-phosphocholine (DPPC) has both its hydrocarbon chains saturated, and, due to the length of these acyl chains, a transition temperature of 41 °C (Figure 4.1). This high transition temperature implies that, at room temperature, the ND systems will be in a gel phase. An investigation was carried out on how the high temperature for reconstituting ND would affect the homogeneity of the assemblies and how stable the ND system would be after preloading drug molecules.

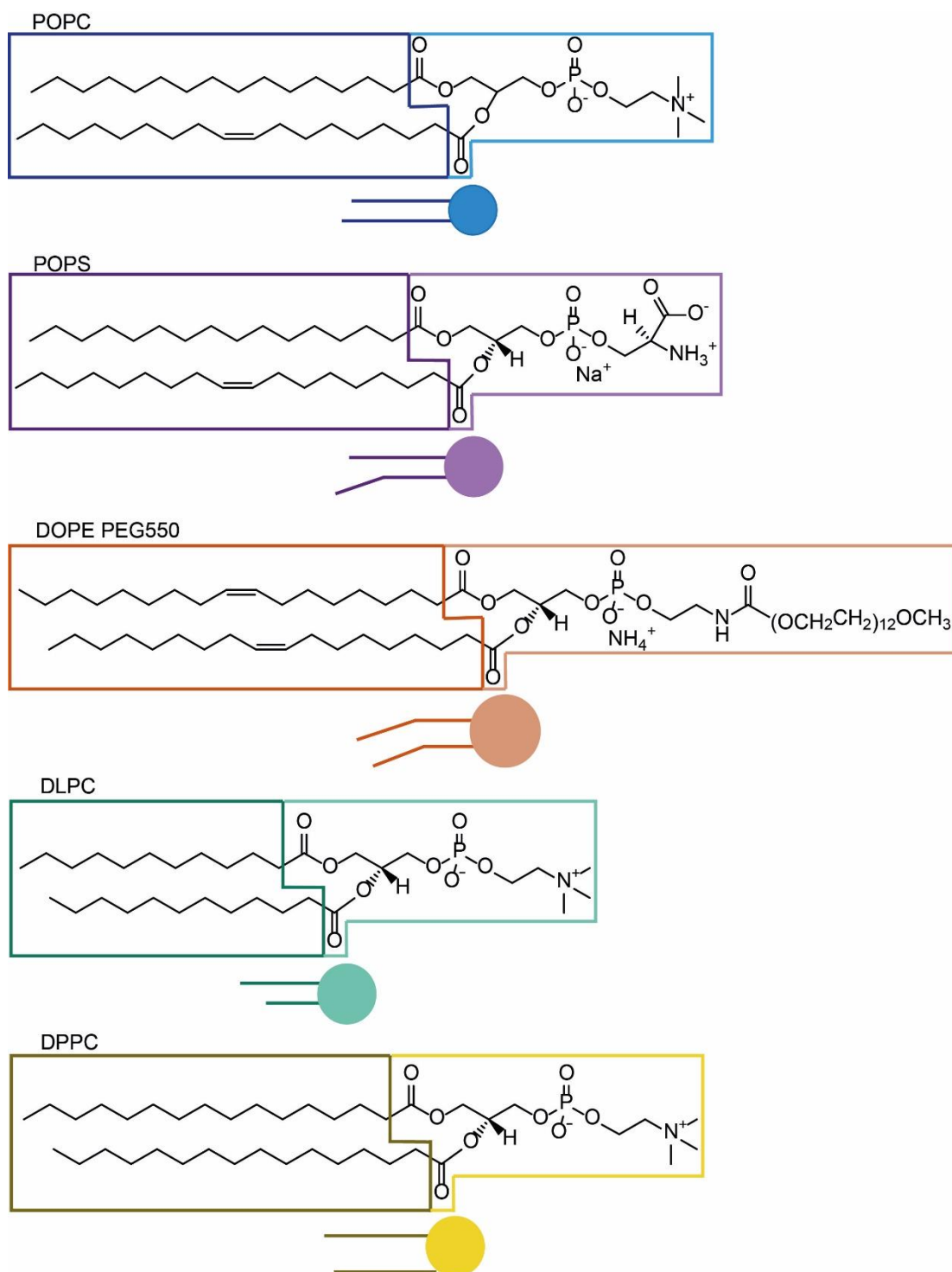


Figure 4.1 Structure of A – POPC; B - 1 - palmitoyl- 2 – oleoyl – *sn* – glycerol – 3 – phospho – L - serine (POPS) Transition Temp. 14 °C; C - 1, 2 - dioleoyl – *sn* – glycerol – 3 – phosphoethanolamine - N - [methoxy (polyethylene glycol)-550] (DOPE PEG550); D - 1, 2 – dilauroyl – *sn* – glycerol – 3 - phosphocholine (DLPC); Transition Temp. -2 °C; E - 1, 2 – dipalmitoyl – *sn* – glycerol – 3 - phosphocholine (DPPC); Transition Temp. 41 °C

4.1.2 Assemblies reconstituted with POPC: POPS

To confirm ND reconstitution and drug loading, the assemblies were analysed by SEC. Subsequently, the drug molecules were loaded in three quantities, for each drug, to the reconstitution mixture in order to observe the influence hydrophobic molecules incorporation has on the size and the formation of the ND assemblies.

4.1.2.1 The monodispersity and size distribution of ND

Initial attempts to form empty ND led to a high yield of large lipid-MSP aggregates, as suggested, on the SEC chromatogram, by the presence of a broad peak with an attached shoulder (Figure 4.2, A). Consistent with literature findings,¹²⁴ the remaining detergent molecules generated instability during ND formation, which resulted in the reconstitution of large spherical and polydisperse assemblies. However, the assembly of monodisperse and stable ND was demonstrated after increasing the POPS composition to 50% and effectively remove the cholate to allow the discoidal self-assembly between lipids and MSP. Subsequently after separation of monodisperse ND from large aggregates, the size distribution of the system was investigated. The analysis of ND showed peaks corresponding to stable empty ND revealing a diameter of 10 nm, regardless of the POPS composition (Figure 4.3).

The chromatograms suggest an optimal amiodarone addition of less than 20 molecules, as the ND-drug peak relative to large lipid–protein–drug aggregates is maximised at this ratio (Figure 4.2, B). Additionally, these assemblies were seen to decrease in size from 10 nm, the diameter of empty ND (50% POPS), to 4.8 nm (Figure 4.3). This result is very unusual, because the diameter of ND is controlled by the MSP belt rather than the composition inside the bilayer domain. Increasing the number of amiodarone molecules led to alterations in the reconstitution of monodisperse assemblies. This was indicated by the height of void volume peaks. A presumable explanation could be that, at higher concentrations, rather than eluting as clusters of free drug, amiodarone formed clusters with the lipid head groups, leading to the ND surface being enlarged. This is consistent with literature studies, where high quantities of positively

charged thioridazine were found to create disorder within a POPC/POPS bilayer, resulting in expansion of the bilayer.¹²⁵

Analysing ND CLB *via* SEC showed that the incorporation of chlorambucil had similar results (Figure 4.2, C). At the lowest chlorambucil addition, the highest population of ND was observed, relative to other aggregates. Moreover, due to electrostatic repulsion with the anionic POPS, the drug molecules did not form large clusters eluted in the void volume. Instead, the excess chlorambucil, for all three ND CLB, was eliminated as free drug aggregates.

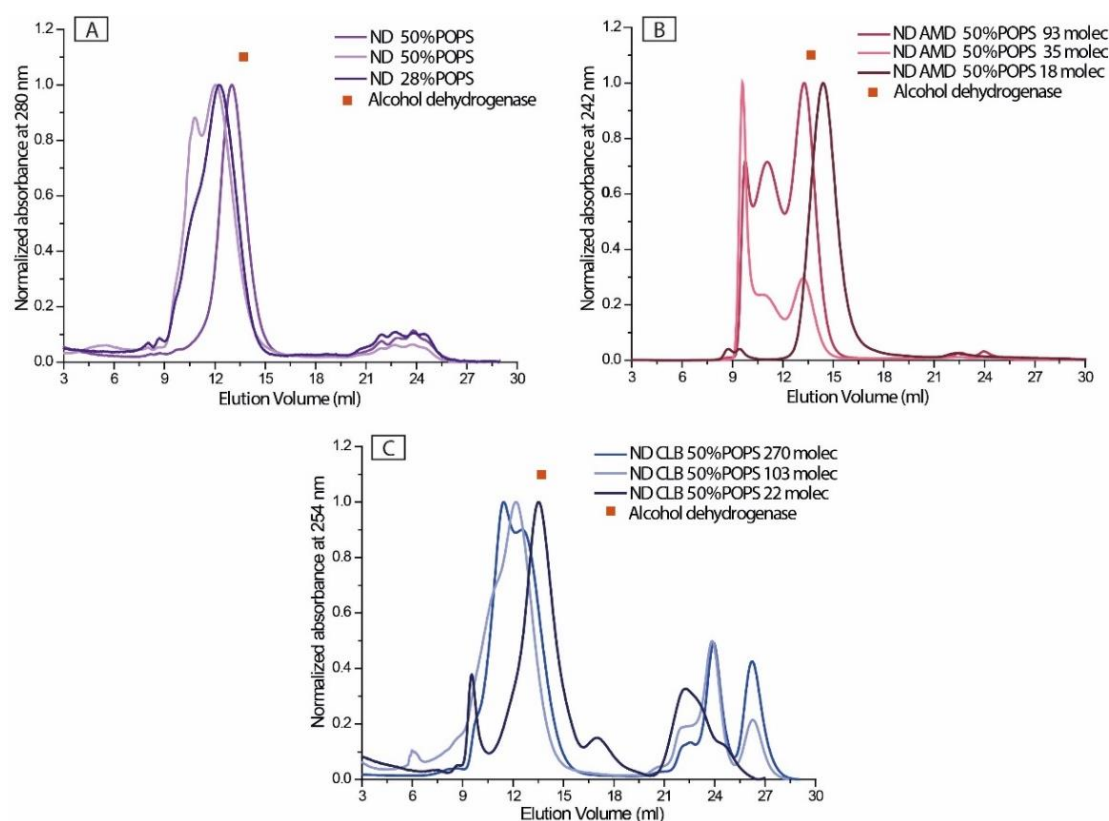


Figure 4.2 SEC chromatograms of empty ND, ND AMD, ND CLB and the elution time of AD: A - empty ND reconstituted with 28% and 50% POPS (280 nm); B - ND AMD reconstituted by preadding 93, 35 and 18 molecules of AMD (242 nm); C - ND CLB reconstituted by preloading 270, 103 and 22 molecules of CLB (254 nm)

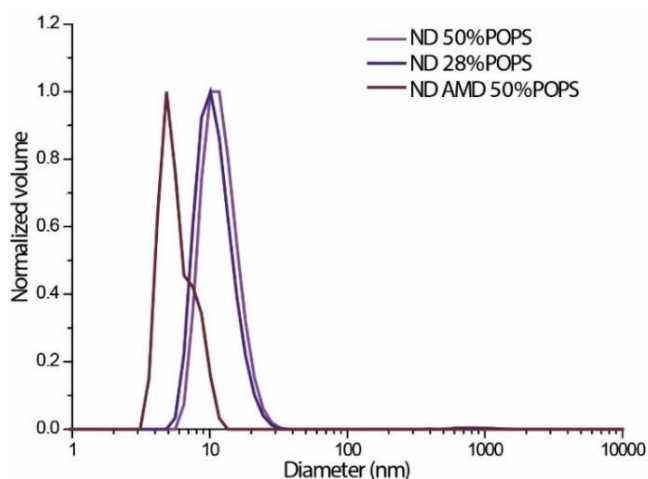


Figure 4.3 DLS of empty and amiodarone loaded ND, reconstituted with 28% and 50% POPS

4.1.2.2 Drug loading efficiency and release profile

The HPLC technique was used to investigate how many drug molecules were loaded within the ND (Figure 4.4). Following the protocol used in the HPLC analysis of drug loaded POPC ND, an accurate calculation of the number of drug molecules loaded per ND was obtained. Subsequently, the rate of drug release were observed on the drugs preloaded ND, as previously described in Chapter 3. As in the previous chapter, an exponential curve was fitted to the drug release data, and using a first order rate equation (Eq. 3.2) the fractional release and half-life of the drug molecules were calculated.

The release profile of amiodarone (1.9 ± 0.8 molecules loaded per ND) showed an initial burst effect, releasing around 60% of the preloaded drug within 3 hours (Figure 4.5, A). Following this burst, the amiodarone release reached a plateau. To interact with the phosphate groups of POPC, the drug molecules must travel further within the bilayer, pass the negatively charged POPS. Nevertheless, electrostatic interactions between POPS and amiodarone facilitated a prolonged anchoring of the drug at the lipid-water interface.¹²⁵ This resulted in the formation of clusters between amiodarone and the lipid head groups, eventually leading to an initial burst and the overall dissociation of only 60% amiodarone. A similar release was observed for amiodarone post-loaded into ND reconstituted with 1:50 MSP to POPC (100% POPC), for which the initial

burst was thought to be associated with amiodarone accumulation near the POPC head groups. The half-life of the drug, calculated from the rate parameter, was $1.75 \text{ h} \pm 0.8$.

In comparison, when chlorambucil was preloaded to ND (8.5 ± 3.8 molecules loaded per ND), the drug profile had a constant release that reached completion within 24 h (Figure 4.5, B). The half-life for chlorambucil was calculated to be $3.9 \text{ h} \pm 0.7$. This lower half-life, compared to ND reconstituted with 100% POPC, indicated a faster release rate associated with electrostatic repulsions between the two negatively charged molecules, chlorambucil and serine head group of POPS. Similarly, the high fluctuation in chlorambucil loading which might indicate instability during drug incorporation, were presumably the result of these repulsive forces between the drug and POPS.

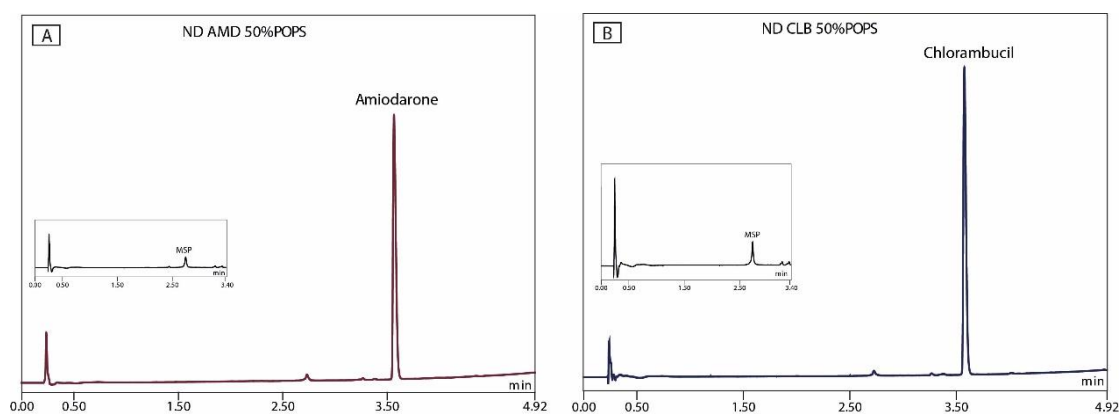


Figure 4.4 HPLC chromatograms of: A - ND AMD (242 nm) and B – ND CLB (254 nm) reconstituted, at 4 °C, with 50% POPS; the inside chromatograms are of the same samples measured at 280 nm to identify the MSP retention time

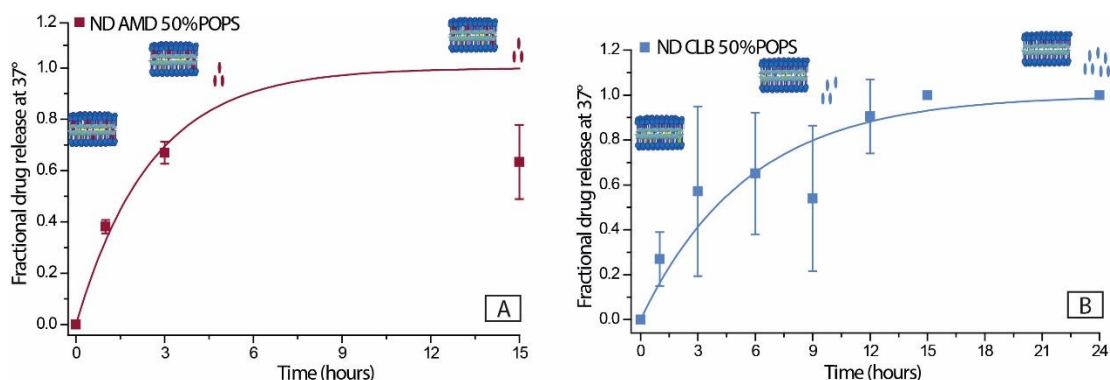


Figure 4.5 Fractional drug release at 37 °C from A - ND AMD (242 nm) and B – ND CLB (254 nm) reconstituted with 50% POPS; $t_{1/2}$ were A - $1.75 \text{ h} \pm 0.8$ and B - $3.9 \text{ h} \pm 0.7$

4.1.3 Assemblies reconstituted with 100% DLPC

4.1.3.1 The monodispersity and size distribution of ND

The reconstitution mixtures of empty ND assembled with 100% DLPC followed the same protocol, although the analysis indicated a lack of reproducible results. The chromatograms of empty ND suggested assemblies were formed with increased polydispersity (Figure 4.6, A). This is shown by the fluctuating width of the ND peak and the presence of a second peak, which could be attributed to monomeric protein assembled into conglomerates with few phospholipids (apparent MW of 38 kDa). However, based on the low absorbance of the second peak, ND are the predominant assemblies formed. Similar observations were seen when the reconstitution was repeated. Nevertheless, the proportionality between ND peak and 38 kDa clusters was lessened. An overall deduction would be that the MSP to DLPC molar ratio used in the ND reconstitution led to the assembly of unstable ND. As a result of keeping the MSP to lipid molar ratio constant (1:65), it was expected DLPC would form smaller ND, with a diameter of 7.5 nm.

The SEC chromatograms of amiodarone loaded ND showed that incorporating the amphiphilic molecules had an effect on stabilising the ND, decreasing its polydispersity (Figure 4.6, B). Regardless of the amount of amiodarone added, the chromatograms indicated a single, narrow peak, corresponding to ND, with apparent MW of around 150 kDa. However, when the reconstitution was repeated, reproducibility of monodisperse ND proved to be an issue. Here, a second, less prominent peak, characteristic for the void volume, was observed. One possibility could be that, upon addition of amiodarone, phospholipids are expelled from the bilayer system, to minimise the energy losses within the system. These phospholipids together with drug molecules anchored to their head groups, potentially assemble into vesicles, with substantially bigger sizes.

In the case of chlorambucil, the analysis showed similar results as to the amiodarone loading (Figure 4.6, C). The formation of small sized aggregates decreased with the addition of chlorambucil, dependent on the number of molecules preloaded. The excess chlorambucil was eliminated as free drug

Part I - Influence of lipid composition on drug incorporation

aggregates. Additionally, for drug loaded ND, the size of the assemblies remained the same as for empty ND (7.5 nm) (Figure 4.7). This is further supported by literature, where one group has demonstrated that the scaffold protein has an adjustable circumference dependent on variations in the number of phospholipids loaded.^{122, 126}

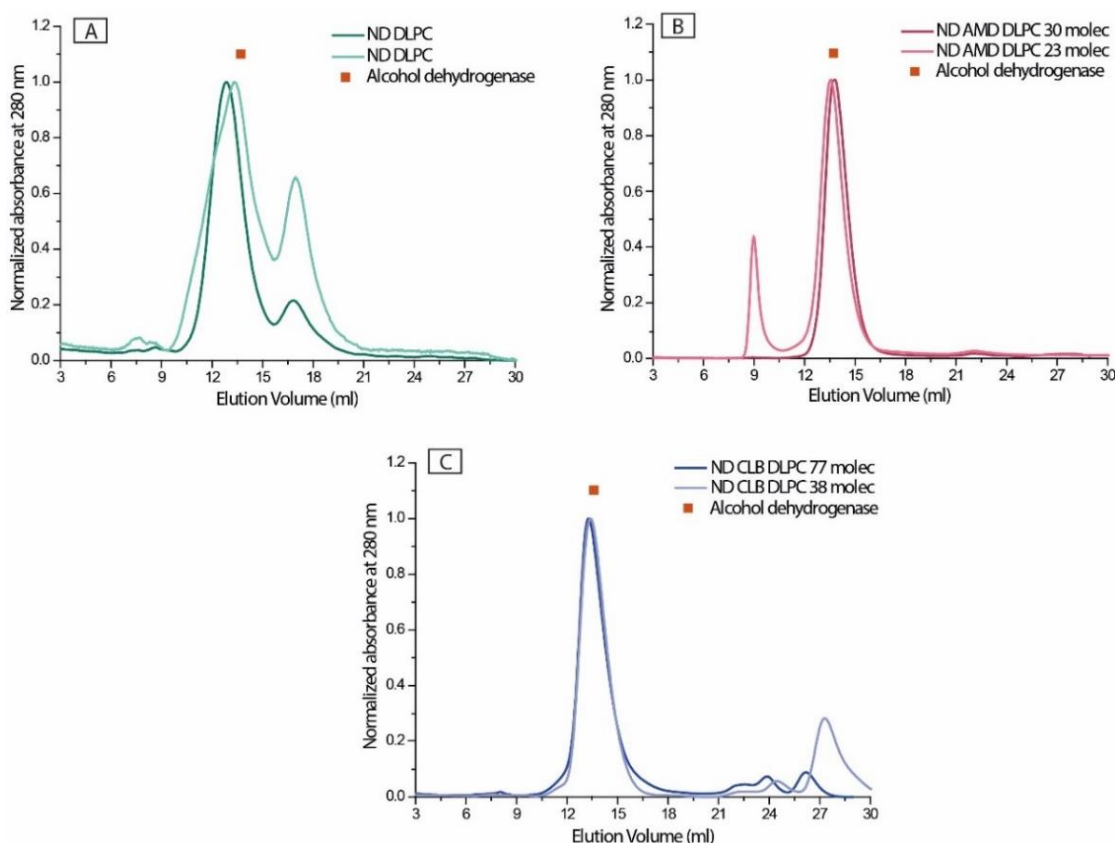


Figure 4.6 SEC chromatograms of empty ND, ND AMD and ND CLB reconstituted with 100% DLPC, and the elution time of AD: A – empty ND (280 nm); B - ND AMD reconstituted by preloading 30 and 23 molecules of AMD (242 nm); C - ND CLB reconstituted by preloading 77 and 38 molecules of CLB (254 nm)

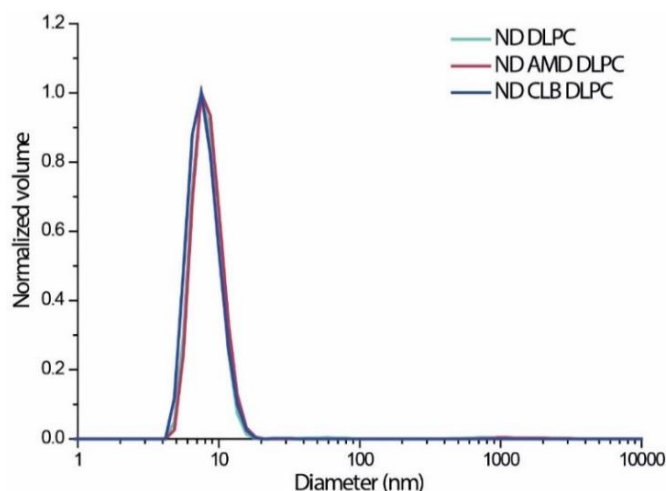


Figure 4.7 DLS of empty ND, ND AMD and ND CLB, reconstituted with 100% DLPC

4.1.3.2 Drug loading efficiency and release profile

The release profile indicated that most chlorambucil molecules (6.4 ± 1.3 molecules per ND) were released in 24 h, and an equilibrium between the concentrations of free and incorporated chlorambucil was achieved (Figure 4.8). Subsequently, no initial burst was observed after the fractional release was plotted. The calculated value for half-life of chlorambucil was $10.2 \text{ h} \pm 3.3$. Although, the release of drug molecules from ND system reconstituted with DLPC was analysed with the idea of being used in future for intravenous delivery of drugs, these DLPC ND assemblies could be used as aerosol delivery to the lungs. In literature, researchers have demonstrated the importance of DLPC liposomes for the aerosol delivery and slow release of various anticancer drugs, such as paclitaxel conjugates¹²⁷ and camptothecin.¹²⁸

The rate of amiodarone release was not investigated, due to the poor incorporation results (1.9 ± 0.2 molecules per ND), given by HPLC (Figure 4.9). The low number of amiodarone incorporated within the shorter chain DLPC could be related to the higher MW of amiodarone, relative to chlorambucil. The high efficiency of incorporating small molecules within DLPC bilayers was also observed in literature studies.¹²⁹ Although the number of amiodarone molecules incorporated per ND was very low, the previously presented SEC analysis demonstrated the positive impact amiodarone addition had on increasing the stability within the ND systems.

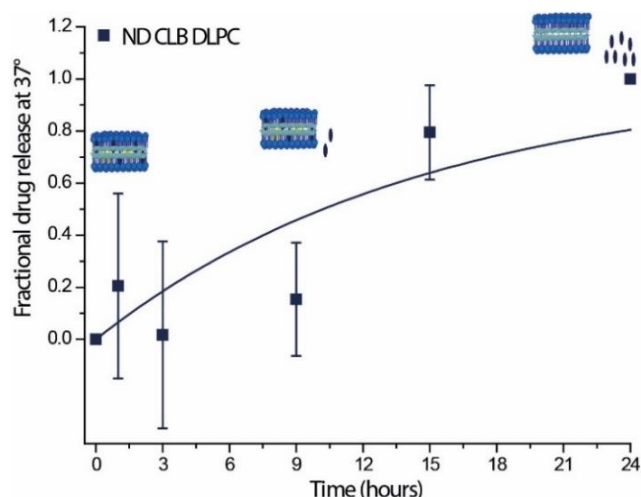


Figure 4.8 Fractional CLB release at 37 °C from ND CLB (254 nm) reconstituted with DLPC; $t_{1/2}$ was $10.2 \text{ h} \pm 3.3$

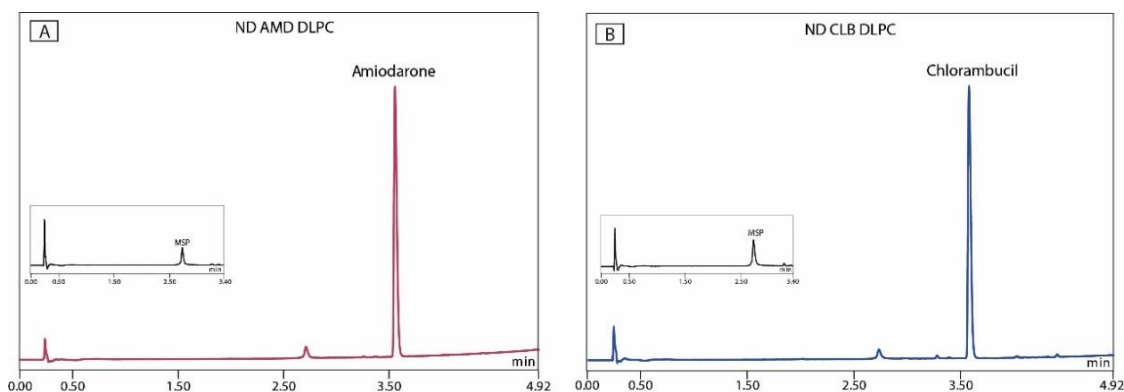


Figure 4.9 HPLC chromatograms of A – ND AMD (242 nm) and B – ND CLB (254 nm), reconstituted, at 4 °C, with 100% DLPC; the inside chromatograms are of the same samples measured at 280 nm to identify the MSP retention time

4.1.4 Assemblies reconstituted with 100% DPPC

4.1.4.1 The monodispersity and size distribution of ND

The reconstitution mixture of empty ND assembled with 100% DPPC was incubated at 42 °C, above the phase transition temperature of DPPC. Similar conclusions, to drug loaded DLPC ND, were drawn for the ND assembled with DPPC. In the SEC chromatogram of empty ND, transitioned to gel phase (analysis at 4 °C), the narrowness of the main peak associated with ND suggested monodisperse and stable ND were assembled (Figure 4.10, A). In order to eliminate the smaller aggregates and have a single peak, the MSP to DPPC molar ratio would need changing. Optimisation studies found in literature

have revealed that the ideal molar ratio for the highest yield of monodisperse ND reconstituted was 1:90.¹³⁰ The lower MSP to DPPC molar ratio, compared to literature ratio,^{80, 131} presumably, also led to the formation of empty ND and drug loaded ND with a small diameter (8.7 nm) (Figure 4.11). A less stable system was consequently created, due to the incomplete DPPC loading within the ND and the need of molecules to adapt to the thickness of the hydrophobic belt at the lipid-protein interface⁸⁰.

When amiodarone molecules were preloaded within ND, the reconstitution of monodisperse assemblies was difficult to reproduce. Additionally, when transitioned to gel phase, by cooling down to room temperature and below, the solution became turbid. This could be a sign of aggregation into micrometer-sized clusters. The SEC chromatogram indicated that incorporating the amiodarone molecules had a two-way effect (Figure 4.10, B). The stability of these systems was reduced proportionally with transition to gel phase and the amount of amiodarone preloaded. The optimal addition of amiodarone was suggested at below 15 molecules, as the peak corresponding to ND, compared to those of large lipid-drug aggregates and membrane protein oligomers, was maximised at this quantity. A presumable explanation could be that, at high amiodarone addition, the discoidal/elliptical¹³¹ ND were entropically forced to disassemble, while the phospholipids and drug molecules were rearranged into structures with favourable energy. A general trend observed for the gel phase assemblies was that, in addition to the tight packing of DPPC tilted hydrocarbon chains,¹³² incorporating the drug molecules had a shrinking effect on the size of the final ND-drug - relative to empty ND. A reason for this shrinkage and the presumed overall poor incorporation of cationic amiodarone could be correlated with the hypothesis developed by Baciú *et al.*¹³³ The study conducted by this research group found that, at physiological pH, the positively charged groups of cationic amphiphilic molecules create instability across the phospholipid bilayer by acting as a catalyst for the separation of phospholipid into a fatty acid and a single-chain lipid. The decrease in lipid loaded into ND, caused by subsequent phase separation of the single-chain lipids, possibly led to adjustments in the circumference of scaffold protein, as mentioned previously. Due to aggregation

problems with amiodarone loaded ND, their loading and release investigation was stopped.

The chromatograms of chlorambucil loaded ND suggested that decreasing the number of molecules preloaded with ND proportionally decreased the height of the peak corresponding to free drug and the shoulder attached to the ND peak (Figure 4.10, C). The absorbance height of this peak of free drug clusters, lowered with preloading less drug molecules, demonstrated that a maximum loading per ND might have been achieved.

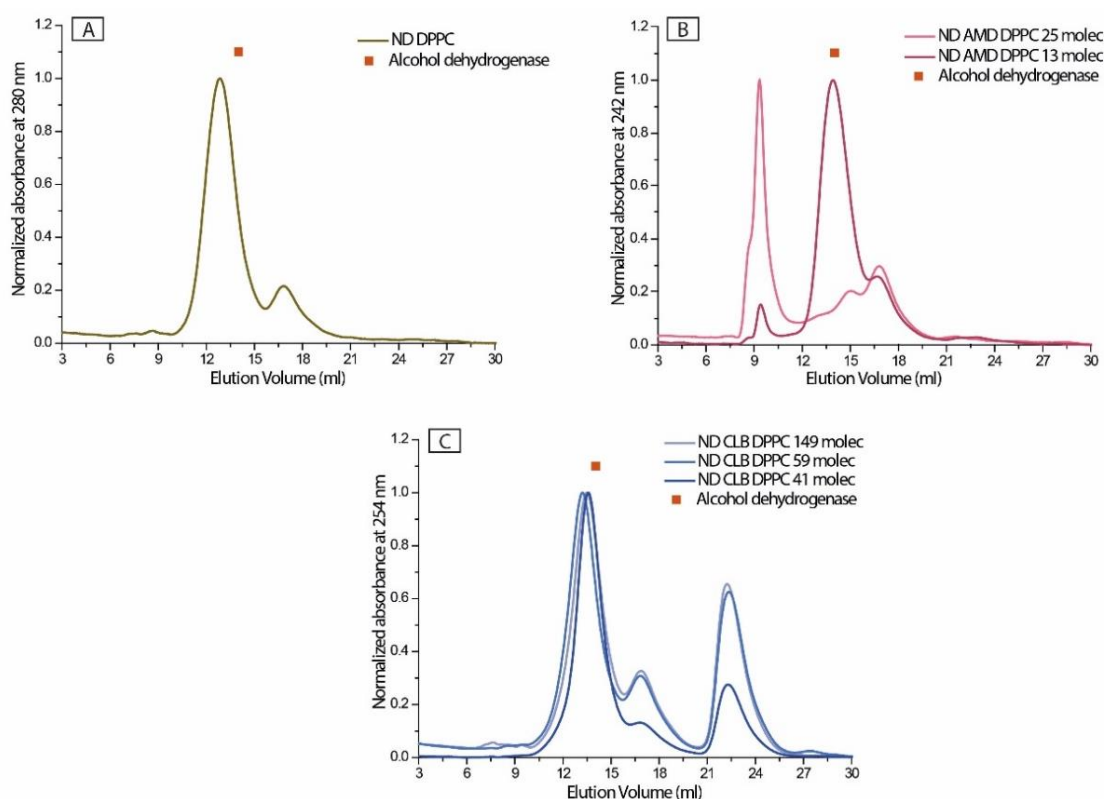


Figure 4.10 SEC chromatograms of empty ND, ND AMD, ND CLB reconstituted with 100% DPPC, and the elution time of AD: A – empty ND (280 nm); B - ND AMD reconstituted by preloading 25 and 13 molecules of AMD (242 nm); C - ND CLB reconstituted by preloading 149, 59 and 41 molecules of CLB (254 nm)

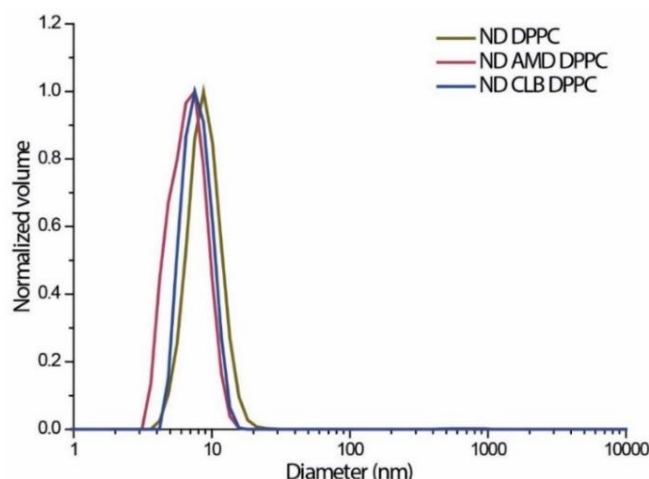


Figure 4.11 DLS of empty ND, ND AMD and ND CLB reconstituted with 100% DPPC

4.1.4.2 Drug loading efficiency and release profile

The rate of chlorambucil released from DPPC ND (7 ± 3.8 molecules loaded per ND, Figure 4.13) indicated that, after 24 h, only 65% of the chlorambucil was release, into the buffer, from the loaded ND (Figure 4.12). Similar to the release from DLPC ND, no initial burst of chlorambucil release was observed. However, the improvement in chlorambucil incorporation might be associated with the longer chains of DPPC.¹³⁴ Although, the oscillation of the number of molecules loaded per ND could be a sign of increased chain-chain interactions. In addition, the calculated value for $t_{1/2}$ of chlorambucil was $16.1 \text{ h} \pm 1.5$. This slow release profile of chlorambucil from DPPC ND is in good agreement with literature findings. Boakye *et al.* showed, in a recent study, that, the release of doxorubicin from DPPC liposomes was minimal for the first 8 h.¹³⁵ In another study involving DPPC liposomes, Dyondi *et al.* observed a slow and sustained paclitaxel release over a time period of 60 h.¹³⁶

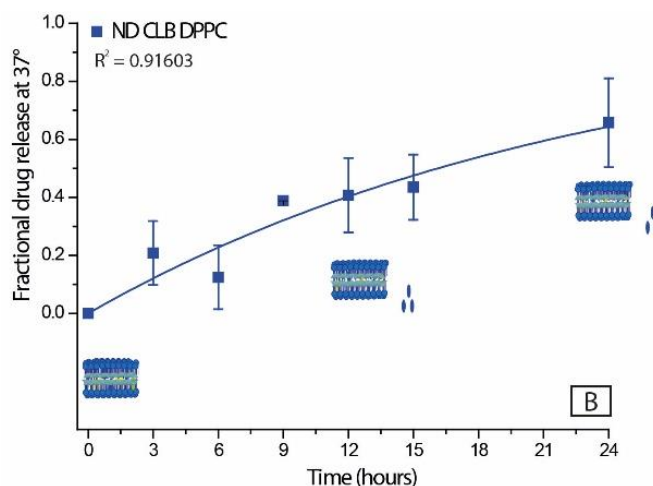


Figure 4.12 Fractional CLB release at 37 °C from ND CLB (254 nm) reconstituted with DPPC; $t_{1/2}$ was $16.1 \text{ h} \pm 1.5$

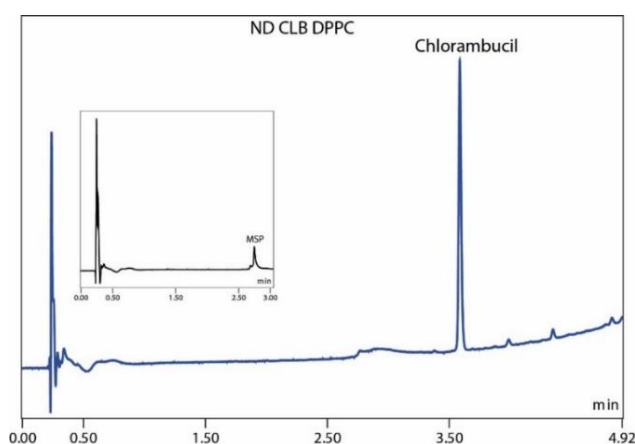


Figure 4.13 HPLC chromatograms of ND CLB (254 nm) reconstituted, at 42 °C, with 100% DPPC; the inside chromatogram is of the same sample measured at 280 nm to identify the MSP retention time

4.1.5 Assemblies reconstituted with POPC: DOPE PEG550

4.1.5.1 The monodispersity and size distribution of ND

The reconstitution mixtures of ND assembled with 10% DOPE PEG550 followed the same protocol, and, as in the case of DLPC ND, the analysis revealed the inability to reproduce monodisperse empty ND. The lack of consistency in forming monodisperse ND could be justified by a potential instability at the acyl chains level, created by repulsive interactions between the saturated and unsaturated pair chains of POPC and DOPE PEG, respectively. Another possibility could be related to steric repulsions caused by the PEG groups. The SEC chromatograms of empty ND indicated a higher apparent MW (210 kDa),

compared to that of empty POPC ND, could be explained by the addition of PEGylated DOPE, which would enlarge the bilayer thickness (Figure 4.14, A). These results were in good agreement with the polydisperse size distribution observed *via* DLS (Figure 4.15). For the empty systems, three different species were seen, with diameter between 11 nm and 396 nm. The most prominent peak is of the assemblies with the smallest diameter, which coincides with empty ND assemblies. The addition of PEGylated DOPE caused an increase in the thickness of the ND bilayer; this could be associated with the larger diameter of the ND, compared with other lipid ND systems.

The chromatograms of ND AMD showed that increasing the number of amiodarone preloaded within ND had a negative influence on the reconstitution of monodisperse assemblies (Figure 4.14, B), as previously seen with the POPC and POPS bilayer. The high preloading of amiodarone within the stabilised bilayer might lead to increased electrostatic repulsive forces, creating an energetically unfavourable packing of lipids and molecules. Lowering the number of molecules preloaded to ND would minimise the repulsion. Hence, below an addition of 20 molecules, the chromatogram revealed a single, narrow peak similar to the elution time specific to ND. However, the appearance of a shoulder in repeated reconstitution indicated a high preference in assembling heterogeneous structures, as seen in one empty ND chromatogram trace.

The analysis of ND CLB showed that, regardless of the number of molecules preloaded with ND, changes in the size of the ND assemblies are hardly noticeable (Figure 4.14, C). However, variations in the absorbance height of the peaks representative to free drug clusters, were observed to be correlated with a negligible increase in the apparent MW of the ND CLB assemblies. This relationship between the enlarged MW and the small peak of free drug, could be associated with drug molecules incorporation within the ND. As more drug molecules interact with the phospholipid head groups, less free molecules are, in solution, to be eliminated as clusters. However, analysis by DLS has found that two species, with a diameter of 6.5 nm and 15.7 nm, were formed. The smaller systems were seen to be predominant in the DLS analysis leading to the conclusion that the ND CLB became polydisperse over time.

Part I - Influence of lipid composition on drug incorporation

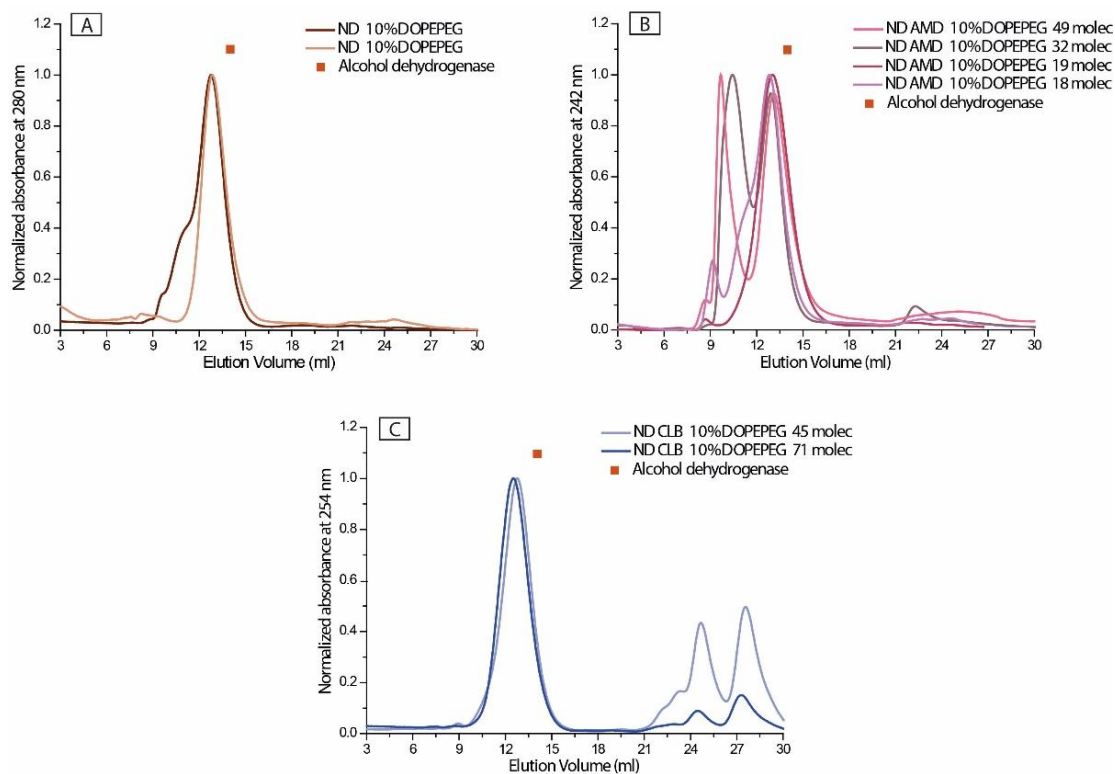


Figure 4.14 SEC chromatograms of empty ND, ND AMD, ND CLB reconstituted with 10% DOPE PEG550, and the elution time of AD: A – empty ND (280 nm); B - ND AMD reconstituted by preloading 49, 32, 19 and 18 molecules of AMD (242 nm); C - ND CLB reconstituted by preloading 71 and 45 molecules of CLB (254 nm)

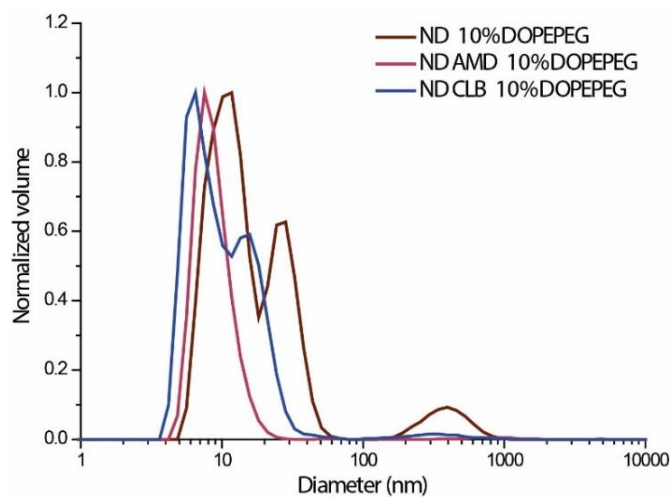


Figure 4.15 DLS of empty ND, ND AMD and ND CLB reconstituted with 10% DOPE PEG550

4.1.5.2 Drug loading efficiency and release profile

Both amiodarone (2.9 ± 2 molecules per ND) and chlorambucil (5.6 ± 0.35 molecules per ND) were released constantly, with no observable initial burst (Figure 4.16, A - for amiodarone release and B – for chlorambucil release). More so, the dissociation of each drug loaded within ND assemblies occurred with an apparent 60% release for amiodarone and 70% for chlorambucil. The half-life of amiodarone and chlorambucil were calculated to be $12.9 \text{ h} \pm 1.3$ and $15.1 \text{ h} \pm 2.6$, respectively. The low level of release, observed within 24 h, was also reported in literature, where Chan *et al.* has highlighted, in his studies, the effect of steric interactions, at the PEGylated head group level, on decreasing the amount of Docetaxel released from hybrid nanoparticles.⁵⁶

However, the addition of PEGylated lipids did not majorly affect the incorporation of chlorambucil. This was observed from the noticeably constant number of chlorambucil molecules incorporated per ND, indicated by the low standard error calculated based on three separate measurements (Figure 4.17). This is in good agreement with the literature, where researchers have reported the low impact on drug partitioning, of stabilised liposomes and disks through incorporation of PEGylated lipids.¹²¹ In addition, the amount loaded per ND was slightly lower than for the ND reconstituted with 100% POPC, however within the error range. The higher number of chlorambucil loaded per ND – comparative to amiodarone – would imply that the drug molecules sit within the bilayer close to the water/membrane interface, interacting with the phospholipid head groups. As the majority of lipids used have long hydrocarbon chains, enhanced van der Waals interactions, at this level, would create the need for a greater force in order to enter the membrane.¹³⁷

Part I - Influence of lipid composition on drug incorporation

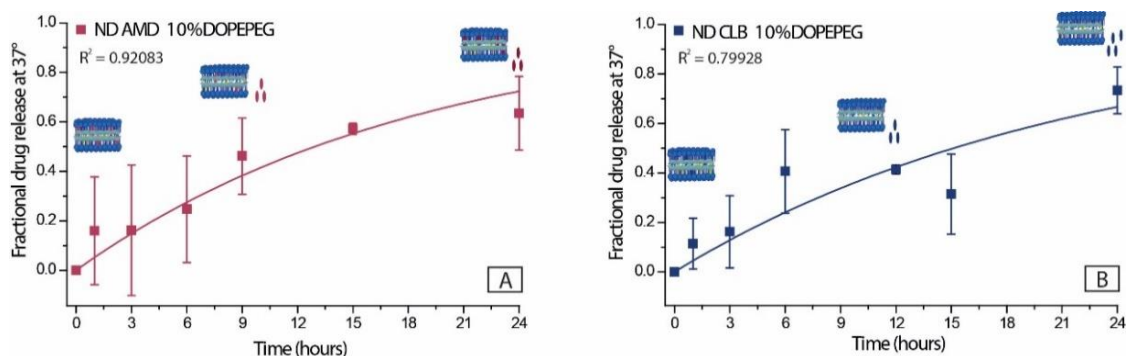


Figure 4.16 Fractional drug release at 37 °C for ND reconstituted with 10% DOPE PEG550: A – ND AMD (242 nm); B – ND CLB (254 nm); $t_{1/2}$ were A - 12.9 h \pm 1.3 and B - 15.1 h \pm 2.6

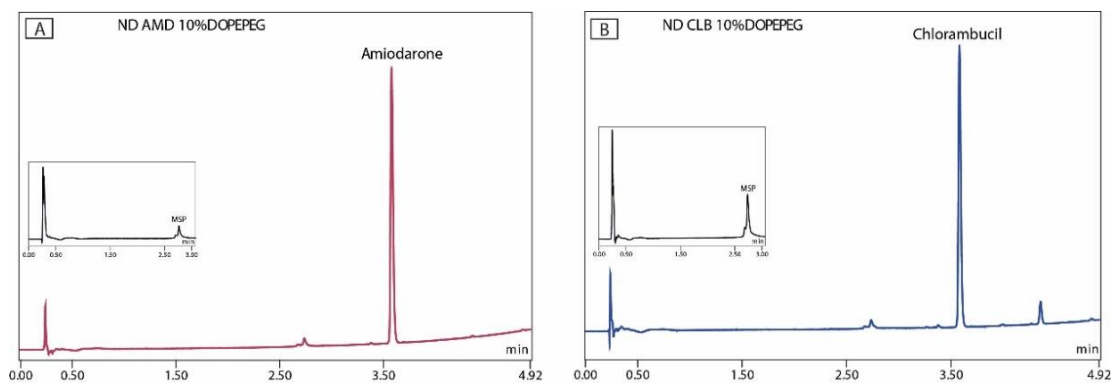


Figure 4.17 HPLC chromatograms of A – ND AMD (242 nm) and B – ND CLB (254 nm) reconstituted, at 4 °C, with 10% DOPE PEG550; the inside chromatograms are of the same samples measured at 280 nm to identify the MSP retention time

4.2 Part II – Influence of bilayer composition on ND reconstitution

In previous chapters we have demonstrated the influence of lipid composition on the reconstitution, and incorporation and release of hydrophobic drug molecules from ND. Although, both MSP to lipid ratio and drug incorporation were seen to have a notable influence on the stability of the assemblies.

In this part, one investigation was conducted on the effect of adding a cationic lipid to ND, on the stability of the system. Cationic lipids were chosen due to their potential in formulating nucleic acids¹³⁸. The second investigation was done on ND formulated by replacing the phospholipid domain with block co-polymers. The use of amphiphilic polymers has many advantages including structural robustness and longer circulation time.

4.2.1 Nanodiscs reconstituted with POPC: DOTAP

The ND were reconstituted by adding a cationic amphiphile to zwitterionic phosphatidylcholine, in ratios of 1 to 2, 5 and 9. Upon inclusion of positively charged 1,2-dioleoyl-3-trimethylammonium-propane (DOTAP), without a phosphate group (Figure 4.18), its effect on packing of the POPC bilayer and the formation of monodisperse ND assemblies was investigated. Recent literature studies highlighted the impact DOTAP addition, to DOPE bilayers, has on enhancing the therapeutic potential for *in vivo* delivery of cytochrome C to H460 cell line, and the efficiency of *in vitro* transfection.^{85, 139, 140}

The SEC chromatogram of empty ND assembled with 9:1 POPC: DOTAP molar ratio showed a single, main peak, corresponding to an apparent MW of 56 kDa (Figure 4.19). Although, the homogeneity of the sample is demonstrated by the absence of other peaks, the extremely low MW of the assemblies suggested that no ND were formed. Most likely, this peak could be the result of protein dimerisation.

When empty ND were reconstituted with a ratio of 5:1 POPC to DOTAP, the corresponding apparent MW was observed to be 135 kDa, similar to ND reconstituted with 100% POPC. A shoulder, of lower relative absorbance, was

also observed, attached to the ND peak. Nevertheless, the stability of assembled ND was enhanced at 5:1 POPC DOTAP molar ratio.

On the SEC chromatogram of empty ND assembled with 2:1 POPC: DOTAP molar ratio, multiple peaks were observed, of species with apparent MW of 201 kDa, 87 kDa, and 38 kDa, respectively. This polydispersity within the sample suggested that electrostatic attractions between POPC and DOTAP head groups, which alter the spatial arrangement of the mixture,¹⁴¹ are preventing the interactions between lipids and the protein belt, required to form the ND. During the reconstitution of ND, the addition of DOTAP in such high ratio, might have facilitated the formation of large aggregates or the fusion of ND assemblies. Our findings are in good agreement with previous studies that have observed this aggregation phenomenon when DOTAP is added, up to 30 mol%, to various PC bilayers.^{142, 143}

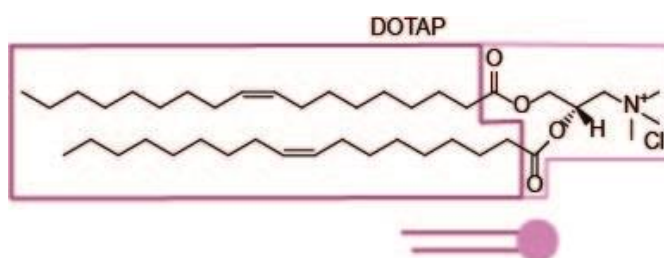


Figure 4.18 Structure of 1,3-bis(sn-3-trimethylammoniumpropyl)-5-(sn-3'-phosphatidyl)-sn-glycerol (chloride salt) (DOTAP); Transition Temp. $<5^{\circ}\text{C}$

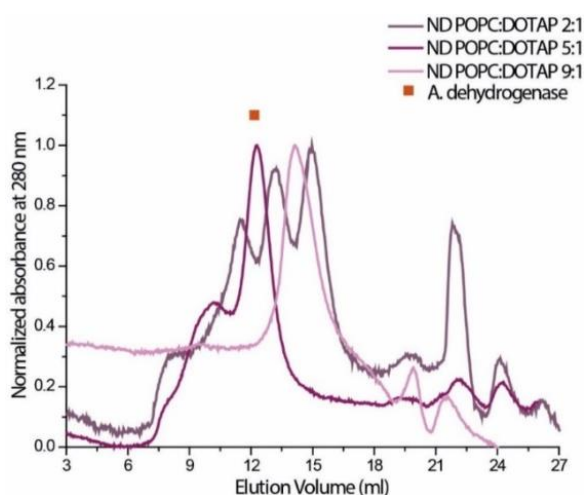


Figure 4.19 SEC chromatograms of empty ND reconstituted with POPC to DOTAP 2:1, 5:1 and 9:1, and the elution time of AD; all samples were measured at 280 nm; AD was eluted at 12.17 mL

4.2.2 Nanodiscs reconstituted with block co-polymers

Going back to the origins of these self-assembled nanostructures, phospholipids were chosen to form the basic component because of their geometrical packing and the MSP affinity to bind to their hydrocarbon chains. From here, a question arose regarding the specificity of phospholipids for being the only amphiphilic nanostructures to assemble into stable and monodisperse ND. Therefore, we investigated the possibility of replacing phospholipids with a block co-polymer and analysed, by SEC, its efficiency in reconstituting stable ND. The block co-polymer chosen was poly(butadiene)-*b*-poly(ethylene oxide) (PB₁₂₀₀-*b*-PEO₆₀₀). Block co-polymers are amphiphilic structures able to form vesicles in solution.¹⁴⁴ The insoluble block, which forms the core of the vesicle, can entrap hydrophobic molecules^{145, 146} or act as a nanoreactor,¹⁴⁷ protecting the cargo, while the soluble block acts as a protective corona, conferring stability to the system. Due to its low CMC,¹⁴⁸ PB-*b*-PEO co-polymer is an attractive alternative in formulating nanocarriers for the delivery of hydrophobic drugs. Recent studies have demonstrated the ability of PB-*b*-PEO nanoparticles to act as carriers for the incorporation and delivery of small molecules such as paclitaxel¹⁴⁹ or fluorescent and hydrophilic dyes.^{150, 151}

The ND were reconstituted following the method described in Chapter 3 as method B (Figure 4.20). The incubation temperature and time before adding bio-beads were varied to find the optimum conditions for the assembly of ND. PB-*b*-PEO was added in smaller quantities (from 1:15 to 1:30 molar ratios), compared to lipid ND, because the hydrophobic domain of this co-polymer is larger than that of lipid and therefore will require a thicker protein belt.

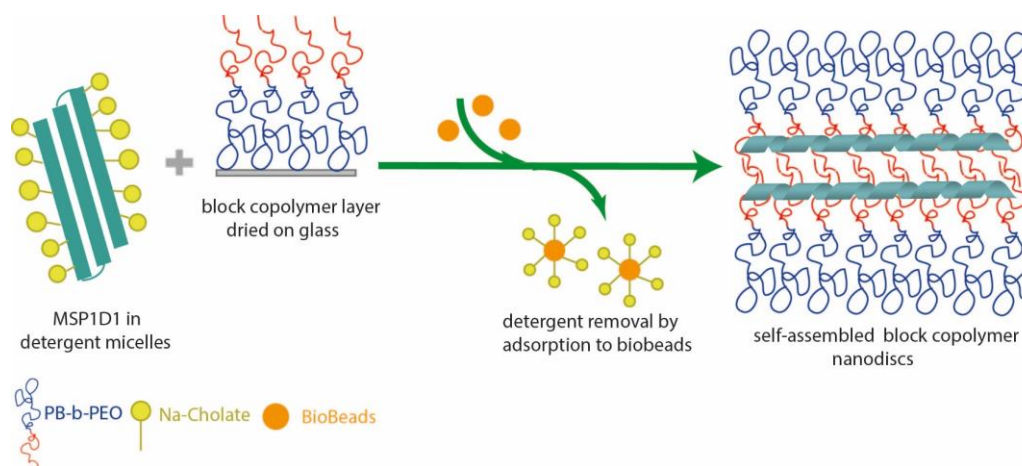


Figure 4.20 Schematic representation of the PB-*b*-PEO ND reconstitution process

The analysis by SEC suggested that a combination of temperature and length of the incubation time before removing the detergent were necessary for the formation of ND (Figure 4.21). The chromatogram of ND assembled with 1:15 MSP to co-polymer molar ratio and incubated at 55 °C for 2.5 h before removing the detergent, showed a high absorbance peak eluted in the void volume, and another peak, with an attached shoulder, corresponding to an apparent MW of 46 kDa. The elution times of these peaks indicated that most co-polymer formed large vesicles with itself, whereas the MSP might have eluted as oligomeric structures. Similar observations were recorded when the incubation temperature was kept at 55 °C, but more PB-*b*-PEO was added to the mixture, and incubated for longer time before removing the detergent. When the temperature was decreased to room temperature and the amount of co-polymer increased again to 1:30 MSP to PB-*b*-PEO, the void volume peak was still present. However, the peak associated with oligomeric MSP disappeared. Instead, we observed a peak eluted at a similar time to alcohol dehydrogenase and POPC ND. When the temperature was decreased to 4 °C, the ND peak was almost inexistent compared to the void volume peak, suggesting that the co-polymer had preferably assembled into large vesicles. The height of this peak indicated that only a small quantity of co-polymer was assembled into ND, however it is a starting point in finding the optimum conditions to reconstitute PB-*b*-PEO and MSP ND.

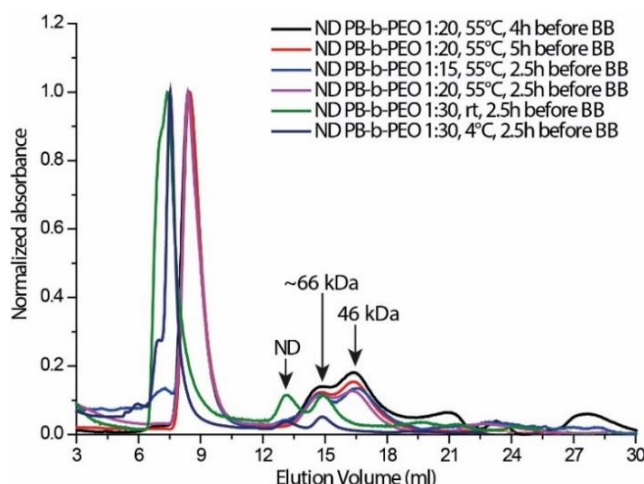


Figure 4.21 SEC chromatograms of PB-*b*-PEO ND reconstituted with 1:15, 1:20 and 1:30 molar ratio, incubated at temperatures between 4 °C and 55 °C; the length of time before removing the detergent was also varied, from 2.5 h to 5 h

4.3 Summary

Using method B for preloading drug molecules, amiodarone and chlorambucil were incorporated into ND assembled with various lipid compositions. SEC analysis showed that DLPC, DPPC and POPC/DOPE PEG550 used in the reconstitution of amiodarone loaded ND had a shrinking effect on the size of the final systems. Whereas, for ND reconstituted with POPC/POPS, the incorporation of higher concentrations of amiodarone led to the formation of clusters with the lipid head groups, eventually, enlarging the ND surface (Table 4.2). Comparatively, changing the lipid composition within ND did not have a major effect on the formation of homogeneous assemblies with incorporated chlorambucil.

The release profile of chlorambucil from ND with POPC/DOPE PEG550, DLPC and DPPC had a slow general trend, the exception being ND reconstituted with anionic POPS. This was probably due to electrostatic repulsions between the two negatively charged molecules. Additionally, similar slow release was observed for the dissociation of amiodarone from ND reconstituted with all the lipid mixtures. The combination of POPC and PEGylated lipid contributed the most to slowing the release of amiodarone, in such that the release did not achieve completion within 24 h. Whereas, for chlorambucil release, this effect was maximised when ND were reconstituted with DPPC composition.

Lipid composition	Amiodarone		Chlorambucil	
	Drug molecules/ND	$t_{1/2}$ /h	Drug molecules/ND	$t_{1/2}$ /h
POPC	10 ± 6.8	5.4 ± 0.7	6.5 ± 1.7	5.8 ± 0.5
50% POPS	1.9 ± 0.8	1.8 ± 0.8	8.5 ± 3.8	3.9 ± 0.7
10%DOPEPEG	2.9 ± 2	12.9 ± 1.3	5.6 ± 0.4	15.1 ± 2.6
DLPC	1.9 ± 0.2	nc	6.4 ± 1.3	10.2 ± 3.3
DPPC	nc	nc	7 ± 3.8	16.1 ± 1.5

Table 4.2 Table of number of amiodarone and chlorambucil incorporated per ND and their half-life for the ND reconstituted with different lipid compositions; nc – not calculated

The efficiency of reconstituting stable and monodisperse ND was also investigated when cationic lipids were incorporated into the bilayer domain and when the phospholipids within the ND were replaced by PB-*b*-PEO. The analysis of ND formed with cationic DOTAP suggested that by increasing the concentration on DOTAP within the bilayer domain, the ND yield is considerably decreased. At the lowest addition of DOTAP, ND formation was absent, instead protein oligomers were presumably formed. In contrast, the highest addition of DOTAP, has promoted the formation of large aggregated vesicles. The appearance of a ND peak was observed only for the ND containing 20% DOTAP. However, the increased polydispersity suggested that further investigation is required to assess ND reconstituted with DOTAP and POPC.

To find the optimum conditions for the assembly of ND, the incubation temperature and time before detergent removal, and the molar ratio between MSP and PB-*b*-PEO were varied. When the incubation temperature of the mixture was decreased to room temperature and the molar ratio was 1:30, the analysis revealed the formation of ND assemblies with a similar elution time to POPC ND. The small absorbance of the ND peak indicated that further investigation is required to determine the optimum conditions for the reconstitution of monodisperse PB-*b*-PEO ND.

5 Chapter 5 – Modified nanodiscs for traceable cellular delivery

5.1 Introduction

The lipid ND systems have been particularly used in the characterisation of membrane proteins; however these self-assembled systems have potential to be used as carriers for drug delivery into cells. For example, recent studies have observed successful delivery of all-*trans* retinoic acid and curcumin to mammalian cells, from lipid nanodiscs formed with ApoA-I and ApoE.^{73, 152, 153} The latter study indicated that an important role in drug uptake and nanodiscs dissociation or internalisation could be played by the cell line used. Here, ApoE was seen to be localised at the cell surface due to its strong affinity to bind to specific receptors found in the glioblastoma multiform cells used.

Sortase A (SrtA) mediated ligation was used to site-specifically modify the scaffold protein, already incorporated in the ND, with fluorescein. Subsequently, their capabilities to enter and deliver chlorambucil to mammalian cells were tested.

5.2 Sortase A mediated modification of the MSP

Prior to the SrtA mediated transpeptidation reaction, the POPC lipids were used to reconstitute the ND assemblies, as our previous investigation showed good results for chlorambucil incorporation and release from these ND. The empty and drug loaded ND assemblies were reconstituted as described in Chapter 3. Following the reconstitution of empty and drug loaded ND, the SrtA mediated ligation of the MSP within the ND was effected by modification of the protocol developed by Williamson *et al.*^{154, 155} In order for the MSP to be labelled *via* SrtA mediated ligation, the N-terminal glycine residue has to be accessible to the LPXTG recognition motif of the depsipeptide label^{156, 157} (Figure 8.19). To facilitate the purification process, MSP has a His₆ attached on the N-terminus, however the MSP1D1 was engineered with a Tobacco Etch Virus (TEV) protease recognition site (ENLYFQG) incorporated between the His₆ tag and the scaffold protein. This mean the His₆ tag can be removed by specifically hydrolysing the amide bond between the QG amino acid residues,⁸⁰ prior to

labelling. The full outline strategy is shown in Figure 5.1. TEV protease, SrtA and fluorescein-depsipeptide used in this study were provided by Dr Daniel Williamson from University of Leeds.

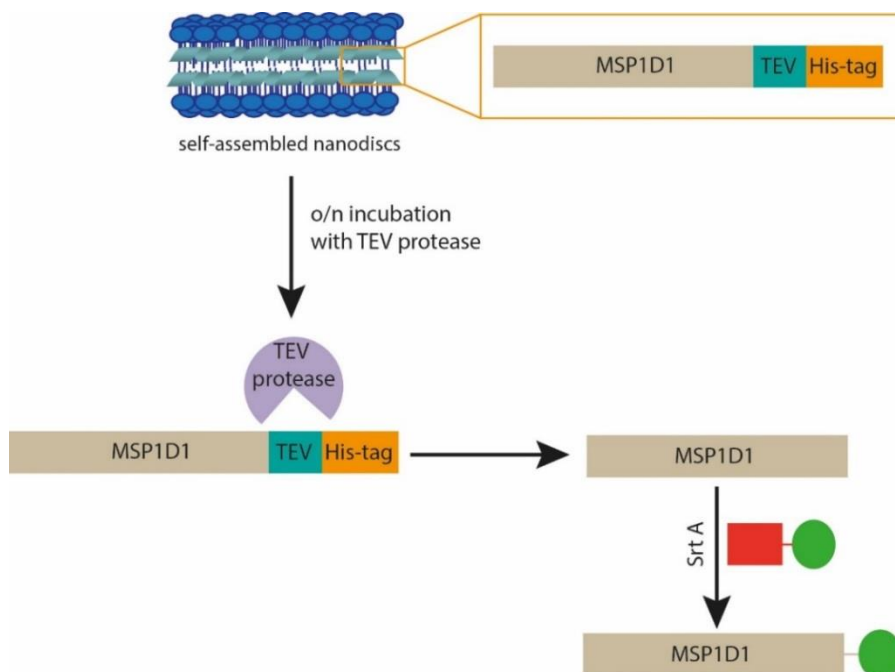


Figure 5.1 SrtA mediated modification of MSP1D1 within ND; to expose the glycine residue on the N-terminus, first the His₆ was removed by enzymatic cleavage; subsequently, SrtA was used to mediate the ligation of fluorescein-depsipeptide and MSP; on the figure, overnight is abbreviated o/n

The reconstituted empty and chlorambucil loaded ND assemblies were incubated overnight at room temperature with TEV protease. We initially attempted to remove the His₆ tag prior to ND formation, however the protein precipitated in solution due to the temperature required during incubation with TEV protease. The ND assemblies with the truncated MSP were separated from the cleavage mixture and non-truncated MSP *via* SEC. On the SEC analysis of ND CLB, a small difference in the elution time was observed between ND before and after HIS-tag removal (Figure 5.2). Further analysis of ND by MS showed a decrease in the MW of some MSP, from 24661 Da to 22043 Da, after the His₆ tag and TEV protease recognition site removal (Figure 5.3). Despite the longer incubation period and the temperature conditions, not all MSP had the His₆ tag cleaved, as analysis by MS showed also the presence of protein with a MW of 24661 Da. The truncation of MSP was also confirmed by SDS-PAGE analysis,

where the gel showed two bands, for empty ND and ND CLB, shifted down the gel from the position of the MSP with the His₆ tag attached (Figure 5.4, Lane 1 for MSP, Lane 2 and 4 for MSP after His₆ tag removal, in empty ND and ND CLB, respectively).

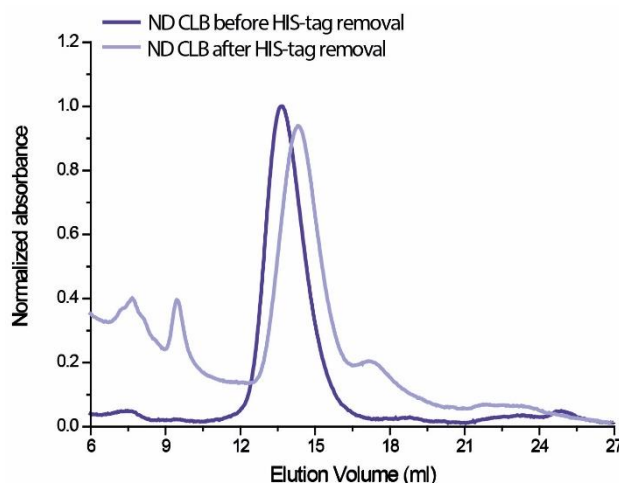


Figure 5.2 SEC chromatogram of ND CLB after His₆ cleavage, showing a later elution time compared to ND CLB before the removal

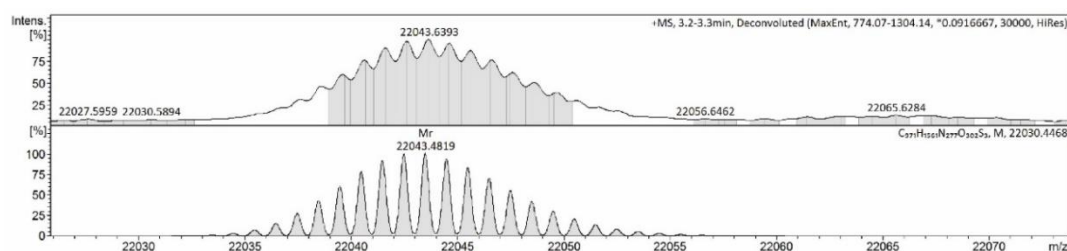


Figure 5.3 Screen shot of mass spectrum of the MSP within ND, after His₆ cleavage (upper image), and simulation of the MSP without the His₆ and TEV protease recognition sequence, based on the chemical formula calculated from the amino acid sequence of MSP¹⁵⁸ (bottom image)

After the His₆ tag cleavage, the MSP incorporated in the ND assemblies was modified *via* SrtA mediated ligation, using fluorescein-depsipeptide for labelling (Figure 8.19, A). The ND were incubated overnight, at room temperature, with 10 equivalents of fluorescein-depsipeptide and 20 mol% of SrtA (Figure 8.19, B). Because the SrtA transpeptidation reaction is reversible, to ensure a high protein modification yield, an excess of depsipeptide label and stoichiometric amounts of SrtA were added to the ND. The overnight incubation time was

another factor to ensure the protein labelling, as the low effective MSP concentration in solution kinetically limits the rate of the ligation.¹⁵⁴

Mass spectrometry and SDS-PAGE of the modified MSP in ND assemblies were, again, used to confirm labelling of ND. More so, the relative degree of fluorescent labelling was assessed by the SDS-PAGE analysis. On the gel a fluorescent MSP band was observed, indicating the successful labelling of the MSP with fluorescein, when in the ND formation (Figure 5.4, Lanes 7 and 8). In addition, when chlorambucil was preloaded within ND, a fluorescent MSP band was also observed. This suggests that drug loading does not affect the SrtA mediated ligation. Another fluorescent band was detected at a MW greater than that of fluorescein-MSP, probably corresponding to the auto labelled SrtA (has a N-terminal glycine), as the purification step was done after the SDS-PAGE analysis. Comparatively, the intensity of the fluorescent MSP band was weaker, however the SDS-PAGE gel showed both MSP unlabelled and fluorescein-MSP bands are barely visible, with only very little difference in their intensities. This could suggest that the majority of MSP was labelled with fluorescein *via* SrtA mediated ligation. The MW of fluorescein modified MSP was determined, *via* MS, to be 22959 Da, in good agreement with its theoretical MW calculated, 22957 Da (Figure 5.5).

The final step in labelling the MSP with fluorescein was removing the SrtA mixture and ND which were not cleaved by incubating overnight the fluorescein-ND with Ni resin, as SrtA has a high affinity to bind to the Ni ions due to its N-terminal His₆ tag. The labelled ND were then separated from the resin by centrifugation. Further tests were selected to study the ability of the fluorescein-ND and chlorambucil loaded fluorescein-ND to enter mammalian cells - Huh7¹⁵⁹ and HeLa cells.¹⁶⁰ Subsequent to treating the cell lines with fluorescently labelled ND, confocal microscopy and MTT cytotoxicity assay were used to show if the MSP translocated into cells and the cytotoxic impact of ND CLB, respectively.

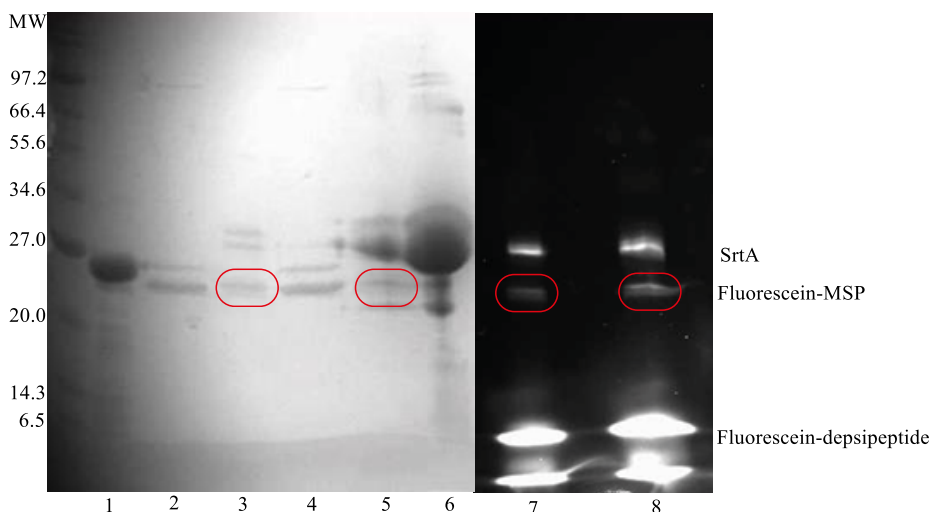


Figure 5.4 SDS-PAGE gel of: Lane 1: MSP; Lane 2: MSP in empty ND with His₆ removed; Lane 3: Fluorescein-MSP in empty ND; Lane 4: MSP in ND CLB with His₆ removed; Lane 5: Fluorescein-MSP in ND CLB; Lane 6: SrtA; Lane 7: UV irradiation of sample showed in Lane 3; Lane 8: UV irradiation of sample showed in Lane 5

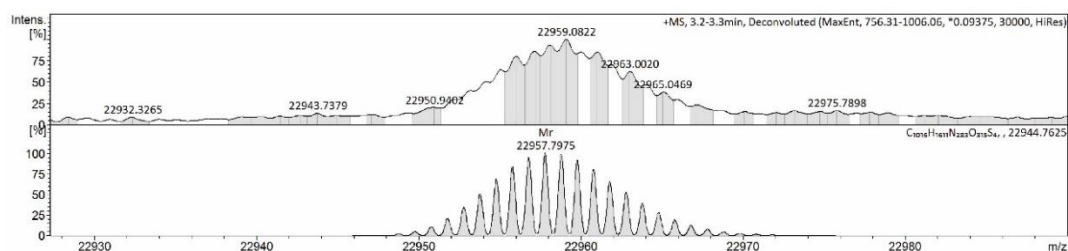


Figure 5.5 Screen shot of mass spectrum of the fluorescein-modified MSP within ND (upper image), and simulation of the modified MSP, based on the chemical formula calculated from the amino acid sequence of MSP¹⁵⁸ and the formula for fluorescein-depsipeptide (bottom image)

5.3 The transport of labelled nanodiscs into mammalian cells

The fluorescein-ND assemblies were screened against Huh7 cells and HeLa cells; these cell lines are derived from human liver and cervical cancer tissues, respectively. The experimental procedures of screening against the cell lines were conducted by Darren Machin, from University of Leeds. Confocal fluorescence microscopy was performed, by myself with the guidance of Darren Machin, to investigate the uptake of empty fluorescein-ND and rhodamine-ND, and chlorambucil loaded fluorescein-ND.

Huh7 cells were incubated with empty and chlorambucil preloaded fluorescein-ND for 2 h and 24 h, before being chemically fixed. The level of background

fluorescence, showed in Figure 8.20, was obtained after exposure of the control Huh7 cells to the blue, green and red lasers; control cells refer to the Huh7 cells not treated with empty or chlorambucil loaded fluorescein-ND. In addition to the nucleus stain (DAPI) identified after excitation at 408 nm, lower intensity fluorescence was also detected with the green and red channels. This could be attributed to autofluorescence from the cells, as aldehyde based fixatives are known to induce fluorescence in cells, after reacting with tissue components.¹⁶¹

The images taken using confocal fluorescence microscopy showed that very little or no amount of fluorescence, attributed to fluorescein-ND, was detected (Figure 5.6). However, in the image depicting the cells treated with chlorambucil loaded ND, changes in the structure of the nucleus, which could lead to disintegration of the nucleus and eventually apoptotic cell death, were identified (Figure 5.7). This observation suggested that chlorambucil has entered the cells, either subsequent or simultaneous to being separated from the ND assemblies. An evidence of fluorescein-MSP internalisation or binding on the cell surface could not be established, probably due to the concentration of ND in the cells being very low.

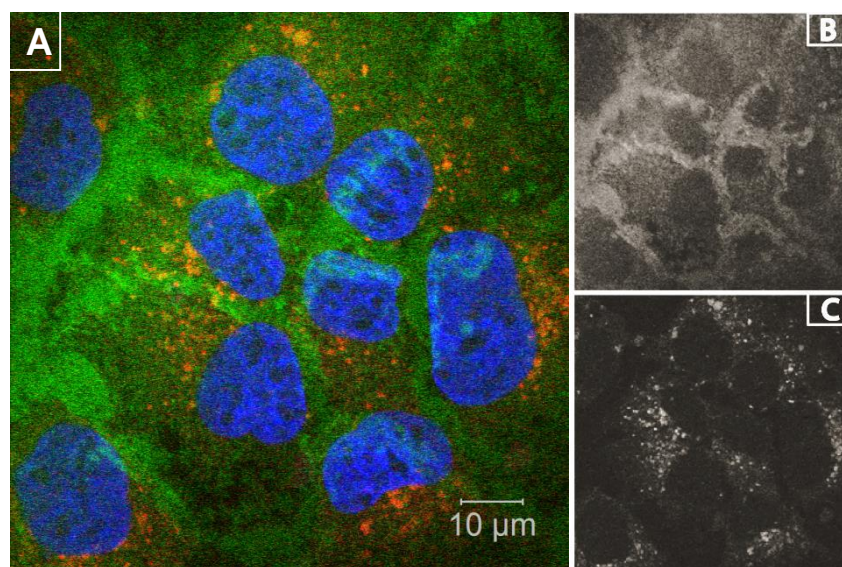


Figure 5.6 Immunostained Huh7 cells incubated with fluorescein-ND assemblies, for 2 h, at 37 °C; A – Merged image; B – green channel, excitation at 488 nm; C – Red channel, excitation at 555 nm

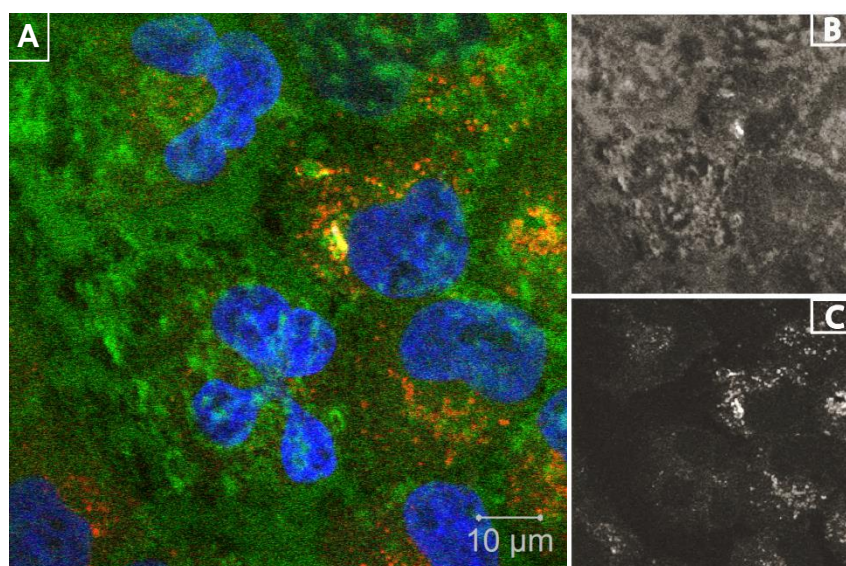


Figure 5.7 Immunostained Huh7 cells incubated with chlorambucil loaded fluorescein-ND assemblies, for 24 h, at 37 °C; A – Merged image; B – green channel, excitation at 488 nm; C – Red channel, excitation at 555 nm

HeLa cells were, as well, incubated with empty fluorescein-ND and rhodamine-ND, for 4 h and 24 h, before being chemically fixed, with 4% paraformaldehyde (PFA). After exposure of the control cells to the blue, green and red lasers, a high intensity background fluorescence was identified with the green channel (Figure 8.21). This, again, could be correlated with autofluorescence from the cells resulted after PFA fixation.

When HeLa cells were incubated with empty fluorescein-ND, dots of higher intensity than the background autofluorescence were detected (Figure 5.8). This could be associated with internalisation of the fluorescent MSP into cells. This is in good agreement with a recent study that has demonstrated the preferential internalisation, by mammalian epithelial cells, of disc-shaped nanoparticles.¹⁶² However, further investigation with organelle-specific immunostaining assays is required to clarify the exact location of the fluorescein-MSP within the cell. A study was reported in literature, where ApoE was shown to bind to the surface of human glioblastoma cells prior to releasing drug molecules, rather than be internalised.¹⁵³ Their findings along with our observations suggest that the cellular uptake is cell-line dependent. The analysis of HeLa cells incubated with empty rhodamine-ND by fluorescent

microscopy showed no changes in the intensity of fluorescence (Figure 5.9). However, these findings might be related to very low rhodamine concentrations in the empty ND, rather than no internalisation of these ND within the cells. Another explanation could be related to the possible diffusion of rhodamine PE within the membrane of the cells.

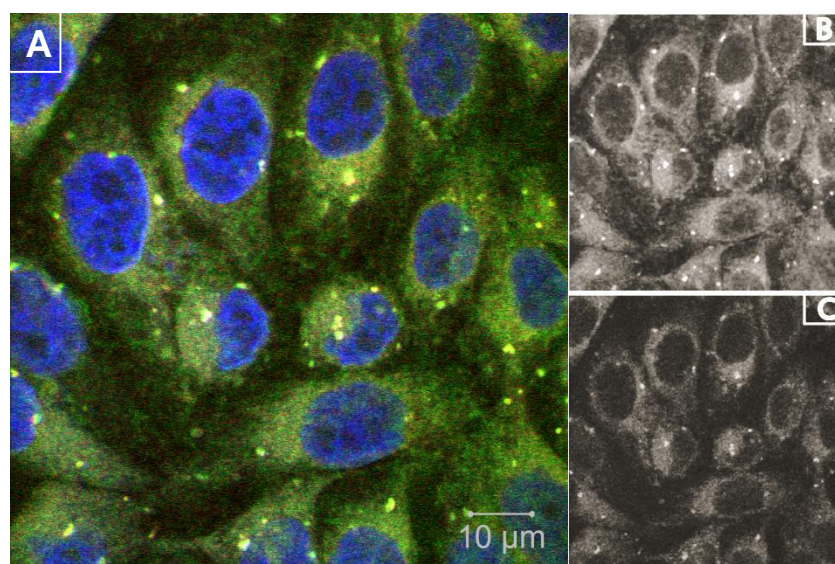


Figure 5.8 Immunostained HeLa cells incubated with empty fluorescein-ND assemblies, for 4 h, at 37 °C; A – Merged image; B – green channel, excitation at 488 nm; C – Red channel, excitation at 555 nm

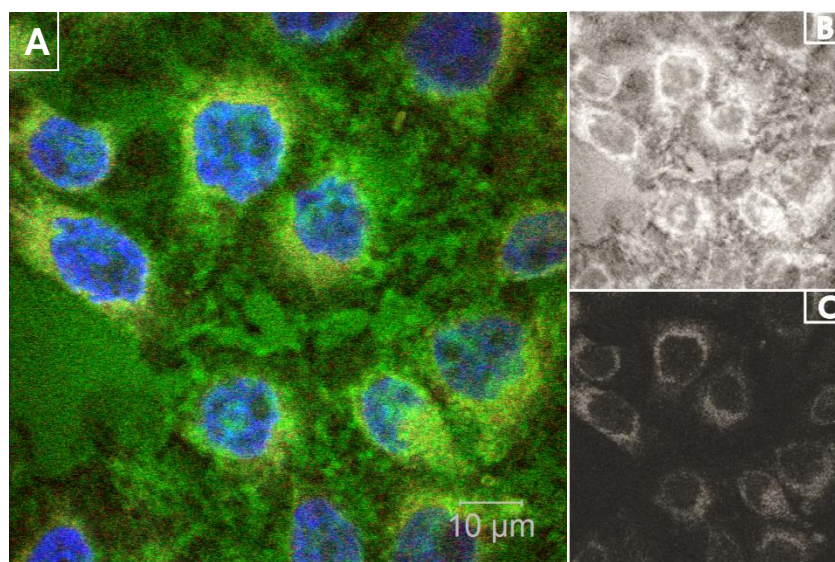


Figure 5.9 Immunostained HeLa cells incubated with empty rhodamine-ND assemblies, for 4 h, at 37 °C; A – Merged image; B – green channel, excitation at 488 nm; C – Red channel, excitation at 555 nm

The cytotoxicity of empty ND, chlorambucil loaded ND and free chlorambucil was determined on HeLa cells using a MTT assay ((3-(4, 5-dimethylthiazol-2-yl)-2,5-diphenyltetrazolium bromide) tetrazolium reduction assay), as described in Chapter 7. The cells were treated for up to 24 h with the same concentration of empty ND, ND CLB and free drug, and the cell viability was determined after measuring the absorbance at 570 nm. Compared with untreated cells, the percentage of apoptotic cells was not affected by the addition of either empty ND, chlorambucil loaded ND or free drug (Figure 5.10). An explanation behind this could probably be related to a very low concentration of chlorambucil in the media. In literature, Singh *et al.* has reported that chlorambucil only at concentrations above 0.1 $\mu\text{g/mL}$ could induce cellular death in breast cancer cells.¹⁶³ More so, the reported IC_{50} of free chlorambucil in HeLa cells is 10 μM .¹⁶⁴ Comparatively, the concentration of chlorambucil in the ND assemblies and as a free drug added to the cells was around 0.05 $\mu\text{g/mL}$. For the ND-drug assemblies and free drug to have a better influence on the viability of the cells, the concentration of chlorambucil added has to be increased, by increasing the concentration of assemblies with which the cells are treated.

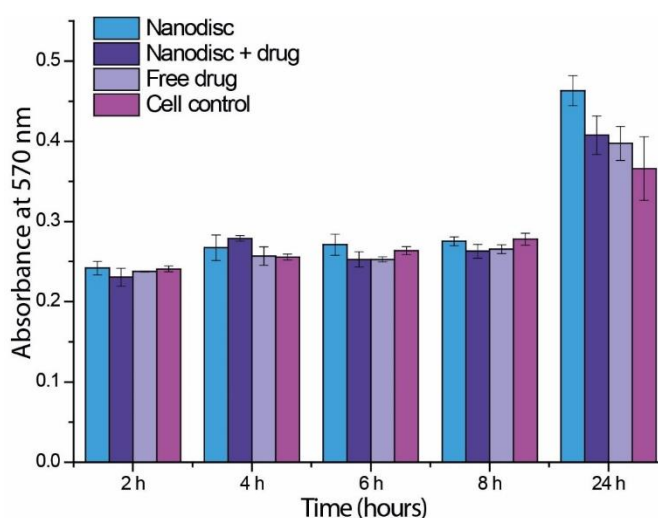


Figure 5.10 MTT cytotoxicity assay of ND, ND CLB and free CLB on HeLa cells; CLB concentration was around 0.05 $\mu\text{g/mL}$

5.4 Summary

Using the SrtA mediated transpeptidation reaction, MSP was chemically modified with fluorescein. Prior to the SrtA mediated ligation, the POPC lipids were used to reconstitute ND assemblies, and the His₆ tag on the N-terminus of MSP was cleaved. After cleavage, the glycine residue required for labelling was revealed. This approach allowed the modification of MSP, with a fluorescent label, while interacting with the phospholipids within the ND. SDS-PAGE and MS analysis were used to identify the fluorescein modified protein within the ND, which had a MW of 22959 Da.

Studies on Huh7 and HeLa cells treated with empty ND and ND CLB were performed to investigate if the MSP was internalised by the cells. The results showed good internalisation of MSP (incorporated into empty ND) by HeLa cells, but little internalisation by Huh7 cells (for empty or drug loaded ND), and no cytotoxic activity of chlorambucil. This suggests that the cellular uptake is cell-line dependent. The lack of cytotoxic activity is probably a consequence of low concentration of ND CLB, with which the cells were treated. Further investigation is required to determine the exact location of fluorescein-MSP within the mammalian cells and the effect of higher concentrations of ND CLB on cell viability.

6 Chapter 6 – Conclusions and future work

After the initial optimisation of protein expression and purification which led to stabilising the protein in a solution of detergent, the ND reconstitution was simplified. This one-step formulation has been adapted for the reconstitution of ND assemblies, by using pure MSP stabilised in Na cholate micelles. The influence of MSP aggregation on the reconstitution and MW of the ND has also been demonstrated with a combination of SEC and DLS analysis.

6.1 Development of drug loaded ND systems

6.1.1 Changes in cargo composition

Conclusions

A new strategy has been developed to generate the optimum conditions for incorporation and release of poorly water soluble drugs from ND. This was achieved by investigating two strategies for loading twelve hydrophobic drugs. The drugs were added either passively, under overnight shaking conditions, to a solution of ND (postloading), or by loading the drug during the reconstitution of ND (preloading). The analysis of drug loaded ND, by SEC and DLS, has demonstrated a minimum impact on the MW and size of the assemblies, with drug molecules preloaded to ND. The amount of hydrophobic molecules loaded into ND was accurately determined with the help of an optimised method of characterisation, using HPLC. When drug molecules were preincorporated into the phospholipid domain of ND reconstituted with the optimised method, an increase in drug incorporated per ND and a slower release rate was observed. The efficiency of drug loading within the POPC bilayer was additionally, correlated with a decrease in membrane thickness. It is reasonable to assume that this approach of optimised reconstitution and drug preload is the optimum option for maximising the efficiency of drug incorporation and increasing the half-life of the transported drug.

Future work

ND have proven to be a versatile platform for incorporating small hydrophobic molecules. If two or more drug molecules would be incorporated into ND, the possibility of using this multiple drugs nanocarrier for combination therapies would increase. If successful, these multi-drug loaded ND could potentially be designed and developed as an optimised treatment for each patient, for clinical applications.

6.1.2 Changes in bilayer domain

Conclusions

Using the optimised preloading methodology, the influence of lipid composition within ND on the formation of stable monodisperse drug loaded ND, on the drug loading capacity and release kinetics of two drugs was observed *via* analysis on SEC, DLS, HPLC and UV spectroscopy. The formation of homogeneous ND assemblies with loaded chlorambucil was insignificantly affected by changes in lipid composition. More so, improvements in the amount of chlorambucil loaded were observed. Comparatively, the analysis of amiodarone loaded ND by SEC has reported that DLPC, DPPC and POPC/DOPE PEG550 compositions had a shrinking effect on the size of the final ND systems. The addition of a negatively charged lipid has intensified the dependence between reconstituting stable monodisperse amiodarone loaded ND and the concentration of amiodarone incorporated –high amiodarone concentration led to the formation of large clusters. Additionally, the number of amiodarone incorporated per ND has significantly decreased when POPC domain within ND was changed. Comparative with release from POPC ND, ND with DOPE PEG550, DLPC and DPPC improved the rate of drug release, leading to a slower general trend. The exception was drug dissociation from ND reconstituted with negatively charged POPS. The combination of POPC and PEGylated lipids contributed the most to slowing the release of amiodarone, in such that the release did not achieve completion within 24 h. For the release profile of chlorambucil, this effect was maximised when ND were reconstituted with DPPC.

Future work

If liposomes – which mimic the cell membrane – were added to the release media, when investigating the release kinetics, the rate of drug release may be affected. The drug release may have a more rapid trend due to the presence of a system into which the drug could be absorbed. More so, plasma could potentially replace the release media. This would lead to investigations into the influence of interactions between ND surface and blood components on the drug release kinetics.

The drug loaded ND systems have been developed for future use in delivering therapeutics to tumour cells by passive targeting, *via* the enhanced permeability and retention (EPR) effect. However, certain limitations, such as poor drug penetration into pancreatic tumour,¹⁶⁵ have stimulated the development of nanocarriers with an active targeting vector attached to the surface, to help improve drug delivery. This targeting ligand will have a high selectivity to bind to a specific receptor on the target cell. There are several ligands that could be used to improve the targeting to cells, and range from small molecules like folic acid,⁴² to macromolecules like antibodies.¹⁶⁶

Additional changes to the bilayer domain of the ND could be made by replacing the phospholipids with block co-polymers. Due to their low CMC,⁴² structural robustness and long circulating time, amphiphilic co-polymers are an attractive alternative in formulating nanodiscs for the incorporation and release of hydrophobic drugs. After initial investigation, assemblies with PB-*b*-PEO co-polymer were observed to have formed with a similar apparent MW as lipid-ND. However, only a small quantity of co-polymer may have assembled into ND. To find the optimum conditions for the reconstitution of monodisperse PB-*b*-PEO ND, several reconstitution parameter could be altered, such as temperature or increasing the incubation time needed for the removal of detergent. Additionally, a different co-polymer could be used.

6.2 Traceable delivery and release of drug

Conclusions

The site-specific modification of scaffold protein has been achieved with the use of SrtA mediated ligation reaction, to allow the label of ND with fluorescein, for *in vitro* imaging. Prior to the SrtA mediated ligation, the His₆ tag on the N-terminus of MSP was cleaved. The SrtA mediated modification approach has allowed the labelling of MSP, with a fluorescent probe, while interacting with the phospholipids within the ND. When mammalian cells were treated with empty and chlorambucil loaded ND good internalisation of MSP by HeLa cells, but little internalisation by Huh7 cells were observed. Chlorambucil showed no cytotoxic activity, presumably as a consequence of low concentration of chlorambucil loaded ND, with which the cells were treated. A new and robust one-step strategy has been developed for reconstituting and loading hydrophobic small molecules into ND systems. With this as a starting platform, several research routes could be investigated.

Future work

A strategy to optimise the labelling of scaffold protein at N-terminus need to be developed as preliminary investigation might have showed that the reaction started sooner than 8 h. However, no strong conclusions could be drawn. To improve the efficiency of the ligation reaction several parameters could be changed. These include reconstitution of ND with a higher concentration and finding a balance between the optimum time and temperature. This will promote the highest yield of labelled protein, in ND formation or free in solution. Finding the optimum balance at a low temperature should improve the imaging of fluorescein-MSP, as well as the efficiency of the ligation reaction.

Although we have demonstrated good internalisation of empty and chlorambucil loaded ND by HeLa cells, further experiments with organelle-specific immunostaining would elucidate the intracellular pathway of the ND. Native HDL is thought to be disintegrated after endocytosis, its apolipoproteins transported to early and late endosomes and finally degraded in lysosomes.¹⁶⁷ Therefore,

is important to identify the organelles involved in the transport and the exact location of fluorescein MSP within the mammalian cells.

The ability of drug loaded ND to induce cellular death needs to be assed further, as preliminary investigation has shown that low concentrations of chlorambucil in loaded ND has prevented chlorambucil to have an apoptotic effect on the cells. Increasing the concentration of assemblies with which the cells are treated would lead to higher concentrations of chlorambucil and therefore influence the cell viability.

7 Chapter 7 – Experimental materials and methods

7.1 Instrumentation and materials

Sterilisation of media, buffers and appropriate equipment was achieved using either a Prestige Medical bench top autoclave or a LTE Touchclave-R autoclave. Bacterial culture was grown using a Stuart Scientific shaker incubator. Cell disruption was performed by using TS series cell disruptor (Constant Systems Ltd, UK). Centrifugation was performed using Avanti J-26 XP (Beckman) Centrifuge.

Purification of MSP1D1 was achieved *via* a Ni-NTA column. SDS-PAGE electrophoresis was performed using a BioRad mini protean 3 apparatus. BIO RAD molecular imager® Gel Doc™ was employed to visualise the polyacrylamide gel using a combination of UV and white light. Mass spectroscopy analysis of ND without His₆ tag and fluorescein-ND was done using a Bruker MicrOTOF accurate MS system.

Drying the lipid film was performed under vacuum using the Edwards pump (model RV3). Nutating Mixer (VWR International) was used as a shaker during ND preparations. Maxi GeBAflex-tube Dialysis kit (MWCO 3.5kDa) (Gene Bio-Application Ltd) was used for the dialysis of ND samples. Bio-Beads® SM-2 Adsorbent (Bio-Rad Laboratories Inc.) was used for the removal of detergent. Size-exclusion chromatography experiments were carried out with Superdex 200 10/300 Chromatographic Separation Columns and run using ÄKTApurifier™ system (GE Healthcare). Thermo scientific NanoDrop 2000 and the Perkin-Elmer UV-vis spectrophotometer with the Lambda 900 software were used to measure the MSP1D1 and drugs absorbance, and to run Total Phosphorus Assays, respectively. DLS measurements were performed using Zetasizer Nano (Malvern) particle size analyser with Zetasizer software. The collected data from DLS and SEC was exported with Microsoft Excel software and analysed with OriginPro software. Circular dichroism spectroscopy of MSP1D1, empty and drug loaded ND was performed by Mr. Nasir Khan on an APP Chriscan CD spectropolarimeter. Reverse phase HPLC analysis was performed

on Agilent 1290 series HPLC system. SAXS experiments were conducted by Dr Amin Dilmaghani with SAXSpace camera (Anton Paar, Graz, Austria) connected to an analytical X-ray generating equipment (ISO-DEBYEFLEX3003, GE Inspection Technologies GmbH).

The phospholipids were obtained from Avanti Polar Lipids Inc. Analytical grade reagents were purchased from Sigma-Aldrich and Fisher Scientific. Plasmid MSP1D1 was purchased from AddGene.

Mammalian cell culture manipulations were performed by Darren Machin inside a Thermo Scientific MSC-Advantage Class II Biological Safety Cabinet. A Sanyo CO₂ cell incubator was used to grow the cells. Fluorescence microscopy analysis of mammalian cell culture slides was performed using a Zeiss LSM510 META upright confocal microscope, coupled with ZEN imaging software. Wavelengths at 408 nm, 488 nm and 555 nm were used to excite the DAPI, fluorescein fluorophores and rhodamine.

7.2 Buffer solutions and media

All solutions were made up to 1 L, with 18.2 M Ω purified water unless stated otherwise. The pH of solutions was adjusted using 6 M NaOH and/or 4 M HCl.

7.2.1 Bacterial growth media

Lysogeny broth media (LB): Tryptone (10 g), 172 mM NaCl and yeast extract (5 g). The solution was autoclaved at 121 °C for 20 min.

Terrific Broth media (TB): tryptone (12 g), yeast extract (24 g) and glycerol (4 mL). After autoclaving at 121 °C, TB media was left to cool, and filter sterilised KH₂PO₄ and K₂HPO₄ solutions were added to a final concentration of 17 mM and 72 mM, respectively.

Auto Induction media (AIM): Tryptone (10 g), yeast extract (5 g), MgCl₂ (2 mM), 1000 x Metals (200 μ l), 50 x Salts (20 mL), 50 % (v/v) glycerol. After autoclaving at 121 °C, 50 % (w/v) glucose and 50 % (w/v) lactose were added.

50 x Salts: 1.25 mM Na₂HPO₄, 1.25 mM KH₂PO₄, 2.5 mM NH₄Cl and 250 mM NaSO₄.

1000 x Metals stock (100 mL): 50 mM FeCl₃•6H₂O, 20 mM CaCl₂•6H₂O, 100 mM MnCl₂•4H₂O, 100 mM ZnSO₄•7H₂O, 1.7 mM CoCl₂•6H₂O, 2 mM CuCl₂•2H₂O, 4.1 mM Na₂MoO₄•2H₂O, 2 mM Na₂SeO₃, 2 mM H₃BO₃, 2 mM NiCl₂•6H₂O, 2 mM NiSO₄•6H₂O and HCl (5 mL/L).

7.2.2 Protein purification buffers

Phosphate buffer saline (PBS): 20 mM NaH₂PO₄ titrated to pH 7.4

Lysis buffer (50 mL): 20 mM PBS pH 7.4. After resuspending the cells, 10% Triton X-100 was added to make 1%

Wash buffers:

Tris buffer I: 40 mM Tris, 0.3 M NaCl, 1% Triton X-100, pH 8

Tris buffer II: 40 mM Tris, 0.3 M NaCl, 50 mM Na-Cholate, 20 mM Imidazole, pH 8

Tris buffer III: 40 mM Tris, 0.3 M NaCl, 50 mM Imidazole, pH 8

Elute buffer: 40 mM Tris, 0.3 M NaCl, 0.4 M Imidazole, 40 mM Na cholate, pH 8

7.2.3 Buffers for SDS-Polyacrylamide gel electrophoresis (SDS-PAGE)

SDS-PAGE loading buffer (pH 6.8): 50 mM Tris HCl, 100 mM DTT, 2% (w/v) sodium dodecyl sulphate (SDS), 10% (v/v) glycerol, 0.1% (v/v) bromophenol blue and complete to volume with water

5x SDS-PAGE running buffer: 125 mM Tris base, 960 mM glycine, 0.5% (w/v) SDS

7.2.4 ND and ND-drug assembly buffer

Method A: 20 mM Tris pH 7.4, 0.1 M NaCl

Method B: 40 mM Tris pH 8, 0.3 M NaCl

7.2.5 SEC chromatography and release studies buffer

20 mM Tris pH 7.4, 0.1 M NaCl

7.3 Methods

7.3.1 Purification of DNA

DNA was purified using QIAprep Spin Miniprep Kit (QIAGEN). A pipette tip of cells from the glycerol stock was resuspended in P1 buffer (250 μ L). To lyse the cells, P2 buffer (250 μ L) was added and gently mixed 4-5 times, causing the solution to go blue. N3 buffer (350 μ L) was added and immediately mixed gently 4-5 times. The white precipitate formed was discarded by centrifugation (17000 rcf, for 10 min) and the supernatant was applied to a QIAprep spin column before further centrifugation at 17000 rcf, for 1 min. The column was washed first with PB buffer (500 μ L) followed by PE buffer (750 μ L) and the supernatant removed after each wash by centrifugation at 17000 rcf, for 1 min. The column was centrifuged again at 17000 rcf, for 1 min to separate any residual buffer. Sterile H₂O (50 μ L) was applied to the centre of the column, left at room temperature for 1 min before the column was centrifuged at 17000 rcf, for 1 min to elute the purified DNA which was then submitted for sequencing to GATC Biotech. The results were analysed using BioEdit sequence alignment editor ClustalW.

7.3.2 Protein overexpression, purification and analysis

The cell preparation was conducted under sterile conditions. 2 μ L of plasmid pMSP1D1 was added to 50 μ L of competent *E. coli* BL21 Gold (DE3), incubated on ice for 30 min and heat-shocked at 42 °C for 45 s before returning on ice for a further 5 min. 200 μ L of LB media was inoculated with the cell/plasmid mixture and incubated at 37 °C, with shaking at 200 rpm, for 1 h. 200 μ L of transformed cells were plated on Agar plates containing kanamycin (50 μ g/mL) and incubated overnight at 37 °C, with shaking at 200 rpm.

A single colony of *E. coli* BL21 Gold (DE3) cells harbouring the pMSP1D1 was used to inoculate LB media (10 mL, 50 µg/mL kanamycin). The starter culture was incubated overnight at 37 °C before adding it to TB or AIM media (1 L, 50 µg/mL kanamycin). For TB media – the culture was grown at 37 °C and induced with 1 mM IPTG (isopropylthio-β-galactoside) when the optical density (OD₆₀₀) reached 2.5. One hour after induction, the temperature was lowered to 28 °C. Four hour after induction, the cells were harvested. For AIM media - the culture was grown at 20 °C for 24 h before harvesting. The cells were isolated by centrifugation (10000 rpm, 10 min), the supernatant discarded and the bacterial pellet stored at -80 °C.

7.3.2.1 Protein purification

The frozen cell pellet was resuspended in lysis buffer (50 mL) and left on ice for 30 min. The suspension was mechanically disrupted using a Constant Systems Cell disruptor (35 kpsi, 4 °C), the lysate cleared by centrifugation (48000×g, 20 min), the pellet discarded and the supernatant passed down on a Ni-NTA column (Qiagen, at rt or 4 °C) pre-equilibrated with PBS buffer. The column was washed sequentially with Tris buffer I, II and III (3×CV each), before the protein was eluted with elution buffer (1×CV). Protein-containing fractions and their purity were identified by SDS-PAGE. The protein was dialysed against 40 mM Tris, 0.3 M NaCl, 40 mM Na cholate, pH 8 before measuring its concentration by UV spectroscopy at 280 nm, using a theoretical extinction coefficient of 21430 M⁻¹ cm⁻¹.

7.3.2.2 Protein analysis

Sodium dodecyl sulphate polyacrylamide gel electrophoresis (SDS-PAGE)

SDS-PAGE was performed using BioRad tetragel apparatus (1 mm plates). A resolving gel of appropriate percentage was prepared using the materials listed in Table 7.1, with the addition of TEMED immediately prior to pouring the gel. The resolving gel was poured to approximately $\frac{3}{4}$ the height of the plate and saturated butanol (0.5 mL) added to the surface. Once the resolving gel has

set, the butanol was removed by washing with water and a stacking gel (5%) was prepared using the materials in Table 7.1. TEMED was added immediately prior to applying the gel to the top of the resolving gel. A comb with a suitable number of lanes was inserted into the stacking gel and left to set.

Components	Resolving gel Volume/mL 12%	Stacking gel Volume/mL 5%
H ₂ O	3.2	2.45
30% acrylamide/bisacrylamide mix	4	0.67
1.5 M Tris, pH 8.8	2.5	na
1.5 M Tris, pH 6.8	na	0.75
10 % Sodium dodecyl persulfate (SDS)	0.1	0.04
15% (w/v) Ammonium persulphate (APS)	0.1	0.04
Tetramethylethylenediamine(TEMED)	0.005	0.005

Table 7.1 Components and quantities for SDS-PAGE resolving and stacking gels; na – not applicable

Once the gel has set, it was put inside an electrophoresis tank, an optimum volume of SDS running buffer was added and the comb was removed. Samples of MSP1D1, ND and fluorescein-ND (10 μ L) were mixed with an equal volume of loading buffer and heated at 95 °C for 5 min. The samples were loaded into different lanes of the gel using a syringe, along with Invitrogen Mark 12 standard protein marker (5 μ L). Electrophoresis was performed at a limiting power of 200 V until the samples were seen to reach the bottom of the gel. The gel was imaged directly by staining with Instant Blue stain. The gels were imaged using EPI-white illumination in the BIO RAD Molecular Imager® Gel Doc™. The gel containing fluorescently labelled MSP1D1 was imaged prior to staining.

Protein concentrations

The absorbance was measured at 280 nm to determine the concentration of MSP1D1. The concentration of protein was calculated with Beer-Lambert Law:

$$A = \varepsilon \times c \times l$$

Equation 7.1 Beer-Lambert Law; A = absorbance, ε = molar extinction coefficient ($\text{mol}^{-1}\text{cm}^{-1}$), c = concentration (mol) and l = path length (cm).

7.3.3 The reconstitution of nanodisc assemblies

7.3.3.1 Phospholipid concentrations

Assay of Total Phosphorus was used to determine the lipid composition - one phosphorus atom corresponds to one phospholipid. In this analysis the inorganic phosphate is digested from organic sample to phospho-molybdic acid by the addition of ammonium molybdate. During heating at 100 °C, the colour of the reduced complex turns blue and gives the complex an absorbance at 820 nm, which facilitates the calculation of phosphorus concentration. The assay was done before every ND preparation, as the lipid is stored in chloroform that evaporates over time even at -20 °C, leading to a change in lipid concentration.

Lipid/ND samples were placed into the bottom of each tube. Into extra six separate tubes the following quantities of phosphorus standard solution were placed: 0 μmoles , 0.0325 μmoles , 0.065 μmoles , 0.114 μmoles , 0.163 μmoles , and 0.228 μmoles . The phosphorus standard solution at different concentrations was used to generate a calibration curve. Subsequently, 0.45 mL 8.9 N H_2SO_4 was added to each tube, before being heated at 200 - 215 °C for 25 min. The tubes were cooled for 5 min before 150 μL H_2O_2 was added. Heating was continued for an additional 30 min, before cooling the tubes to room temperature. To the cooled solutions, deionized water (3.9 mL), 2.5% ammonium molybdate (VI) tetrahydrate solution (0.5 mL) and 10% ascorbic acid solution (0.5 mL) were added to all tubes, then vortexed and heated at 100 °C for 7 min.

The absorbance of each standard calibrant was plotted against its number of moles. A linear function was fitted to the resulting calibration curve and the concentration of phosphorus in each sample was calculated (Figure 7.1). The

lipid concentrations calculated using the equation generated by the calibrants were found to be between 26 mM and 31 mM.

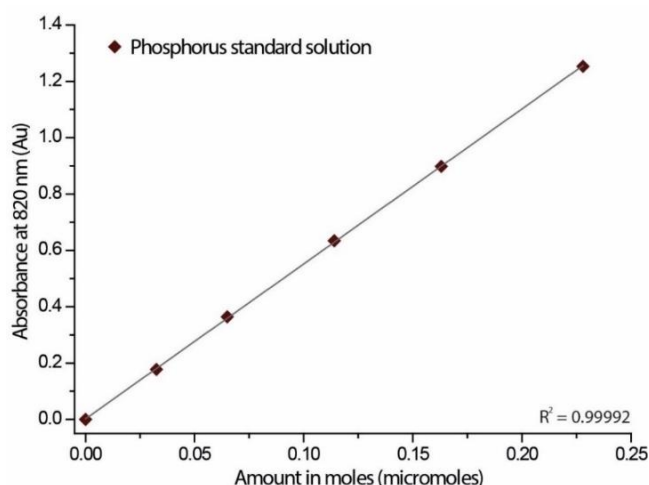


Figure 7.1 Calibration curve for determining the total phosphorus in the phospholipid samples generated using the phosphorus standard solution at different concentrations

7.3.3.2 Method A of reconstitution

An appropriate volume of lipid dissolved in chloroform (concentration calculated with phosphorus assay) was dried to a thin film under vacuum. The prepared lipid was then dispersed in a solution of Na cholate in ND buffer (1:1.54 and 1:2 POPC to Na cholate molar ratio), to form micelles, at room temperature, by gentle vortexing and sonication. The detergent was added at a concentration of 50 mM so that its final concentration would be around the critical micelle concentration. Following this, an appropriate volume of MSP1D1 (1:65 and 1:50 MSP to lipid molar ratio) in elution buffer was added. The solution was incubated with gentle shaking for 90 min, close to the transition temperature of the lipid (4 °C for POPC, 50% POPS, DLPC, 10% DOPEPEG, and 42 °C for DPPC). An appropriate amount of wet bio-beads (0.3 g per mL of ND), previously washed with 2 volumes of methanol and 4 volumes of ND buffer, were added. The mixture was incubated for 5-6 h, close to the transition temperature of the lipid. The bio-beads were then separated by careful pipetting.

7.3.3.3 Method B of reconstitution

An appropriate volume of lipid dissolved in chloroform (concentration calculated with phosphorus assay) was dried to a thin film under vacuum. The prepared

lipid was then incubated with a solution of MSP stabilised in Na cholate micelles (MSP in elution buffer) (1:65:100 and 1:50:100 MSP to lipid to Na cholate molar ratio), by gentle shaking for 2.5 h, close to the transition temperature of the lipid. From here, the reconstitution followed method A. Briefly, an appropriate amount of wet bio-beads (0.3 g per mL of ND) were added and the mixture and incubated for 4 to 5 h, close to the transition temperature of the lipid. The bio-beads were then separated.

The size and monodispersity of the reconstituted ND were verified by analysis *via* size exclusion chromatography and dynamic light scattering.

7.3.4 The reconstitution of ND with block co-polymers

The ND were formulated following method B of reconstitution. The molar ratios of MSP to polymer used were 1:15, 1:20 and 1:30. The incubation temperature and time before adding bio-beads were varied to find the optimum conditions for the assembly of ND. The conditions used were as followed: 1:15 MSP to polymer, mixtures incubated at 55 °C for 2.5 h before adding the bio-beads; 1:20 MSP to polymer, mixtures incubated at 55 °C for 2.5, 4 or 5 h before adding the bio-beads; 1:30 MSP to polymer, mixtures incubated at 4 °C or room temperature for 2.5 h before adding the bio-beads. Subsequently, for all mixtures, the bio-beads were separated after 5 h.

7.3.5 The reconstitution of drug loaded ND

For each drug incorporation method the ND were formed following both methods of reconstitution.

7.3.5.1 Method 1 – postloading

Firstly, empty ND were reconstituted using the above methods. To the solution of empty ND, an appropriate amount of drug (in powder form) was added. The mixture was incubated overnight with gentle shaking, close to the transition temperature of the lipid. The unincorporated drug was separated by size exclusion chromatography.

7.3.5.2 Method 2 – preloading

An appropriate volume of drug and lipid were dissolved in chloroform (concentration of lipid calculated with phosphorus assay) and dried to a thin film under vacuum. The prepared lipid and drug were then incubated with a solution of 50 mM Na cholate or with a solution of MSP stabilised in Na cholate micelles (MSP in elution buffer) (1:65:100 and 1:50:100 MSP to lipid to Na cholate molar ratio). Subsequently, the preloading of drug followed method A or method B of ND reconstitution.

The size, monodispersity, loading efficiency and rate of drug release of the reconstituted drug loaded ND were verified by analysis *via* size exclusion chromatography, dynamic light scattering, HPLC and UV spectroscopy.

7.3.6 Analysis of MSP1D1 and of empty and drug loaded ND

7.3.6.1 Analysis by mass spectrometry

Samples were diluted to 50% (v/v) with H₂O before being loaded directly into the instrument. Prior to MS analysis, the samples were automatically diluted with 0.1% TFA 50%, MeCN (v/v) in H₂O. Processing and deconvolution of multiple charge states was performed using BioPharma Compass 1.1 Software.

7.3.6.2 Analysis by circular dichroism

CD spectroscopy was used to observe how the secondary structure of the scaffold protein changes when interacting with the lipid domain of the ND and with the drug molecules incorporated. The secondary structure is determined by measurements in the far-UV region (190 - 250 nm). In this region, the signal appears when the peptide bond is located in a regular, folded environment. Three different conformations, α -helix, β -sheet and random coil structures, generate a characteristic shape and magnitude of CD spectra (Figure 7.2).

Samples of MSP, ND and ND-drug suspended in elution buffer were measured on CD spectropolarimeter. For measurements in the far-UV (190-260 nm) the CD signal is recorded in a 1 mm path-length cell using a sample with concentration of around 20 μ M.

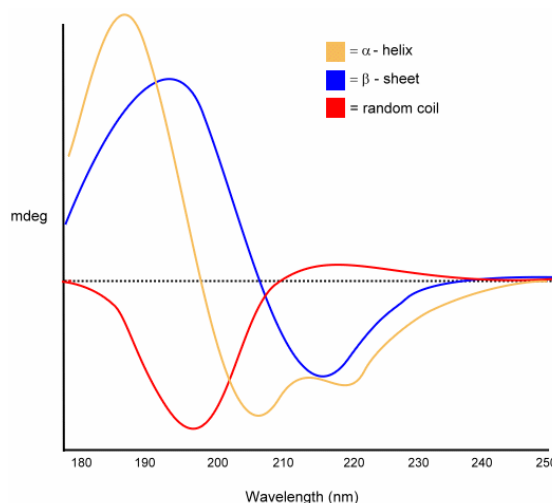


Figure 7.2 CD spectra of poly-L-lysine in α -helix, β -sheet and random coil conformations¹⁶⁸

7.3.6.3 Analysis of size and monodispersity by size exclusion chromatography

Size-exclusion chromatography can be used to separate components based on their molecular size and shape by using a bed of porous particles. These solid phase beads contain spaces of different sizes that will control the elution path of the analysed sample. Molecules smaller than the pore size enter the porous particles and have a longer path and retention time than larger molecules that can only enter the gel bed but not the pore bed. The size and shape of the analysed molecules is proportional with the fraction of pores the molecules can enter. Hence, the molecules will have an average resistance time in the pores.¹⁶⁹ However, only molecules with masses between the higher and lower pore size can be separated. Samples that surpass these margins will not be separated and therefore cannot be analysed by SEC.

Samples of MSP1D1 (in elution buffer), ND and drug-loaded ND (250 μ L) were applied to a Superdex 200 10/300 Chromatographic Separation Column (GE Healthcare), previously equilibrated with filtered 20 mM Tris pH 7.4, 0.1 M NaCl (1 \times CV), using the ÄKTA purifierTM system. The analysis was run at 280 nm and the absorbance wavelength characteristic for every drug molecule (Table 7.2). The samples were eluted in 20 mM Tris buffer, 0.1 M NaCl, at a flow rate of 0.5 mL/min. Fractions were collected at 0.25 mL. All fractions containing MSP1D1, ND or ND-drug were identified using UV-vis spectroscopy (absorbance

measured at 280 nm). The identified MSP1D1, ND and ND-drug samples were stored at 4 °C. Data collected was exported with Microsoft Excel and plotted with Origin Pro.

Drug molecule	UV absorbance used in the SEC analysis
Amiodarone (AMD)	242 nm
Chloroquine (CLQ)	343 nm
Chlorambucil (CLB)	254 nm
Thioridazine (TRD)	262 nm
Oxymethazoline (OXM)	315 nm
Novobiocin (NVB)	324 nm
Tamoxifen (TMX)	277 nm
Camptothecin (CPT)	218 nm
Indomethacin (IND)	318 nm
Clofazimine (CFZ)	486 nm
Rimantadine (RMD), Curcumin (CCM) and Fluorescein (FLC)	280 nm

Table 7.2 Drug molecule and their absorbance wavelength at which the analysis by SEC was conducted

A set of calibrants with different MW, were run through the column (Figure 7.3). Blue Dextran, which has a MW of 2 MDa, was used to identify the void volume of the column. This void volume is associated with the fastest elution time it takes a sample to pass through the column. The close elution time between Blue Dextran and Thyroglobulin is presumably related with the highest pore size of the column. For this reason we can speculate that the largest samples which can elute in the void volume might be smaller than 2 MDa. The subsequent analysis of purified protein, ND and ND-drug were not affected by this conclusion.

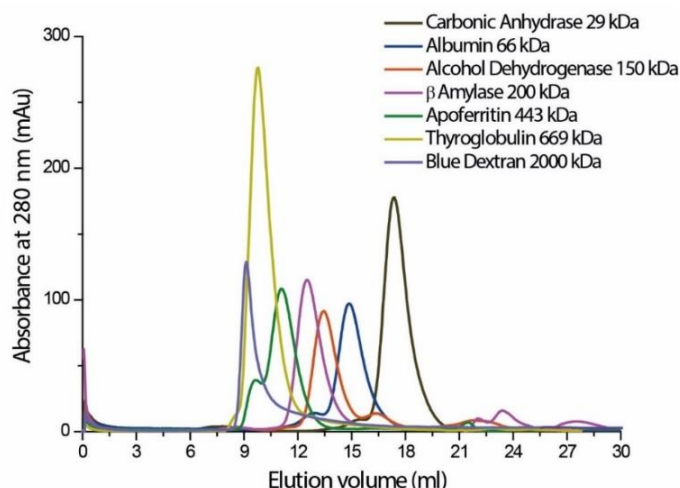


Figure 7.3 SEC chromatograms of the calibrants with known MW used to calculate the apparent MW of all samples passed through the column

To compare the estimated mass of ND to its expected MW,⁸⁰ the elution volume found during SEC analysis was placed on a calibration graph. The known MW of each standard calibrant was plotted against the ratio of its elution volume (V_e) and the void volume (V_o) of the column (Figure 7.4). The resulting calibration curve was modelled by a linear function and the apparent MW of the sample was calculated. The equation generated by the calibrants was used to further estimate the ND's apparent mass.

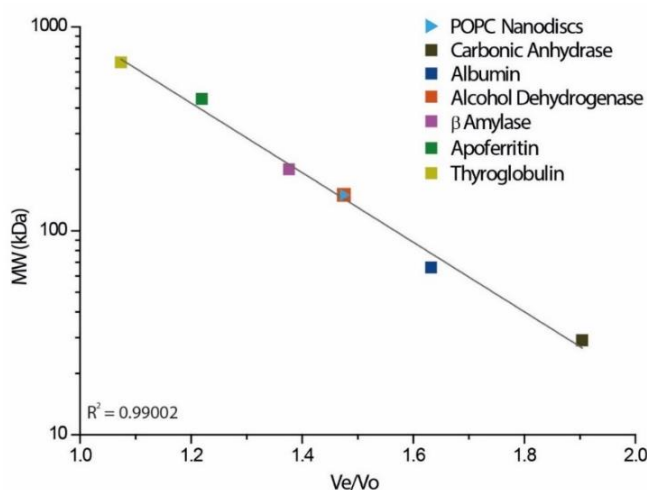


Figure 7.4 Calibration curve of the SEC elution times of calibrants with known MW and POPC; ND have an apparent MW of 150 kDa

7.3.6.4 Analysis of size distribution by dynamic light scattering

The principle behind the technique of DLS is that a sample is illuminated by a laser beam and the intensity of the scattered light fluctuations is detected at a known scattering angle θ . The intensity fluctuations of the scattered light are determined by the size, shape and interactions of the particles.

DLS measures the speed at which the particles are diffusing due to Brownian motion and relates it to the size of the particles. The larger particles will have a slower Brownian motion, while smaller particles will move more rapidly. This is related with slower changes in signal for large particles while the correlation continues for a long time. In the case of small particles, the correlation will decrease more rapidly. The signal arose from the random Brownian motion of the particles can be defined as an autocorrelation function (Eq. 7.2), which is extracted as a function of delay time (τ) from the data processed using a correlator.

$$G(\tau) = \exp^{-2\Gamma\tau}$$

Equation 7.2 Autocorrelation function; τ = the time difference of the correlator; Γ = the decay rate.

The correlator measures the degree of similarity between two signals or one signal with itself at different time intervals and converts the fluctuations into an intensity correlation function. By analysing the intensity correlation function, the translational diffusion coefficient is obtained:

$$\Gamma = q^2 D$$

Equation 7.3 Γ = decay rate; D = translational diffusion coefficient; q = wave vector; The wave vector reflects the distance the particles are travelling and is dependent on the scattering angle:

$$q = \frac{4\pi n}{\lambda} \sin \frac{\theta}{2}$$

Equation 7.4 n = refractive index of dispersant; λ = wavelength of the laser; θ = scattering angle.

From the translational diffusion coefficient, D , which describes the rate of the Brownian motion, the diameter of a particle is calculated using the Stokes-Einstein equation:

$$d(H) = \frac{kT}{3\pi\eta D}$$

Equation 7.5 Stokes-Einstein equation; $d(H)$ = hydrodynamic diameter; k = Boltzmann's constant; the value is $1.380650 \times 10^{-23} \text{ J K}^{-1}$; T = absolute temperature; η = viscosity.

The hydrodynamic diameter is a value that indicates how a particle diffuses within a fluid and, for non-spherical particles is the diameter of a sphere that has the same average translational diffusion coefficient as the particle being measured.

Unfiltered samples of MSP1D1, ND and drug-loaded ND collected from SEC were characterised by size and polydispersity with a Zetasizer Nano (Malvern) particle size analyser. The samples were measured using a disposable micro cuvette (70 μL), at 4 °C. For accurate results, the samples were equilibrated for 5 min and, for each sample, three measurements were made. Data collected was exported with Microsoft Excel and plotted with Origin Pro.

7.3.6.5 Analysis of drug loading per ND using HPLC

In this separation technique the solvent used is polar and the silica bed particles within the column have long hydrocarbon chains attached to the surface in order to make it non-polar. Attractions will tend to form between non-polar compounds in the sample and the hydrocarbon groups. These interactions will make them less soluble in the polar solvent and slow them down on their way through the column.¹⁷⁰

Samples of drug loaded ND were analysed by reverse phase HPLC at 280 nm and drugs absorbance wavelengths to evaluate the number of drug molecules incorporated per ND. The drug loaded ND samples were resuspended in TFE in order to disassemble the systems. MSP and free drug in TFE were run on the HPLC column to obtain a calibration curve which was used by the Agilent

Chemstation software to automatically generate a calculated amount of the analysed components. The given amount of components was further used to calculate the number of drug molecules loaded per ND, by dividing the concentration of drug loaded ND by the concentration of empty ND.

7.3.6.6 Analysis of drug loading per ND using UV spectroscopy

Similarly to HPLC analysis, UV spectroscopy was employed to determine the number of drug molecules loaded per ND, using two methods of calculation described in Chapter 3. Prior to analysis, drug loaded ND, MSP and drugs were suspended in TFE.

7.3.6.7 Analysis of rate of drug release from ND by UV spectroscopy

Dialysis tubes containing ND with loaded drug were put in 900 mL of 20 mM Tris pH 7.4, 100 mM NaCl. Samples of ND containing drug (10 μ L) were taken at specific time intervals and the concentration of drug was determined by UV-vis spectroscopy measurements on a NanoDrop. The release studies of all drug-loaded ND assemblies were performed in triplicate. The fractional release and half-life of drug molecules were calculated as described in Chapter 3.

7.3.7 The reconstitution of drug loaded MLV and ULV and their analysis by SAXS

An appropriate volume of POPC (5 wt%) and drug (20 mol%) dissolved in chloroform were dried overnight into a thin film under vacuum. The prepared lipid and drug were then dispersed in dH₂O (200 μ L), at room temperature, by gentle vortexing. The vortexing was conducted in 10 cycles, each of 15-20 sec, with 5 minutes break in between. The drug loaded MLVs and ULVs were then kept in the fridge prior to analysis by Dr Amin Dilmaghani.

7.3.8 Sortase mediated ligation of MSP with a fluorescent probe

SrtA and fluorescein depsipeptide were prepared in HEPES buffer by Dr Daniel Williamson, at University of Leeds.

Prior to the SrtA mediated ligation, TEV protease was used for the cleavage of His₆ tag attached to the N-terminus of MSP1D1. ND (137 μ L, 27 μ M) was incubated, overnight, in the presence of TEV protease (2.74 μ L, 1 μ M final concentration), at 4 °C. The reaction was monitored by MS, however complete cleavage was not observed. The reaction mixture was separated by SEC.

SrtA (8.6 μ M final concentration, 480 μ M stock concentration), ND (27 μ M) and fluorescein depsipeptide (5 equivalents, 2 mM stock concentration) were mixed together to form a total volume of 55.5 μ L. The mixture was then left at room temperature. After 6 h, an additional 4 equivalents of depsipeptide was added and the incubation continued overnight. The reaction mixture was monitored by MS and SDS-PAGE. Once the MSP had been modified, the ND mixture was immediately purified either using nickel resin or by SEC.

The reaction mixture was incubated with nickel affinity resin (Qiagen) for up to 4 h, by gently shaking. The mixture was subsequently separated from the resin by centrifugation and careful pipetting, and washed with ND buffer.

7.3.8.1 Mammalian cell culture

Media, buffers and reagents

PBS (100 mL): A single PBS tablet was dissolved in H₂O. The solution was autoclaved for 20 minutes at 121 °C.

1% or 4% BSA (50 mL): 1% or 4% bovine serum albumin (BSA) was dissolved in PBS

0.1% Triton (50 mL): 0.1% (v/v) triton was dissolved in PBS

4% PFA (100 mL): 4% (w/v) paraformaldehyde was dissolved in PBS with heating at 70 °C, filtered (0.2 µm) and left to cool to room temperature before use.

General passage procedure, cell preparation before transfection and the protein transfection procedure were conducted by Mr Darren Machin, at University of Leeds.

Cell fixation

The growth media or transfection solution was removed from each well plate and the cells were washed with PBS (2 × 1 mL) before being treated with 4% PFA (1 mL) for 10 minutes at room temperature. The cells were washed and stored in PBS (2 × 1 mL) at 4 °C for no longer than a week. Transfection experiments were stored in the dark to prevent photo-bleaching of the fluorophore.

Cell immobilisation and confocal fluorescence microscopy

The cells were plated at 150000 cells/well, on round coverslips in 12-well plates. After 24 h, the medium was replaced and the cells were incubated with 2 µL samples (empty and chlorambucil loaded fluorescein-ND, empty rhodamine-ND) or left untreated. After 4 h and 24 h, the medium was removed and cells were washed with 2 × 1 mL PBS, fixed with 4% PFA for 10 minutes and washed again with 2 × 1 mL PBS. The cells were mounted onto a glass slide with Prolong® Gold Antifade Reagent with DAPI (15 µL) – used to stain nuclei. The slides were left overnight in the dark before being sealed with nail varnish to preserve the cells. The cells were stored at 4 °C in the dark for weeks to months without degradation. Confocal images were acquired on a Zeiss LSM510 META upright confocal microscope.

7.3.8.2 MTT assay

The cytotoxicity of empty ND, chlorambucil loaded ND and free chlorambucil was determined on HeLa cells using a MTT assay. Cells were plated out in 96 well plate - 1×10^4 cells per well. These were left overnight to grow up in 100 µL

medium. On the day, MTT Mw414 (Sigma) was dissolved in serum free medium at 1 mg/mL – conducted in sterile conditions. After removing the medium from wells, 100 μ L MTT solution was added per well, covered with aluminium foil and incubated at 37 °C for 30 minutes. The MTT solution was discarded and replaced with 100 μ L DMSO and shook for 5 min at 60 rpm, to dissolve the purple precipitate. The cells were treated for up to 24 h with the same concentration of empty ND, ND CLB and free drug, and the cell viability was determined after measuring the absorbance at 570 nm.

8 Chapter 8 – Appendix

```
      10      20      30      40      50      60
MSP1D1  ....|...|...|...|...|...|...|...|...|...|...|
Seq Data GATGGAGAAATCCCCCTCTAGAATATTTGTTACTTTAAGAAGGAGATAT.....

      70      80      90     100     110     120
MSP1D1  ...|...|...|...|...|...|...|...|...|...|...|
Seq Data CATCATCATCATCATCATCAGATTATGATATTCCCTACTACTGAGAATTGTATTTTCAG

      130     140     150     160     170     180
MSP1D1  ...|...|...|...|...|...|...|...|...|...|...|
Seq Data GGTTCCTACCTTCAGTAACTTCGCGAACTTGGGCCCGTGACGAGGAATTCGGGAC

      190     200     210     220     230     240
MSP1D1  ...|...|...|...|...|...|...|...|...|...|...|
Seq Data AACCCTGGAAAAAGAAACCGAGGGACTGCGTCAGGAAATGTCCAAAGATTAGAAAGAGGTG

      250     260     270     280     290     300
MSP1D1  ...|...|...|...|...|...|...|...|...|...|...|
Seq Data AAGGCCAAGGTCAGCCATATCTCGATGACTTTCAGAAAAATGGCAGGAAGAGATTGGAA

      310     320     330     340     350     360
MSP1D1  ...|...|...|...|...|...|...|...|...|...|...|
Seq Data TTATATCGTCAAAAGGTGGAACCGCTGCGTTCGGAACTGCAAGAGGGGGCAGCCAAAAA

      370     380     390     400     410     420
MSP1D1  ...|...|...|...|...|...|...|...|...|...|...|
Seq Data CTCCATGAGCTCCAAGAGAAGCTCAGCCATTAGGCGAAGAAATCGCGATCGCCCCGT

      430     440     450     460     470     480
MSP1D1  ...|...|...|...|...|...|...|...|...|...|...|
Seq Data GCACATGTTGATGCACTCCGACTCATTGGCGCGGTATTCGGATGAACCTCGCCAGCGT

      490     500     510     520     530     540
MSP1D1  ...|...|...|...|...|...|...|...|...|...|...|
Seq Data TTGGCCGCACGTCTCGAGGCGCTGAAAGAAACGGGGGTGCCGCTTGGCTGAGTACCAC

      550     560     570     580     590     600
MSP1D1  ...|...|...|...|...|...|...|...|...|...|...|
Seq Data GCGAAAGCGACAGAACCTGAGCACCTTGAGCGAAAAAGCGAAACCGGCGCTGGAAGAT

      610     620     630     640     650     660
MSP1D1  ...|...|...|...|...|...|...|...|...|...|...|
Seq Data CTACGCCAGGGCTTATTGCCTGTTCTTGAGAGCTTTAAAGTCAGTTTCTGTGAGCTCTG

      670     680     690     700     710     720
MSP1D1  ...|...|...|...|...|...|...|...|...|...|...|
Seq Data GAAGAATATACTAAAAAGCTGAATACCCAGTAAGCTT.....GCGGCCGCACTCGAGCACCA

      730     740     750     760     770     780
MSP1D1  ...|...|...|...|...|...|...|...|...|...|...|
Seq Data CCACCACTGAGATCCGGCTGCTAACAAAGCCCGAAAGGAGCTGAGTTGGCTGCTGC
```

Figure 8.1 DNA sequence of MSP1D1

```

      10      20      30      40      50      60
MSP1D1      . . . . . TMGHHHHHHHDYDIPTTENLYFQGSTFSKLRQQLGPVTOEFWD
Seq Data    DGEFPL*NILFTLRRRY. . . . .

      70      80      90      100     110     120
MSP1D1      . . . . . NLEKETEGLRQEMSKDLEEVKAKVQPYLDDFQKKWQEEMLYRQKVEPLRAELQEGARQK
Seq Data    . . . . .

      130     140     150     160     170     180
MSP1D1      . . . . . LHELQEKLSPLGEMRDRARAHVDALRTHLAPYSDELQRQLAARLEALKENGGLARLAEYH
Seq Data    . . . . .

      190     200     210     220     230     240
MSP1D1      . . . . . AKATEHLSTLSEKAKPALEDLRQGLLPVLESFKVSFLSALEEYTKKLNTQ*AX
Seq Data    . . . . . *CGRTRAPP

      250     260     270     280     290     300
MSP1D1      . . . . . PPPLRSGC*QSPKGS*VGCCHR*AITSIPTWGL*TGLEGFFAERRNYIRIGEDWAPCSGA
Seq Data    . . . . .

      310     320     330     340     350     360
MSP1D1      . . . . . LSAAGVVVTRSVTATLASALAPAPFAFFPSFLATFAGFFRQALNRGLPLGFRFSALRHLD
Seq Data    . . . . .

      370     380     390     400     410     420
MSP1D1      . . . . . PPKLD*GDGSRNGPSP**TVFRPLTLESTFFNSGLLVQTGTTLNPIPGYSFDLKGILPIS
Seq Data    . . . . .

      430     440     450     460
MSP1D1      . . . . . AYWVKN*PDLFKIYPEF*QNFTAYNLGGTFPGKWAGNPNLVIF
Seq Data    . . . . .

```

Figure 8.2 Amino acids sequence of MSP1D1

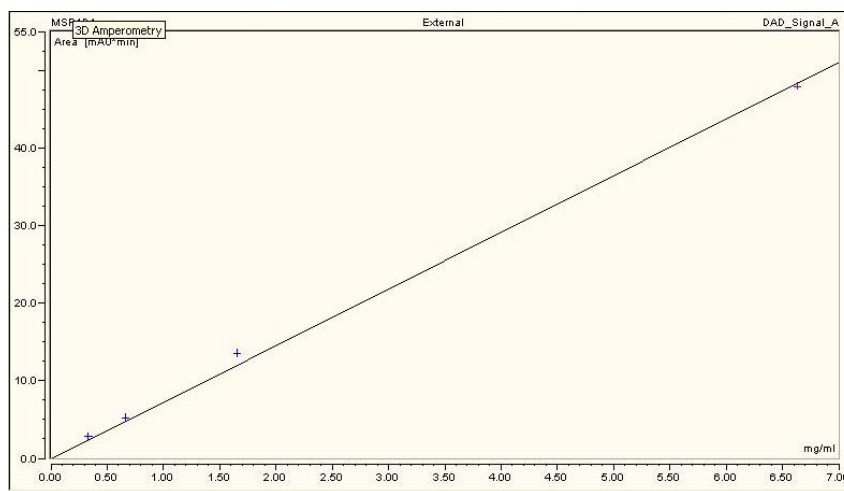


Figure 8.3 Calibration curve generated after HPLC analysis, at 280 nm, of a series of MSP with known concentrations

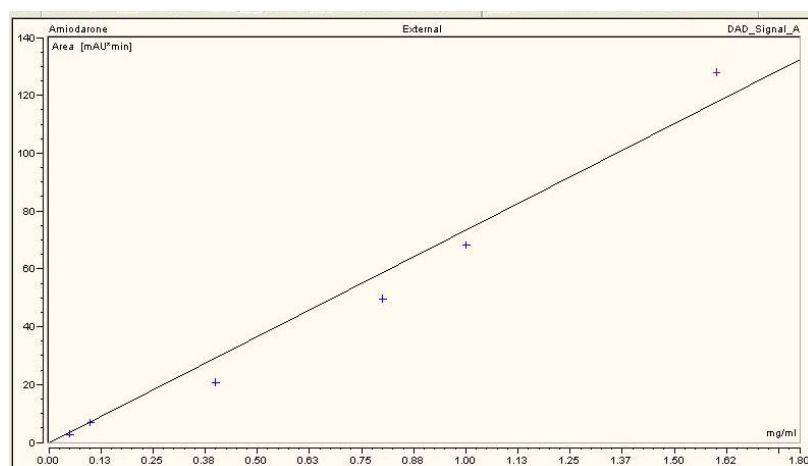


Figure 8.4 Calibration curve generated after HPLC analysis, at 242 nm, of a series of AMD with known concentrations

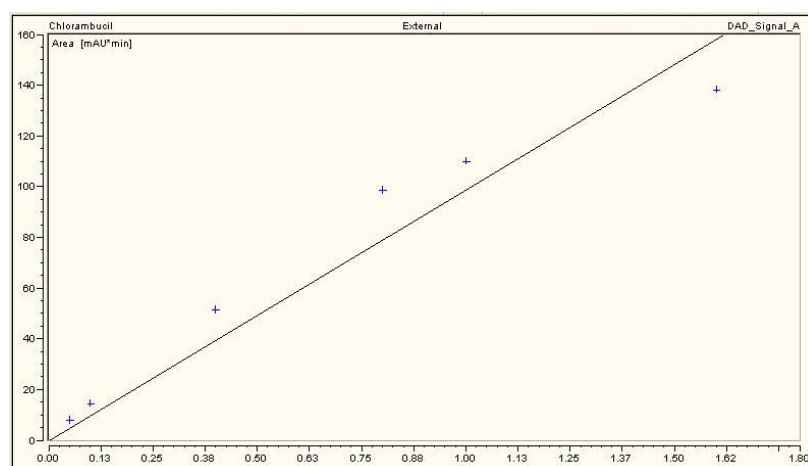


Figure 8.5 Calibration curve generated after HPLC analysis, at 254 nm, of a series of CLB with known concentrations

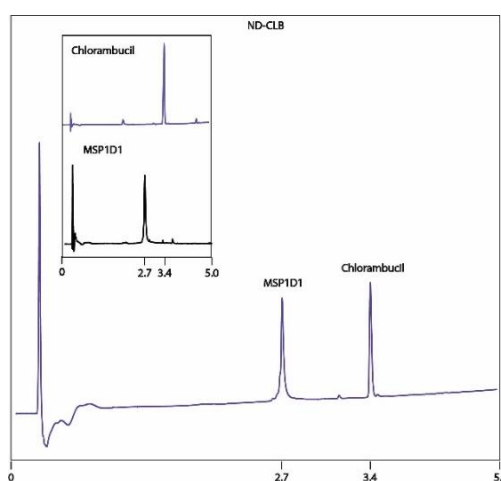


Figure 8.6 HPLC chromatogram of ND CLB measured at 254 nm; the inside chromatograms are an example of CLB and MSP with a known concentration measured at 254 nm and 280 nm, respectively; CLB was preloaded to ND reconstituted using method B

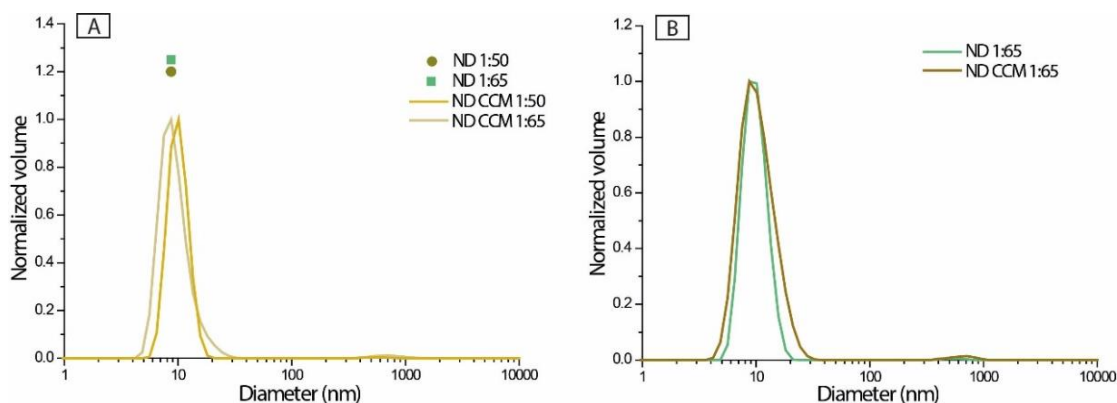


Figure 8.7 DLS of: A – CCM postloaded to ND (1:50 and 1:65 molar ratios); B - CCM preloaded to ND (1:65 molar ratio); reconstituted using method A

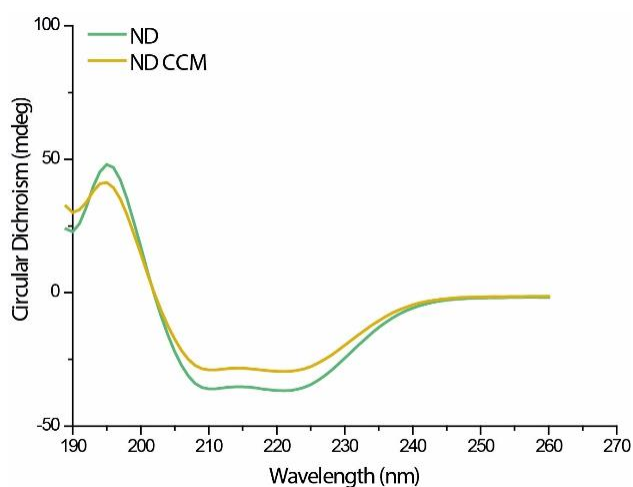


Figure 8.8 CD spectra of ND and ND CCM; CCM was postloaded to ND (1:65 molar ratio) using method A

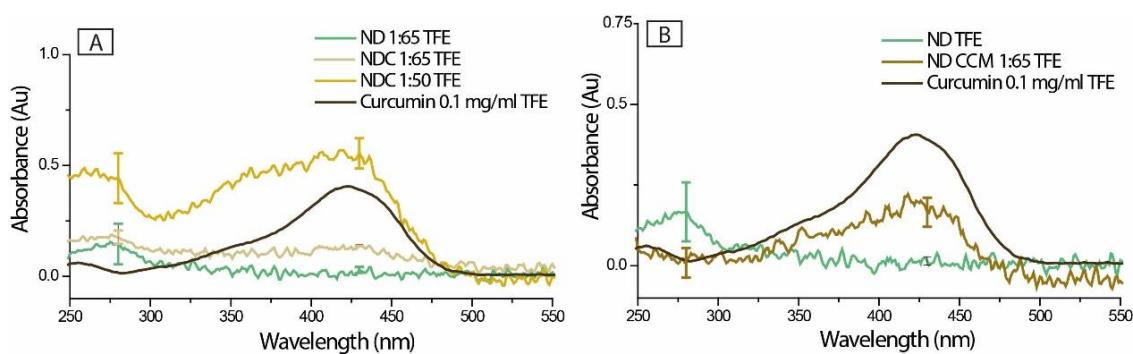


Figure 8.9 UV spectra of ND CCM resuspended in TFE: A – CCM was postloaded to ND using method A; B - CCM was preloaded to ND using method A; the analysis was conducted at 430 nm

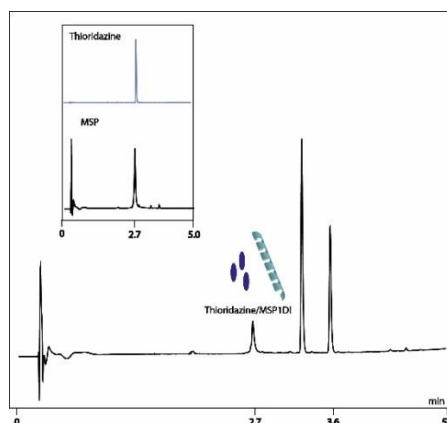


Figure 8.10 HPLC chromatogram of ND TRD, at 262 nm, the inside chromatograms are an example of TRD and MSP with a known concentration measured at 262 nm and 280 nm, respectively; TRD was preloaded to ND reconstituted with method B

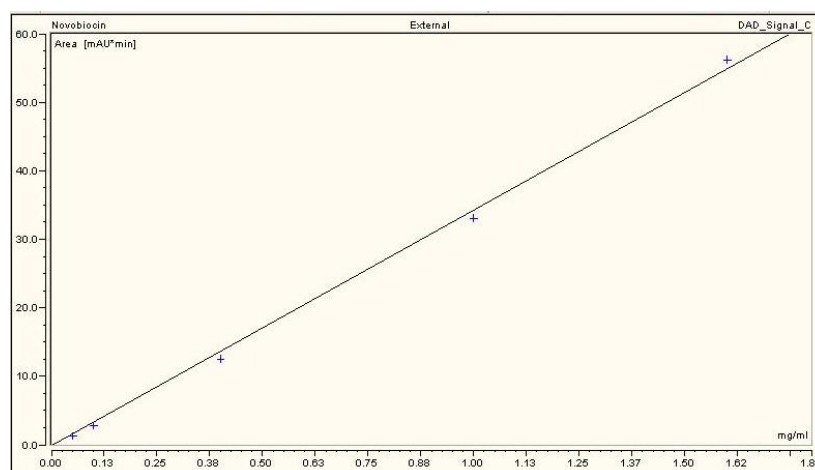


Figure 8.11 Calibration curve generated after analysis, at 324 nm, of a series of NVB with known concentrations by HPLC

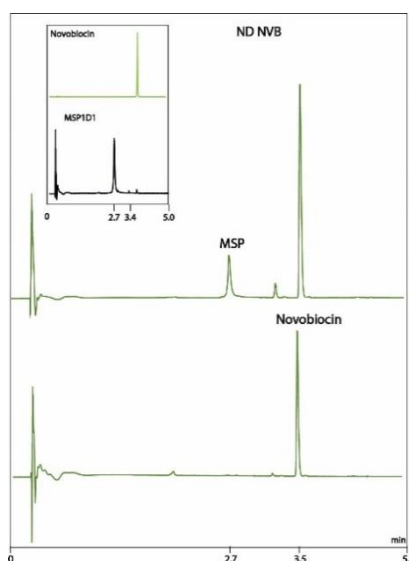


Figure 8.12 HPLC chromatograms of ND NVB, at 280 nm (upper), and 324 nm (lower); drugs were preloaded to ND reconstituted with method B

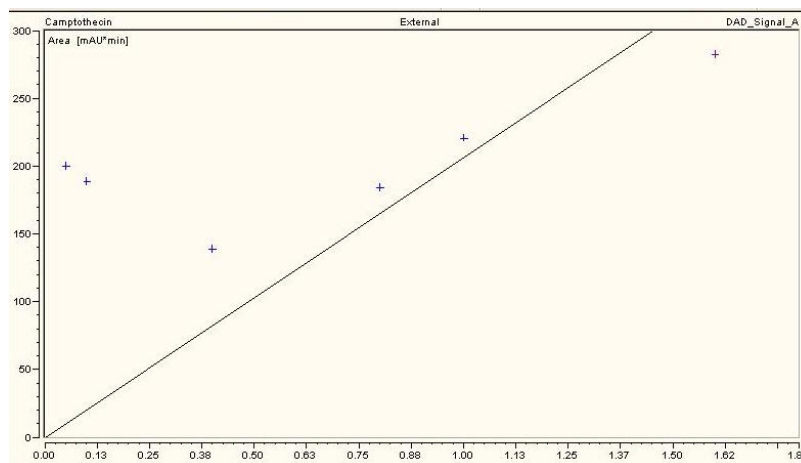


Figure 8.13 Calibration curve generated after analysis, 218 nm, of a series of CPT with known concentrations by HPLC

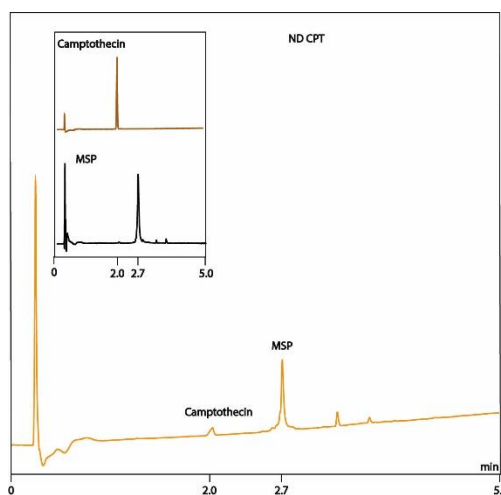


Figure 8.14 HPLC chromatogram of ND CPT, at 218 nm, the inside chromatograms are an example of CPT and MSP with a known concentration measured at 218 nm and 280 nm, respectively; CPT was preloaded to ND reconstituted with method B

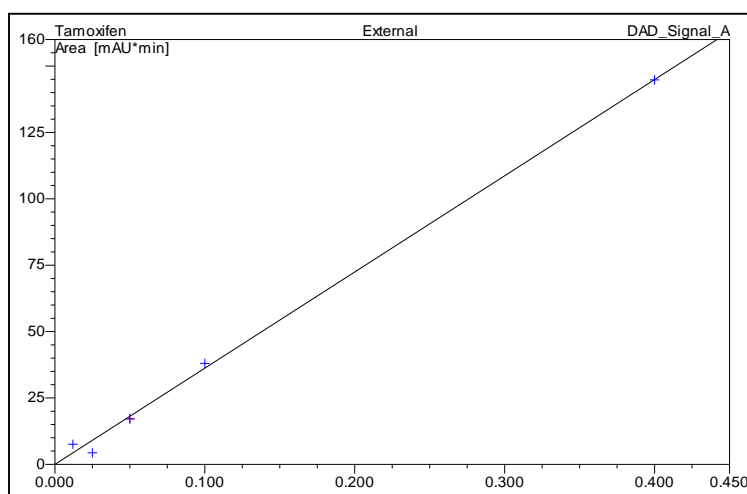


Figure 8.15 Calibration curve generated after analysis, 277 nm, of a series of TMX with known concentrations by HPLC

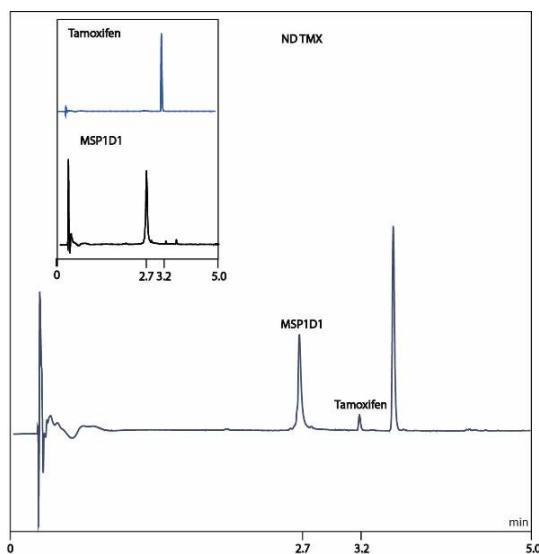


Figure 8.16 HPLC chromatogram of ND TMX, at 277 nm, the inside chromatograms are an example of TMX and MSP with a known concentration measured at 277 nm and 280 nm, respectively; TMX was preloaded to ND reconstituted with method B

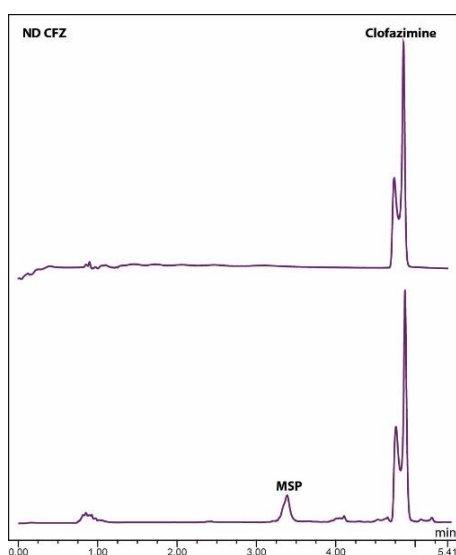


Figure 8.17 HPLC chromatograms of ND CLF, at 486 nm (upper), and 280 nm (lower); samples prepared by Noha and analysed by me; drugs were postloaded to ND reconstituted with method B

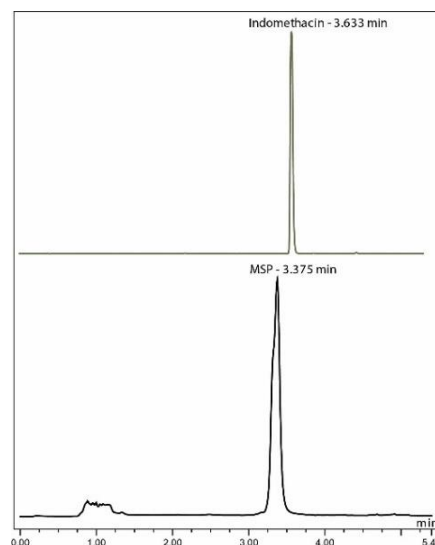


Figure 8.18 HPLC chromatogram of IND at 318 nm (upper) and of MSP at 280 nm (lower)

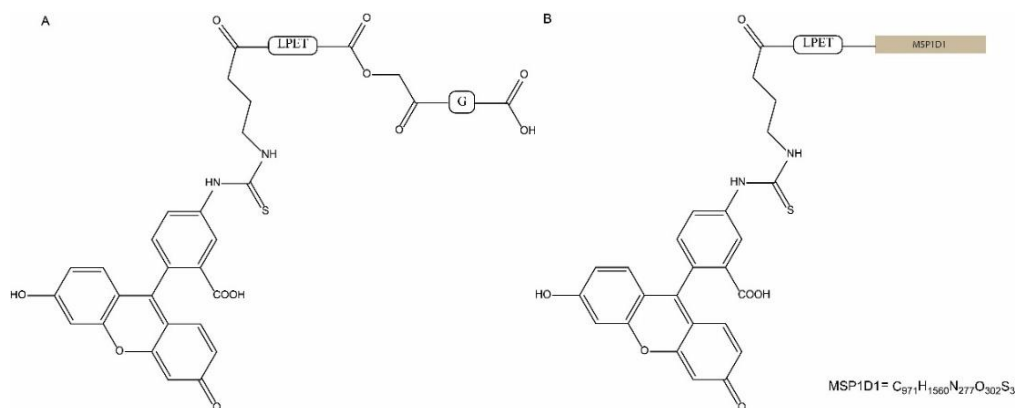


Figure 8.19 Structures of: A - fluorescein-depsipeptide; B - fluorescein modified MSP, within ND assemblies

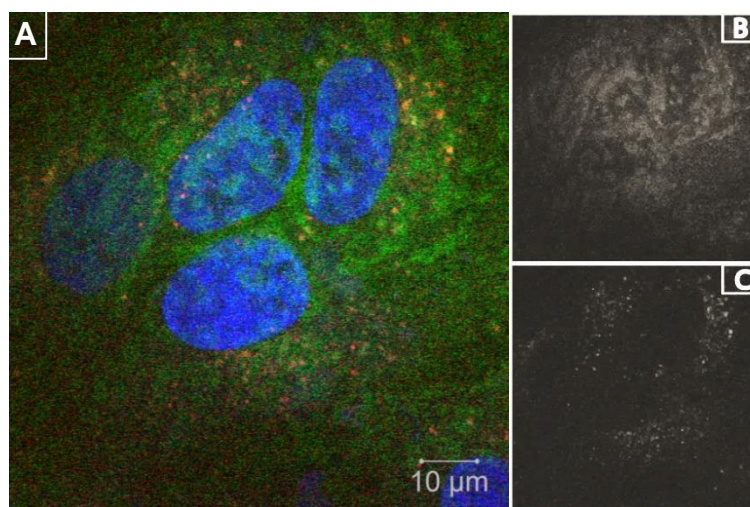


Figure 8.20 Immunostained Huh7 cells, control cells, after 24 h, at 37 °C; A – Merged image; B – green channel, excitation at 488 nm; C – Red channel, excitation at 555 nm

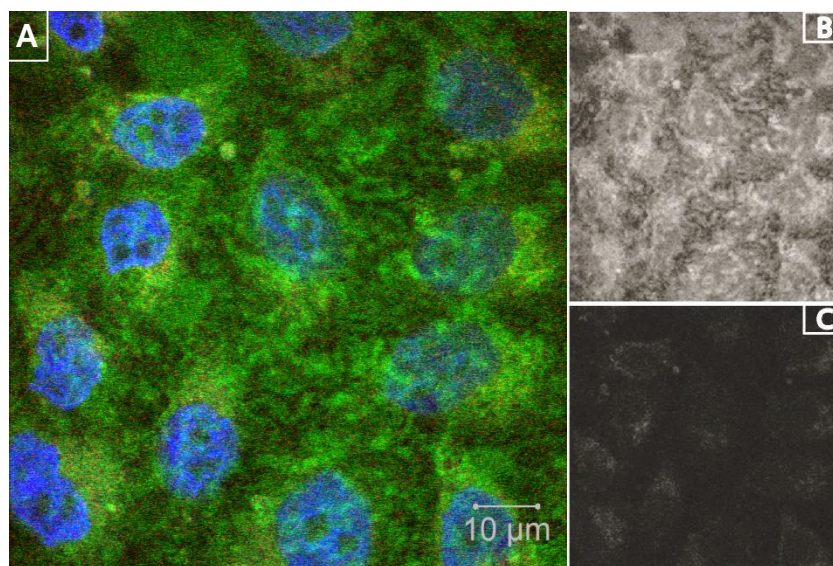


Figure 8.21 Immunostained HeLa cells, control cells, after 24 h, at 37 °C; A – Merged image; B – green channel, excitation at 488 nm; C – Red channel, excitation at 555 nm

9 Chapter 9 – References

1. M. L. Etheridge, S. A. Campbell, A. G. Erdman, C. L. Haynes, S. M. Wolf and J. McCullough, *Nanomedicine-Nanotechnology Biology and Medicine*, 2013, **9**, 1-14.
2. M. K. Teli, S. Mutalik and G. K. Rajanikant, *Current Pharmaceutical Design*, 2010, **16**, 1882-1892.
3. E. M. Aleassa, M. Xing and R. Keijzer, *Pediatric Surgery International*, 2015, **31**, 611-616.
4. A. Wicki, D. Witzigmann, V. Balasubramanian and J. Huwyler, *Journal of Controlled Release*, 2015, **200**, 138-157.
5. T. R. Society, Nanoscience and nanotechnologies: opportunities and uncertainties, <http://www.nanotec.org.uk/finalReport.htm>, (accessed October, 2015).
6. N. N. Initiative, What is nanotechnology?, <http://www.nano.gov/nanotech-101/what/definition>, (accessed October, 2015).
7. R. B. Shah and M. A. Khan, *Nanopharmaceuticals: challenges and regulatory perspective*, 2009.
8. Y. Namiki, T. Fuchigami, N. Tada, R. Kawamura, S. Matsunuma, Y. Kitamoto and M. Nakagawa, *Accounts of Chemical Research*, 2011, **44**, 1080-1093.
9. G. Bozzuto and A. Molinari, *International Journal of Nanomedicine*, 2015, **10**, 975-999.
10. V. Kumar Khanna, *ISRN pharmacology*, 2012, **2012**, 571394-571394.
11. P. Kopel, D. Wawrzak, V. Milosavljevic, A. Moulick, M. Vaculovicova, R. Kizek and V. Adam, *Advances in Nanotechnology*, 2015, **14**.

12. L. M. Bergström, *Thermodynamics of self-assembly*, INTECH Open Access Publisher, 2011.
13. D. Chandler, *Nature*, 2005, **437**, 640-647.
14. J. Israelachvili, *Intermolecular and Surface Forces*, Academic Press, second edition edn., 1991.
15. G. Verma and P. A. Hassan, *Physical Chemistry Chemical Physics*, 2013, **15**, 17016-17028.
16. P. Sharma, S. Ganta, W. A. Denny and S. Garg, *International Journal of Pharmaceutics*, 2009, **367**, 187-194.
17. A. Lamprecht, Y. Bouligand and J. P. Benoit, *Journal of Controlled Release*, 2002, **84**, 59-68.
18. H. B. Ruttala and Y. T. Ko, *Colloids and Surfaces B-Biointerfaces*, 2015, **128**, 419-426.
19. A. Ben-Naim, *Hydrophobic Interactions*, Plenum Press, New York 1980.
20. G. S. Hartley, *Aqueous solutions of paraffin-chain salts; a study in micelle formation*, Hermann & cie, Paris, 1936.
21. A. Leo, C. Hansch and D. Elkins, *Chemical Reviews*, 1971, **71**, 525-+.
22. V. Pliška, in *Lipophilicity in Drug Action and Toxicology*, Wiley-VCH Verlag GmbH, 2008, DOI: 10.1002/9783527614998.ch16, pp. 263-293.
23. M. S. Ku and W. Dulin, *Pharmaceutical Development and Technology*, 2012, **17**, 285-302.
24. P. Khadka, J. Ro, H. Kim, I. Kim, J. T. Kim, H. Kim, J. M. Cho, G. Yun and J. Lee, *Asian Journal of Pharmaceutical Sciences*, 2014, **9**, 304-316.
25. P. C. L. Kwok and H.-K. Chan, *Current Pharmaceutical Design*, 2014, **20**, 474-482.

26. P. Bhatnagar, V. Dhote, S. C. Mahajan, P. K. Mishra and D. K. Mishra, *Current Drug Delivery*, 2014, **11**, 155-171.
27. J. Rios-Doria, A. Carie, T. Costich, B. Burke, H. Skaff, R. Panicucci and K. Sill, *Journal of Drug Delivery*, 2012, **2012**, 1-8.
28. D. C. Buehler, D. B. Toso, V. A. Kickhoefer, Z. H. Zhou and L. H. Rome, *Small (Weinheim an der Bergstrasse, Germany)*, 2011, **7**, 1431.
29. G. Caracciolo, *Nanomedicine: Nanotechnology, Biology and Medicine*, 2015, **11**, 543-557.
30. Y. Li, M. Kroeger and W. K. Liu, *Macromolecules*, 2012, **45**, 2099-2112.
31. Antibody opsonisation, <http://www.innovateus.net/health/what-opsonization>, (accessed October, 2015).
32. L. A. Lane, X. Qian, A. M. Smith and S. Nie, in *Annual Review of Physical Chemistry*, Vol 66, eds. M. A. Johnson and T. J. Martinez, 2015, vol. 66, pp. 521-547.
33. E. Blanco, H. Shen and M. Ferrari, *Nature Biotechnology*, 2015, **33**, 941-951.
34. P. Decuzzi and M. Ferrari, *Biophysical Journal*, 2008, **94**, 3790-3797.
35. V. P. Torchilin, *Advanced Drug Delivery Reviews*, 2006, **58**, 1532-1555.
36. F. Chen, E. B. Ehlerding and W. Cai, *Journal of Nuclear Medicine*, 2014, **55**, 1919-1922.
37. E.-J. Cha, I.-C. Sun, S. C. Lee, K. Kim, I. C. Kwon and C.-H. Ahn, *Macromolecular Research*, 2012, **20**, 319-326.
38. S. Decato, T. Bemis, E. Madsen and S. Mecozzi, *Polymer Chemistry*, 2014, **5**, 6461-6471.
39. Y. Jiao, Y. Sun, X. Tang, Q. Ren and W. Yang, *Small*, 2015, **11**, 1962-1974.

40. Y. Chen, W. Zhang, Y. Huang, F. Gao, X. Sha and X. Fang, *International Journal of Pharmaceutics*, 2015, **488**, 44-58.
41. M. L. Adams, A. Lavasanifar and G. S. Kwon, *Journal of Pharmaceutical Sciences*, 2003, **92**, 1343-1355.
42. V. N. Rao, H. Dinda, P. Venu, J. Das Sarma and R. Shunmugam, *Rsc Advances*, 2014, **4**, 45625-45634.
43. H. Shen, M. Zhou, Q. Zhang, A. Keller and Y. Shen, *Colloid and Polymer Science*, 2015, **293**, 1685-1694.
44. X. Zhai, W. Huang, J. Liu, Y. Pang, X. Zhu, Y. Zhou and D. Yan, *Macromolecular Bioscience*, 2011, **11**, 1603-1610.
45. T. Thanh-Huyen, N. Chi Thanh, L. Gonzalez-Fajardo, D. Hargroye, D. Song, P. Deshinukh, L. Mahajan, D. Ndaya, L. Lai, R. M. Kasi and X. Lu, *Biomacromolecules*, 2014, **15**, 4363-4375.
46. N. F. Steinmetz, *Molecular Pharmaceutics*, 2013, **10**, 1-2.
47. Q. Zhao, W. Chen, Y. Chen, L. Zhang, J. Zhang and Z. Zhang, *Bioconjugate Chemistry*, 2011, **22**, 346-352.
48. Q. Zeng, H. Wen, Q. Wen, X. Chen, Y. Wang, W. Xuan, J. Liang and S. Wan, *Biomaterials*, 2013, **34**, 4632-4642.
49. L. Shan, S. Cui, C. Du, S. Wan, Z. Qian, S. Achilefu and Y. Gu, *Biomaterials*, 2012, **33**, 146-162.
50. A. A. A. Aljabali, S. Shukla, G. P. Lomonossoff, N. F. Steinmetz and D. J. Evans, *Molecular Pharmaceutics*, 2013, **10**, 3-10.
51. K. Niikura, N. Sugimura, Y. Musashi, S. Mikuni, Y. Matsuo, S. Kobayashi, K. Nagakawa, S. Takahara, C. Takeuchi, H. Sawa, M. Kinjo and K. Ijro, *Molecular Biosystems*, 2013, **9**, 501-507.
52. D. Ren, F. Kratz and S.-W. Wang, *Small*, 2011, **7**, 1051-1060.

53. E. Kastner, V. Verma, D. Lowry and Y. Perrie, *International Journal of Pharmaceutics*, 2015, **485**, 122-130.
54. R. Duncan and R. Gaspar, *Molecular Pharmaceutics*, 2011, **8**, 2101-2141.
55. C.-H. Chu, Y.-C. Wang, H.-Y. Huang, L.-C. Wu and C.-S. Yang, *Nanotechnology*, 2011, **22**.
56. J. M. Chan, L. Zhang, K. P. Yuet, G. Liao, J.-W. Rhee, R. Langer and O. C. Farokhzad, *Biomaterials*, 2009, **30**, 1627-1634.
57. L. Zhang, J. M. Chan, F. X. Gu, J.-W. Rhee, A. Z. Wang, A. F. Radovic-Moreno, F. Alexis, R. Langer and O. C. Farokhzad, *Acs Nano*, 2008, **2**, 1696-1702.
58. K. Hadinoto, A. Sundaresan and W. S. Cheow, *European Journal of Pharmaceutics and Biopharmaceutics*, 2013, **85**, 427-443.
59. P. K. K. Vivek Kumar Gupta, S. Ramesh, S. P. Misra, Alok Gupta, *Int. J. Res. Pharm. Sci.*, 2010, **1**, 163-169.
60. E. D. Enger, F. C. Ross and D. B. Bailey, *Concepts in biology*, Dubuque, IA McGraw-Hill 13th ed. edn., 2009.
61. A. Diller, C. Loudet, F. Aussenac, G. Raffard, S. Fournier, M. Laguerre, A. Grelard, S. J. Opella, F. M. Marassi and E. J. Dufourc, *Biochimie*, 2009, **91**, 744-751.
62. R. Vacha and D. Frenkel, *Langmuir*, 2014, **30**, 4229-4235.
63. Y. Liu, M. Li, Y. Yang, Y. Xia and M.-P. Nieh, *Biochimica Et Biophysica Acta-Biomembranes*, 2014, **1838**, 1871-1880.
64. M. Zhang, R. Huang, S.-C. Im, L. Waskell and A. Ramamoorthy, *Journal of Biological Chemistry*, 2015, **290**, 12705-12718.

65. I. Kucharska, T. C. Edrington, B. Liang and L. K. Tamm, *Journal of Biomolecular Nmr*, 2015, **61**, 261-274.
66. W. Zhang, J. Sun and Z. He, *Asian Journal of Pharmaceutical Sciences*, 2013, **8**, 143-150.
67. M. N. Triba, D. E. Warschawski and P. F. Devaux, *Biophys J*, 2005, **88**, 1887-1901.
68. M. Cuchel, S. Lund-Katz, M. de la Llera-Moya, J. S. Millar, D. Chang, I. Fuki, G. H. Rothblat, M. C. Phillips and D. J. Rader, *Arteriosclerosis, thrombosis, and vascular biology*, 2010, **30**, 526-532.
69. P. G. Frank and Y. L. Marcel, *Journal of Lipid Research*, 2000, **41**, 853-872.
70. J. P. Segrest, D. W. Garber, C. G. Brouillette, S. C. Harvey and G. M. Anantharamaiah, in *Advances in Protein Chemistry; Lipoproteins, apolipoproteins, and lipases*, ed. V. N. Schumaker, 1994, vol. 45, 303-369.
71. T. H. Bayburt, Y. V. Grinkova and S. G. Sligar, *Nano Letters*, 2002, **2**, 853-856.
72. T. H. Bayburt and S. G. Sligar, *Febs Letters*, 2010, **584**, 1721-1727.
73. K. A. Redmond, T.-S. Nguyen and R. O. Ryan, *International Journal of Pharmaceutics*, 2007, **339**, 246-250.
74. A. W. Shaw, M. A. McLean and S. G. Sligar, *Febs Letters*, 2004, **556**, 260-264.
75. B. J. Baas, I. G. Denisov and S. G. Sliger, *Archives of Biochemistry and Biophysics*, 2004, **430**, 218-228.
76. T. H. Bayburt and S. G. Sligar, *Protein Science*, 2003, **12**, 2476-2481.

77. T. Boldog, S. Grimme, M. Li, S. G. Sligar and G. L. Hazelbauer, *Proceedings of the National Academy of Sciences of the United States of America*, 2006, **103**, 11509-11514.
78. E. Serebryany, G. A. Zhu and E. C. Y. Yan, *Biochimica et biophysica acta*, 2012, **1818**, 225-233.
79. A. J. Leitz, T. H. Bayburt, A. N. Barnakov, B. A. Springer and S. G. Sligar, *Biotechniques*, 2006, **40**, 601.
80. I. G. Denisov, Y. V. Grinkova, A. A. Lazarides and S. G. Sligar, *Journal of the American Chemical Society*, 2004, **126**, 3477-3487.
81. A. Nath, A. J. Trexler, P. Koo, A. D. Miranker, W. M. Atkins and E. Rhoades, in *Methods in Enzymology, Vol 472: Single Molecule Tools, Pt A: Fluorescence Based Approaches*, ed. N. G. Walter, 2010, vol. 472, pp. 89-117.
82. A. Das and S. G. Sligar, *Biochemistry*, 2009, **48**, 12104-12112.
83. T. Kawai, J. M. M. Caaveiro, R. Abe, T. Katagiri and K. Tsumoto, *Febs Letters*, 2011, **585**, 3533-3537.
84. T. K. Ritchie, Y. V. Grinkova, T. H. Bayburt, I. G. Denisov, J. K. Zolnerciks, W. M. Atkins and S. G. Sligar, in *Methods in Enzymology; Liposomes, Pt F*, ed. N. Duzgunes, 2009, vol. 464, pp. 211-231.
85. S. K. Kim, M. B. Foote and L. Huang, *Biomaterials*, 2012, **33**, 3959-3966.
86. F. Hagn, M. Etzkorn, T. Raschle and G. Wagner, *Journal of the American Chemical Society*, 2013, **135**, 1919-1925.
87. A. Das, S. S. Varma, C. Mularczyk and D. D. Meling, *Chembiochem*, 2014, **15**, 892-899.
88. K. G. Nelson, J. V. Bishop, R. O. Ryan and R. Titus, *Antimicrobial Agents and Chemotherapy*, 2006, **50**, 1238-1244.

89. D. C. Buehler, D. B. Toso, V. A. Kickhoefer, Z. H. Zhou and L. H. Rome, *Small*, 2011, **7**, 1432-1439.
90. I. G. Denisov, M. A. McLean, A. W. Shaw, Y. V. Grinkova and S. G. Sligar, *Journal of Physical Chemistry B*, 2005, **109**, 15580-15588.
91. A. W. Shaw, V. S. Pureza, S. G. Sligar and J. H. Morrissey, *Journal of Biological Chemistry*, 2007, **282**, 6556-6563.
92. F. Zehender, A. Ziegler, H. J. Schoenfeld and J. Seelig, *Biochemistry*, 2012, **51**, 1269-1280.
93. ap-lab, Circular Dichroism, http://www.ap-lab.com/circular_dichroism.htm, (accessed November, 2015).
94. N. J. Greenfield, *Nature Protocols*, 2006, **1**, 2876-2890.
95. M. N. Oda, M. S. Budamagunta, M. S. Borja, J. Petrlova, J. C. Voss and J. O. Lagerstedt, *Febs Journal*, 2013, **280**, 3416–3424.
96. A. Singh, A. M. Evens, R. Anderson, J. Beckstead, N. Sankar, S. Bhalla, S. Yang, T. Forte, R. Ryan and L. I. Gordon, *Blood*, 2009, **114**, 1433-1434.
97. Y.-L. Luo, X.-L. Yang, F. Xu, Y.-S. Chen and X. Zhao, *Colloid and Polymer Science*, 2014, **292**, 1061-1072.
98. H. Song, S. Nie, X. Yang, N. Li, H. Xu, L. Zheng and W. Pan, *International Journal of Nanomedicine*, 2010, **5**, 933-942.
99. A. Perez-de-Luque, Z. Cifuentes, J. A. Beckstead, J. C. Sillero, C. Avila, J. Rubio and R. O. Ryan, *Pest Management Science*, 2012, **68**, 67-74.
100. M. Ghosh, A. T. K. Singh, W. Xu, T. Sulchek, L. I. Gordon and R. O. Ryan, *Nanomedicine-Nanotechnology Biology and Medicine*, 2011, **7**, 162-167.

101. S. H. Kim, J. A. Kaplan, Y. Sun, A. Shieh, H.-L. Sun, C. M. Croce, M. W. Grinstaff and J. R. Parquette, *Chemistry-a European Journal*, 2015, **21**, 101-105.
102. U. Pison, T. Welte, M. Giersig and D. A. Groneberg, *European Journal of Pharmacology*, 2006, **533**, 341-350.
103. H. Zeng, C. Shi, J. Huang, L. Li, G. Liu and H. Zhong, *Biointerphases*, 2015, **11**, 1934-8630.
104. T.-S. Nguyen, P. M. M. Weers, V. Raussens, Z. Wang, G. Ren, T. Sulchek, P. D. Hoeprich, Jr. and R. O. Ryan, *Biochimica Et Biophysica Acta-Biomembranes*, 2008, **1778**, 303-312.
105. M. Trumbore, D. W. Chester, J. Moring, D. Rhodes and L. G. Herbette, *Biophysical Journal*, 1988, **54**, 535-543.
106. d. bank, chlorambucil, <http://www.drugbank.ca/drugs/DB00291>, 2014).
107. D. Yanagisawa, H. Taguchi, A. Yamamoto, N. Shirai, K. Hirao and I. Tooyama, *Journal of Alzheimers Disease*, 2011, **24**, 33-42.
108. E. Kupetz and H. Bunjes, *Journal of Controlled Release*, 2014, **189**, 54-64.
109. X.-Y. Ke, V. W. L. Ng, S.-J. Gao, Y. W. Tong, J. L. Hedrick and Y. Y. Yang, *Biomaterials*, 2014, **35**, 1096-1108.
110. V. Law, C. Knox, Y. Djoumbou, T. Jewison, A. C. Guo, Y. Liu, A. Maciejewski, D. Arndt, M. Wilson, V. Neveu, A. Tang, G. Gabriel, C. Ly, S. Adamjee, Z. T. Dame, B. Han, Y. Zhou and D. S. Wishart, *Nucleic Acids Research*, 2014, **42**, D1091-D1097.
111. D. S. Wishart, T. Jewison, A. C. Guo, M. Wilson, C. Knox, Y. Liu, Y. Djoumbou, R. Mandal, F. Aziat, E. Dong, S. Bouatra, I. Sinelnikov, D. Arndt, J. Xia, P. Liu, F. Yallou, T. Bjorndahl, R. Perez-Pineiro, R. Eisner,

- F. Allen, V. Neveu, R. Greiner and A. Scalbert, *Nucleic Acids Research*, 2013, **41**, 801-807.
112. B. T. Kurien, A. Singh, H. Matsumoto and R. H. Scofield, *Assay and Drug Development Technologies*, 2007, **5**, 567-576.
113. B. Drasler, D. Drobne, A. Sadeghpour and M. Rappolt, *Chemistry and Physics of Lipids*, 2015, **188**, 46-53.
114. W. Kopec, J. Telenius and H. Khandelia, *Febs Journal*, 2013, **280**, 2785-2805.
115. N. Shimokawa, M. Nagata and M. Takagi, *Physical Chemistry Chemical Physics*, 2015, **17**, 20882-20888.
116. N. Kučerka, M.-P. Nieh and J. Katsaras, *Biochimica et Biophysica Acta (BBA) - Biomembranes*, 2011, **1808**, 2761–2771.
117. N. Dan, *Biochimica et Biophysica Acta (BBA) - Biomembranes*, 2002, **1564**, 343–348.
118. W. K. Surewicz, R. M. Epand, H. J. Pownall and S. W. Hui, *Journal of Biological Chemistry*, 1986, **261**, 6191-6197.
119. B. J. Orlando, D. R. McDougale, M. J. Lucido, E. T. Eng, L. A. Graham, C. Schneider, D. L. Stokes, A. Das and M. G. Malkowski, *Archives of Biochemistry and Biophysics*, 2014, **546**, 33-40.
120. S. Kaufmann, O. Borisov, M. Textor and E. Reimhult, *Soft Matter*, 2011, **7**, 9267-9275.
121. E. Johansson, C. Engvall, M. Arfvidsson, P. Lundahl and K. Edwards, *Biophysical Chemistry*, 2005, **113**, 183-192.
122. N. Skar-Gislinge, J. B. Simonsen, K. Mortensen, R. Feidenhans'l, S. G. Sligar, B. L. Moller, T. Bjornholm and L. Arleth, *Journal of the American Chemical Society*, 2010, **132**, 13713-13722.

123. Z. O. Shenkarev, E. N. Lyukmanova, O. I. Solozhenkin, I. E. Gagnidze, O. V. Nekrasova, V. V. Chupin, A. A. Tagaev, Z. A. Yakimenko, T. V. Ovchinnikova, M. P. Kirpichnikov and A. S. Arseniev, *Biochemistry-Moscow*, 2009, **74**, 756-765.
124. A. Y. Shih, P. L. Freddolino, S. G. Sligar and K. Schulten, *Nano Letters*, 2007, **7**, 1692-1696.
125. W. Kopec and H. Khandelia, *Journal of Computer-Aided Molecular Design*, 2014, **28**, 123-134.
126. N. Skar-Gislinge and L. Arleth, *Physical Chemistry Chemical Physics*, 2011, **13**, 3161-3170.
127. T. Y. Zakharian, A. Seryshev, B. Sitharaman, B. E. Gilbert, V. Knight and L. J. Wilson, *Journal of the American Chemical Society*, 2005, **127**, 12508-12509.
128. N. V. Koshkina, B. E. Gilbert, J. C. Waldrep, A. Seryshev and V. Knight, *Cancer Chemotherapy and Pharmacology*, 1999, **44**, 187-192.
129. M. Luxnat and H. J. Galla, *Biochimica et biophysica acta*, 1986, **856**, 274-282.
130. Sligarlab, Nanodisc protocols, <http://sligarlab.life.uiuc.edu/nanodisc/protocols.html>, (accessed October, 2015).
131. A. Y. Shih, I. G. Denisov, J. C. Phillips, S. G. Sligar and K. Schulten, *Biophysical Journal*, 2005, **88**, 548-556.
132. S. Leekumjorn and A. K. Sum, *Biochimica Et Biophysica Acta-Biomembranes*, 2007, **1768**, 354-365.
133. M. Baciú, S. C. Sebai, O. Ces, X. Mulet, J. A. Clarke, G. C. Shearman, R. V. Law, R. H. Templer, C. Plisson, C. A. Parker and A. Gee, *Philosophical Transactions of the Royal Society a-Mathematical Physical and Engineering Sciences*, 2006, **364**, 2597-2614.

134. M. H. Ali, B. Moghaddam, D. J. Kirby, A. R. Mohammed and Y. Perrie, *International Journal of Pharmaceutics*, 2013, **453**, 225-232.
135. C. H. A. Boalwe, K. Patel and M. Singh, *International Journal of Pharmaceutics*, 2015, **489**, 106-116.
136. D. Dyondi, A. Sarkar and R. Banerjee, *Journal of Biomedical Nanotechnology*, 2015, **11**, 1225-1235.
137. S. Garcia-Manyes, L. Redondo-Morata, G. Oncins and F. Sanz, *Journal of the American Chemical Society*, 2010, **132**, 12874-12886.
138. L. P. J. Heyes, K. Bremner, I. MacLachlan, *J Control Release*, 2005, 276-287.
139. D. Li, G. Li, P. Li, L. Zhang, Z. Liu, J. Wang and E. Wang, *Biomaterials*, 2010, **31**, 1850-1857.
140. Y. Perrie, P. M. Frederik and G. Gregoriadis, *Vaccine*, 2001, **19**, 3301-3310.
141. P. Jurkiewicz, A. Olzynska, M. Langner and M. Hof, *Langmuir*, 2006, **22**, 8741-8749.
142. J.-F. Labbe, F. Cronier, R. C.-Gaudreault and M. Auger, *Chemistry and Physics of Lipids*, 2009, **158**, 91-101.
143. R. B. Campbell, S. V. Balasubramanian and R. M. Straubinger, *Journal of Pharmaceutical Sciences*, 2001, **90**, 1091-1105.
144. E. Kaditi, G. Mountrichas and S. Pispas, *European Polymer Journal*, 2011, **47**, 415-434.
145. N. Nishiyama and K. Kataoka, *Pharmacology & Therapeutics*, 2006, **112**, 630-648.
146. J. H. Park, S. Lee, J.-H. Kim, K. Park, K. Kim and I. C. Kwon, *Progress in Polymer Science*, 2008, **33**, 113-137.

147. N. Hoda, L. Budama, B. A. Cakir, O. Topel and R. Ozisik, *Materials Research Bulletin*, 2013, **48**, 3183-3188.
148. O. Topel, B. A. Cakir, L. Budama and N. Hoda, *Journal of Molecular Liquids*, 2013, **177**, 40-43.
149. S. Li, B. Byrne, J. Welsh and A. F. Palmer, *Biotechnology Progress*, 2007, **23**, 278-285.
150. W. Mueller, K. Koynov, K. Fischer, S. Hartmann, S. Pierrat, T. Basche and M. Maskos, *Abstracts of Papers of the American Chemical Society*, 2009, **237**.
151. W. Mueller, K. Koynov, S. Pierrat, R. Thiermann, K. Fischer and M. Maskos, *Polymer*, 2011, **52**, 1263-1267.
152. A. T. K. Singh, A. M. Evens, R. J. Anderson, J. A. Beckstead, N. Sankar, A. Sassano, S. Bhalla, S. Yang, L. C. Plataniias, T. M. Forte, R. O. Ryan and L. I. Gordon, *British Journal of Haematology*, 2010, **150**, 158-169.
153. M. Ghosh and R. O. Ryan, *Nanomedicine*, 2014, **9**, 763-771.
154. D. J. Williamson, M. A. Fascione, M. E. Webb and W. B. Turnbull, *Angewandte Chemie-International Edition*, 2012, **51**, 9377-9380.
155. D. J. Williamson, M. E. Webb and W. B. Turnbull, *Nature Protocols*, 2014, **9**, 253-262.
156. M. W.-L. Popp and H. L. Ploegh, *Angewandte Chemie-International Edition*, 2011, **50**, 5024-5032.
157. A. H. Gaspar, L. A. Marraffini, E. M. Glass, K. L. DeBord, H. Ton-That and O. Schneewind, *Journal of Bacteriology*, 2005, **187**, 4646-4655.
158. M. R. Wilkins, E. Gasteiger, A. Bairoch, J. C. Sanchez, K. L. Williams, R. D. Appel and D. F. Hochstrasser, *Methods in molecular biology (Clifton, N.J.)*, 1999, **112**, 531-552.

159. H. Nakabayashi, K. Taketa, K. Miyano, T. Yamane and J. Sato, *Cancer Research*, 1982, **42**, 3858-3863.
160. G. O. Gey, W. D. Coffman and M. T. Kubicek, *Cancer Research*, 1952, **12**, 264-265.
161. H. Corrodi and G. Jonsson, *Journal of Histochemistry and Cytochemistry*, 1967, **15**, 65-78.
162. R. Agarwal, V. Singh, P. Journey, L. Shi, S. V. Sreenivasan and K. Roy, *Proceedings of the National Academy of Sciences of the United States of America*, 2013, **110**, 17247-17252.
163. S. Barman, S. K. Mukhopadhyay, M. Gangopadhyay, S. Biswas, S. Dey and N. D. P. Singh, *Journal of Materials Chemistry B*, 2015, **3**, 3490-3497.
164. M. Ikbal, B. Saha, S. Barman, S. Atta, D. R. Banerjee, S. K. Ghosh and N. D. P. Singh, *Organic & Biomolecular Chemistry*, 2014, **12**, 3459-3469.
165. P. P. Provenzano, C. Cuevas, A. E. Chang, V. K. Goel, D. D. Von Hoff and S. R. Hingorani, *Cancer Cell*, 2012, **21**, 418-429.
166. S. Bhattacharyya, R. Bhattacharya, S. Curley, M. A. McNiven and P. Mukherjee, *Proceedings of the National Academy of Sciences of the United States of America*, 2010, **107**, 14541-14546.
167. S. Jackle, F. Rinninger, T. Lorenzen, H. Greten and E. Windler, *Hepatology*, 1993, **17**, 455-465.
168. R. S. Farid, Circular Dichroism (CD) Spectroscopy, <http://www.proteinchemist.com/cd/cdspec.html>, (accessed November, 2015).
169. Department of Chemistry, University of Adelaide, *Size Exclusion Chromatography*, <http://www.chemistry.adelaide.edu.au>, (accessed November, 2015).

170. K. D. Fifeild F. W., *Principles and practice of analytical chemistry*, Stanley Thornes (Publishers) Ltd, Cheltenham, 4th edition edn., 1999.